To the Graduate Council:

I am submitting herewith a thesis written by An Yan entitled "Study of Two-Phase Flow Patterns and Frictional Pressure Drop in Helical and Spiral Coils". I have examined the final copy of this thesis for form and content and recommend that it be accepted in partial fulfillment of the requirements for the degree of Master of Science, with a major in Mechanical Engineering.

Edward G. Keshock

Edward G. Keshock, Major Professor

We have read this thesis
and recommend its acceptance:

Accepted for the Council:

Associate Vice Chancellor
and Dean of The Graduate School

STATEMENT OF PERMISSION TO USE

In presenting this thesis in partial fulfillment of the requirements for the Master of Science degree at The University of Tennessee, Knoxville, I agree that the Library shall make it available to borrowers under rules of the Library. Brief quotations from this thesis are allowable without special permission, provided that accurate acknowledgement of the source is made. Permission for extensive quotation from or reproduction of this thesis in whole or parts may be granted by my major professor, or in his absence, by the Head of Interlibrary Service when, in the opinion of either, the proposed use of the material is for scholarly purposes. Any copying or use of the material in this thesis for financial gain shall not be allowed without my written permission.

Signature Anyan [signature]

Date 5/27/92

STUDY OF TWO-PHASE FLOW PATTERNS AND FRICTIONAL PRESSURE DROP IN HELICAL AND SPIRAL COILS

A Thesis
Presented for the
Master of Science
Degree
The University of Tennessee, Knoxville

An Yan

August 1992

ACKNOWLEDGEMENTS

I am greatly indebted to two people without whom this thesis would have never been completed; Dr. E. G. Keshock, my major professor, who made the original proposal, obtained the funding for the work presented here, and advised the whole experiment and thesis writing processes, whose patience, long time support, and guidance made this work possible, Mr. Adel Omrani, who helped me with the experiment from the very beginning to the end.

I would also like to thank my other advisory committee members, Dr. J. W. Hodgson and Dr. J. R. Parsons, for their helpful comments and their understanding in my situation.

Thanks are also due to Mr. D. Higdon, Mr. S. Hunly, and the staff members of the Mechanical and Aerospace Engineering Department machine shop for their assistance during the experimental stage of this study.

Most importantly, I would like to thank my husband, Zhichao Guo, without his love, support and encouragement I would have given up long time ago.

ABSTRACT

Experimental studies of flow pattern and pressure drop for air-water and R113 liquid/vapor flow in helical and spiral coils were conducted. Five test sections, namely, helical coils having a circular cross-section and three rectangular cross-sections of different aspect ratios, along with a circular cross-section spiral tube, were utilized in the study.

Five sets of the flow pattern test data -- helical coil vertical up-flows for both air-water and R-113 in a circular cross-section tube, R-113 in a near-square cross-section tube, and spiral horizontal outward flow of both air-water and R-113 in a circular cross-section tube -- are analyzed and compared with a modified Baker map, the Taitel & Dukler map, the Choe, Weinberg, & Weisman map, and the Uddin map. None of the maps are able to adequately predict both the helical and spiral coil test data. An empirical correlation of the slug-annular transition was developed for both helical vertical-up flow and spiral horizontal outward flow which gives good agreement with the test data.

Three sets of the pressure drop test data -- helical coil vertical up-flows for both air-water and R-113 in a circular cross-section tube, and R-113 in a near-square cross-section tube -- are analyzed and compared with homogenous and Lockhart-Martinelli models. All of them predict pressure drops only approximately in the slug and developing-annular flow regions. Empirical correlations were developed to calculate the critical Reynolds number and friction factors for R-113 helical coil vertical up-flow in both circular and near-square cross-section tubes.

TABLE OF CONTENTS

LIST OF TABLES

LIST OF FIGURES

FIGURE PAGE

NOMENCLATURE

A Cross-section area of tube or flow channel; Constant in eq.(1.1c)

A^* Y-axis parameter in Uddin's flow map

a Constant in eq.(1.18)

b Constant in eq. (1.18)

C Constant in eq. (1.1c), a dimensionless pressure gradient

c Constant in eq. (1.18)

D Diameter of coil

DP^* X-axis parameter in Uddin's flow map

DP Pressure drop

d Inner diameter of tube or flow channel

De Dean number, $De = Re\sqrt{(r/R)} = Re\sqrt{(d/D)}$

d_h Hydraulic diameter of rectangular tube

D_{max} Maximum diameter of spiral

D_{min} Minimum diameter of spiral

D^* Dimensionless secondary flow velocity in core region (?for single phase flow)

dp/dz Pressure gradient

e Constant in eq. (1.18)

f Fanning friction factor, $\lambda = 4f$

f_c Fanning friction factor for coils or curved tubes

f_s Fanning friction factor for straight tubes

g Gravitational acceleration

g_c Gravitational conversion factor, = 32.174 $(lb_m\text{-}ft)/(lb_f\text{-}sec^2)$ in English units, = 1 $(kg\text{-}m)/N\text{-}sec^2)$ in SI units

G Mass velocity, $G = \rho W$

H Height of the rectangular cross section in helical coil

H_c Height of coil

K Dean number, $K = De$

L Flow channel length or tube length

n_1 Number of turns from the origin to the inner start of the spiral, $n_1 = D_{min}/2p$

n_2 Number of turns from the origin to the end of the spiral, $n_2 = D_{max}/2p$

p Pressure; Coil pitch

P Pressure

r Radius of tube or flow channel

R Radius of coil

R_c Modified coil radius for helical coil

Re Reynolds number, $Re = \rho W d/\mu = Gd/\mu$

Re_{crit} Critical Reynolds number

U Radial component of velocity, superficial velocities of two-phase flow

u Dimensionless radial component of velocity, $u = U(r/\nu)$

V Circumferential component of velocity

v Dimensionless circumferential component of velocity, $v = V(r/\nu)$

W Axial component of velocity, width of the rectangular cross section in helical coil

w Dimensionless axial component of velocity, $w = W(r/\nu)$

x Quality of two-phase flow

X Lockhart-Martinelli parameter

z Elevation

Greek Symbols

α Void fraction

ΔP Pressure drop

δ Dimensionless thickness of boundary layer, boundary layer thickness divided by r

δ_m Peripheral mean value of δ

η Co-ordinate in radial direction in the cross section

θ Axial co-ordinate

λ Friction factor, density correction factor in Modified Baker's flow map

μ Viscosity (dynamic)

ν Kinematic viscosity, $\nu = \mu/\rho$

ρ Density

σ Surface tension

ψ Circumferential co-ordinate, viscosity & surface tension correction factor in Modified Baker's flow map

Subscripts

1 Values in the core region

a Accelarational pressure drop

c Coil, coiled tube

cal Calculated quantity

crit Critical Reynolds number

f Frictional pressure drop

g Gas phase, gravitational pressure drop

l Liquid phase

m Measured quantity, mean value

measured Measured quantity

room Quantity at room temperature

s Straight tube, superficial velocity

tot Total pressure drop between two ΔP transducer taps

TP Two-phase mixture

CHAPTER 1 INTRODUCTION

1.1 Introduction

A coiled tube with a constant radius of the coil is called a *helically coiled tube* (or *helical coil*). A *spiral coil* is a tube coiled into a plane with gradually increasing radius of the coil (see Figure 1.1).

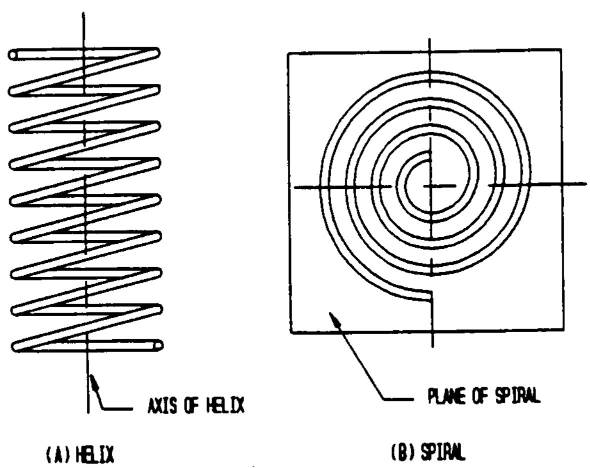

Figure 1.1 Coil Type

Helical and spiral coiled tube heat exchangers are widely used in the petrochemical, biomedical, pharmaceutical, power generation, refrigeration and aero-space industries. They have two main advantages over straight tubes: 1) heat transfer coefficients in coils are higher than in straight tubes, 2) coils allow a significantly greater heat transfer area to be packed into a given space than do straight tubes. Also, the flow-induced centrifugal forces make possible the successful use of heat exchangers under zero-gravity conditions, i.e. in space applications. It has been shown that the added artificial body force substantially improves two-phase heat transfer rates [34]. In recent years, considerable interest has been generated in the design of helical (or spiral) heat exchangers which can provided uninterrupted and uniform performance under adverse gravity loading [17].

The optimum design of helical and spiral coiled heat exchangers for two-phase systems requires an analytical description of the heat, mass and momentum transfer characteristics associated with the flowing two-phase mixture in the coils. Since the transfer characteristics depend strongly upon the spatial configuration formed by the two phases (generally known as flow pattern or flow regime), the fundamental problems become (1) determining the possible flow patterns and (2) being able to predict which flow patterns will exist for a given set of conditions. Additionally, being able to predict the pressure drop along such coiled two-phase systems is of equal importance for design purposes.

A particular characteristic which makes the flow in a coil or a curved tube quite different from that in a straight tube, is that there is a variation of centrifugal force acting on the fluid across the tube, which produces a pressure gradient in the tube cross section [39]. This pressure gradient yields a so-called *secondary flow* -- a pair of symmetrical recirculation patterns superimposed on the main flow. A schematic diagram of the secondary flow in a helically coiled tube for single phase flow is given in Figure 1.2.

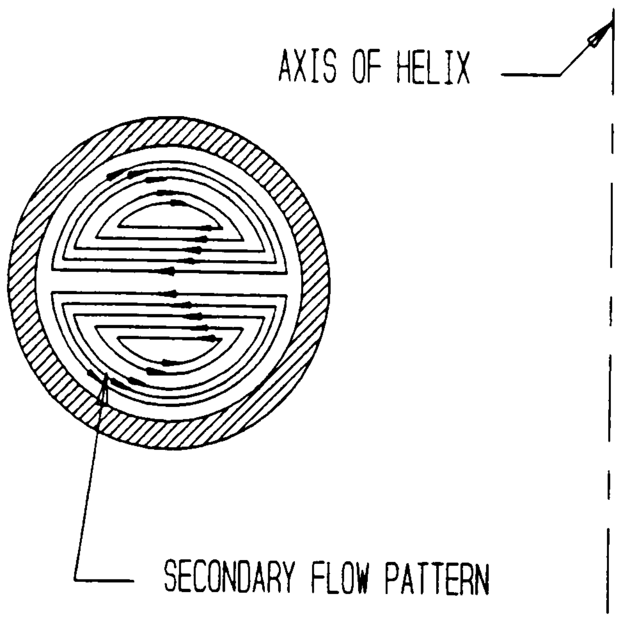

Figure 1.2 Schematic diagram of the secondary flow in a helically coiled tube for single phase flow

Because of the complicated spatial distribution of two-phase flow, an attempt to schematically depict the secondary flow for two-phase flow in a coil is extremely difficult. No such accurate visualization or characterization have yet been seen in the literature. This makes the theoretical analysis of two-phase flow dynamics in coiled tubes very difficult.

Another factor which makes the study of two-phase flow in helical or spiral coils complicated is that their geometrical orientations and flow directions make a great difference in flow dynamics. The following diagram (Figure 1.3) summarizes the applicable combinations of flow directions and geometrical orientations for helical and spiral coils. For a helical coil, its orientation is described with respect to the orientation of its axis. For example, vertical flow in a helical coil indicates that the axis of the helix

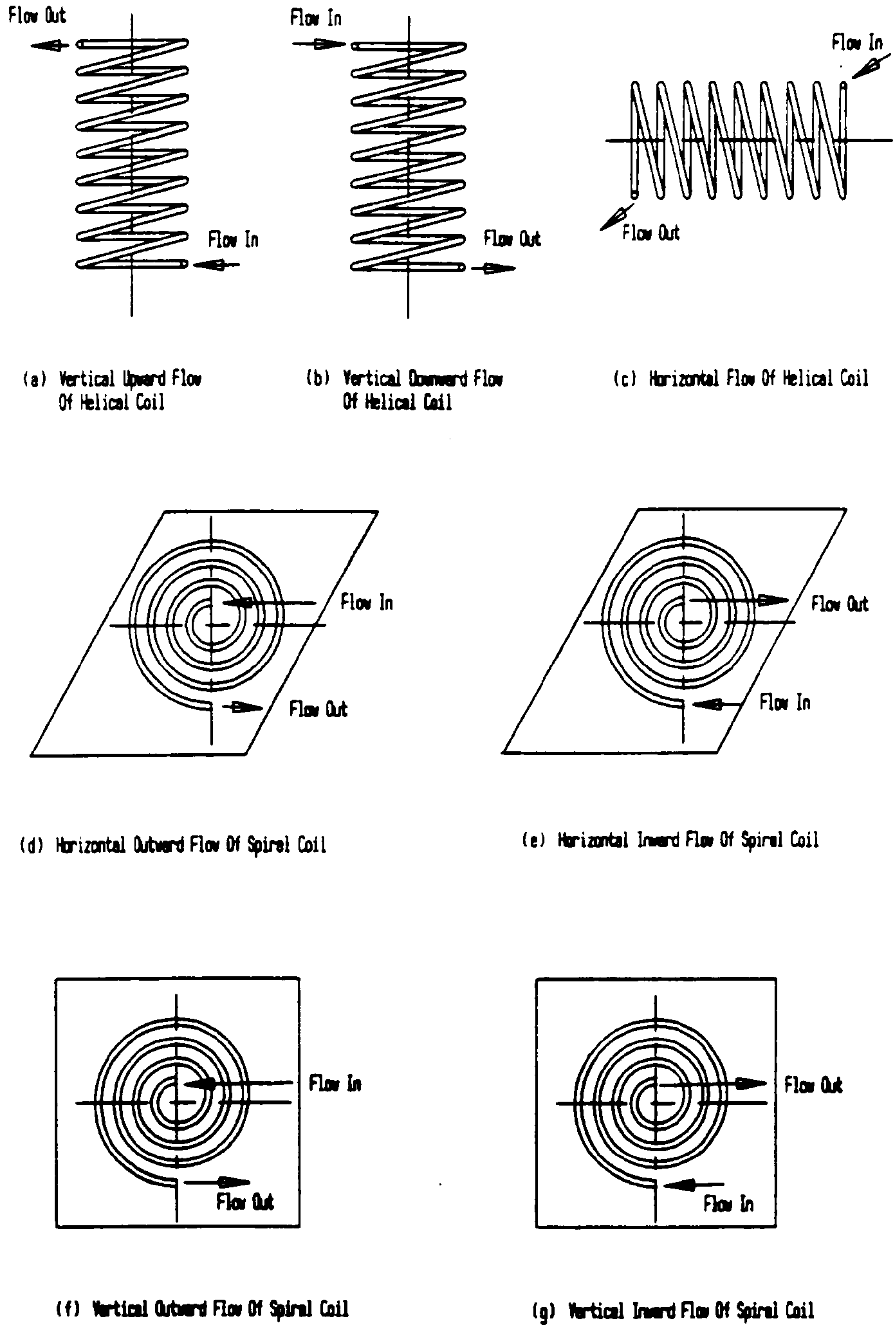

Figure 1.3 Combinations of flow directions and geometrical orientations for helical and spiral coils

is oriented vertically. Similarly, for horizontal flow, the axis is oriented horizontally (see Figure 1.3 (a),(b),(c)). However, the orientational characterization of a spiral coil is described in terms of the plane of the spiral, so that horizontal flow for a spiral coil means that the coil lies in a horizontal plane. In helical upward flow the fluids flow into the coil from the bottom and out from the top, whereas in helical downward flow the fluids flow into the coil from the top and exit from the bottom. Inward flow for a spiral coil means that the fluid flows in at the largest outer coil diameter and exits out of the smallest inner coil turn in the center [41]. And, outward flow indicates the opposite flow direction (see Figure 1.3 (d),(e),(f),(g)).

1.2 Literature Review

Up to now, many papers have reported the characteristics of single phase flow and pressure drop in helical or spiral coils, but the work done in studying the properties of two-phase flow dynamics and pressure drop in coiled systems is very limited.

1.2.1 Single Phase Flow in Coils

Understanding the effects of centrifugal forces and secondary flow on the flow dynamics and pressure drop in single phase flow can aid in understanding the same matters in two-phase flow. Therefore, some discussion of past studies of single phase flow in coils is beneficial at this point.

Analysis of Flow Field

As early as 1927, Dean [22] first made a theoretical study of fully developed laminar single phase flow in a curved pipe. Using a perturbation method he tried to find the deviation of a velocity profile from the Poiseuille flow pattern by solving the Navier–Stokes equations. He pointed out that a secondary flow is set up (see Figure 1.2) due to centrifugal forces. Considerations of dynamic similarity resulted in a parameter $K = Re(r/R)^{1/2}$, which is now called the Dean number, and is denoted by De. However, his solution is applicable only in quite small Dean number regions ($De < 36$), and his formula for the resistance coefficient is not useful enough for practical use. His assumption of a parabolic velocity distribution was shown to be incorrect according to the experimental results by Williams [62], Ito [28] and others in ranges of practical importance. Their results showed that the greatest axial velocity occurs near the outside wall of the tube. Figure 1.4 [28] shows the distortion of the velocity distribution in single phase flow by the secondary flow effect.

Using the boundary layer assumptions, Barua [7] and Ito [28] theoretically analyzed laminar and turbulent flow in coils, and obtained relatively good agreement with experimental results. In 1965 and 1967, Mori and Nakayama [38,39] reported a complete theoretical analysis of the flow field for fully developed laminar and turbulent single phase flow in curved pipes and removed the incompleteness in Barua and Ito's analyses.

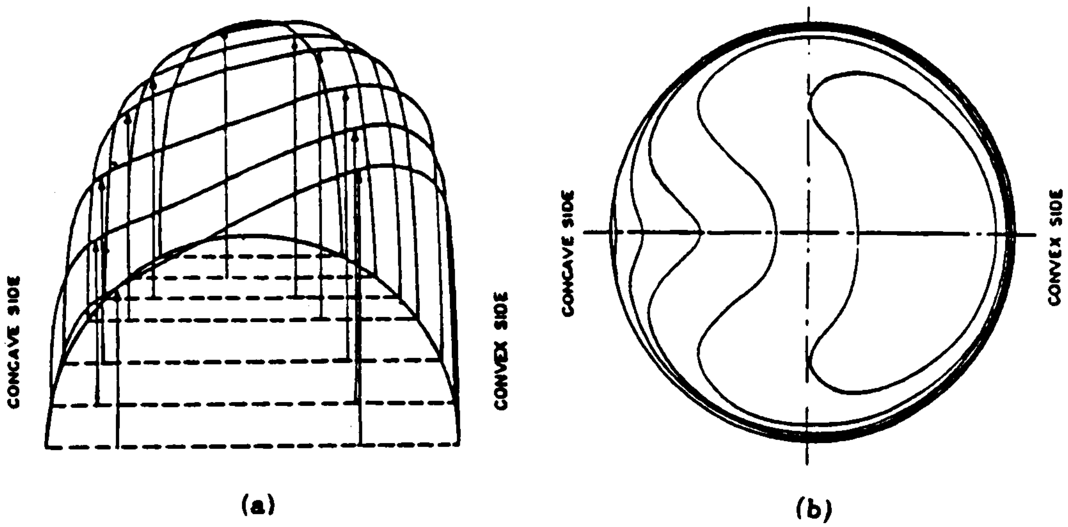

Figure 1.4 (a) Axial-velocity profile in a curved pipe
(b) Diagram showing lines of constant axial velocity

In Mori and Nakayama's analysis, the stress caused by the secondary flow is considered in addition to the viscous stress, and the flow field is divided into two regions -- a core region and a thin boundary layer region along the wall. The *core region* is the center region over the entire tube cross section except for the thin layer adjacent to the tube wall, where stresses caused by the secondary flow predominate, and viscous stress is ignored. The *boundary layer region* is the very thin layer close to the tube wall where both viscous stress and the stresses associated with the secondary flow can *not* be ignored. Using an approach analogous to that which results in the Reynolds stress in turbulent flow analyses, they introduced a relation between the velocities of secondary flow and the stresses caused by the secondary flow. Thus, through a force balance, and applying other basic laws such as the conservation of mass, they obtained the velocity distributions in curved tubes. The velocity components in the core region for both laminar and turbulent flows are expressed as follows:

$$u_1 = D^* \cos\psi \qquad (1.1a)$$

$$v_1 = -D^* \sin\psi \qquad (1.1b)$$

$$w_1 = A + (C/D^*)(\eta/r)\cos\psi \qquad (1.1c)$$

where the suffix 1 denotes the values in the core region, A is a constant, and C is a dimensionless pressure gradient introduced by them (which is constant when the flow is steady). These three core velocity distribution equations actually express the secondary flow in the core region by a uniform flow D^* toward the outer side of channel (see Figure 1.5). The dimensionless velocity of the uniform secondary flow in the core region is denoted by D^*, and the dimensionless thickness of the boundary layer is denoted by δ. Since the variation of δ with peripheral angle is found to be negligible, δ is replaced by its peripheral mean value δ_m. D^* and δ_m are obtained as follows:

$$D^* = \begin{cases} 0.9656\ De^{1/2} & \text{(laminar flow)} \quad (1.2) \\ 0.0852\ Re^{4/5}\ (r/R)^{1/10} & \text{(turbulent flow)} \quad (1.3) \end{cases}$$

$$\delta_m = \begin{cases} 4.6311\ De^{-1/2} & \text{(laminar flow)} \quad (1.4) \\ 0.2566\ [Re\ (r/R)^2]^{-1/5} & \text{(turbulent flow)} \quad (1.5) \end{cases}$$

It should be noted that in the laminar region D^* and δ_m are functions of only one parameter, De $(=Re(r/R)^{1/2})$; but in the turbulent region they are functions of both the Reynolds number and the curvature ratio, r/R. The velocity profiles and the two regions are depicted in Figure 1.5.

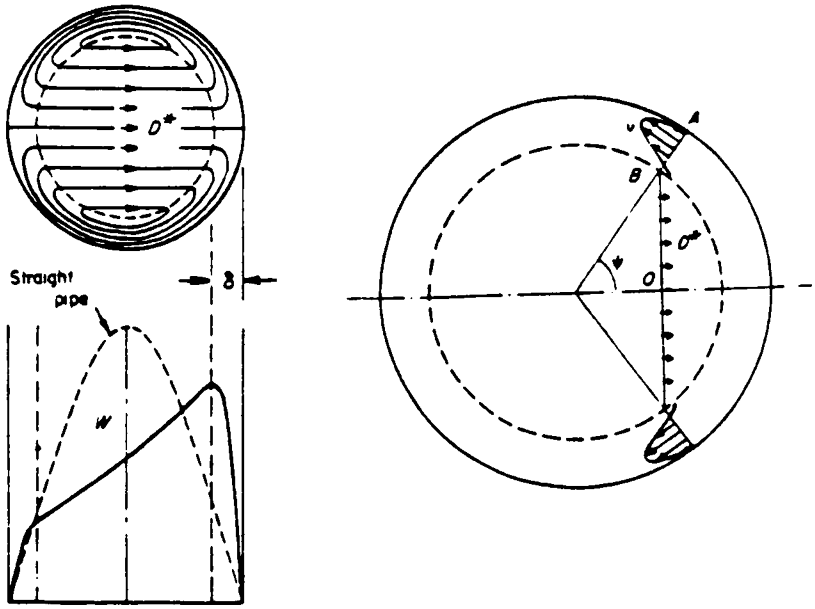

Figure 1.5 Velocity distributions and two flow regions in cross section for single phase flow in a curved pipe

Their analytical flow resistance formulae of f_c/f_s for fully developed laminar flow and for turbulent flow gave good agreement with both their experimental results and other previously successful empirical correlations (such as Ito's) which gives strong support to their theoretical analyses. Their successful analyses have proven that the additive flow resistance in a curved pipe is caused by stresses due to secondary flow. They further have shown that in the De range of practical interest (De > 36), the flow pattern of the secondary flow in the tube cross section is divided into two regions (see Figure 1.6) and differs from the homogeneous region (also see Figure 1.6). The homogeneous region was introduced by Dean [22] for small values of De (< 36), but this is outside the range of practical interest.

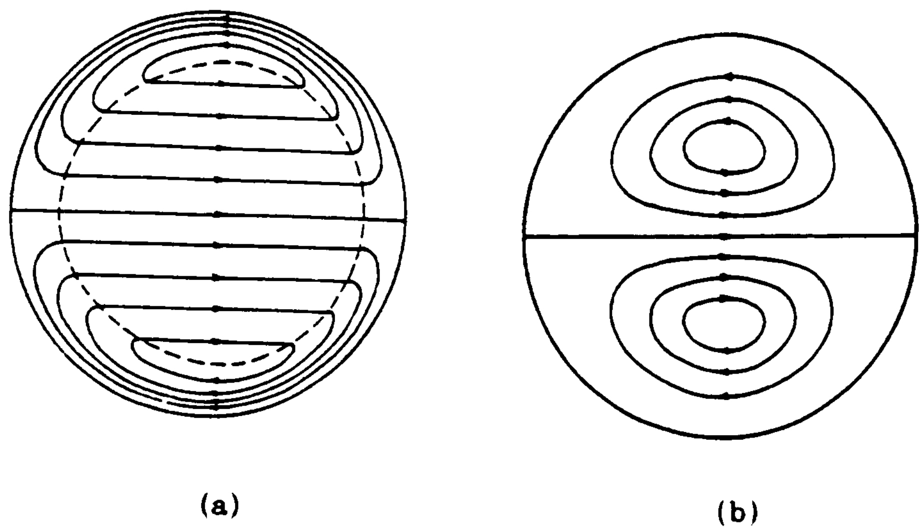

Figure 1.6 (a) Flow pattern of secondary flow for large De, by Mori [38]
(b) Flow pattern of secondary flow for small De, by Dean [22]

In the case of large De values, as shown in Figure 1.6(a), the secondary flow actually flows uniformly toward the outside wall in most parts of the cross section, except for a thin layer near the wall which flows back within the thin layer close to the tube wall.

Critical Reynolds Number

For turbulence to develop in a fluid flowing through a straight tube the inertia forces need to overcome the opposing viscous forces. For turbulence to develop in a fluid flowing through a coil the inertia forces need to overcome both the opposing centrifugal forces and the viscous forces. In another words, the secondary flow caused by the centrifugal forces has a stabilizing effect on laminar fluid flow. Thus, the critical Reynolds number at which the flow changes from laminar to turbulent in a coil is considerably higher than that in a straight tube. Its value is a function of the curvature ratio of the coil. The curvature ratio of a coil is defined as the ratio of the cross-sectional inside diameter of the tubing to the diameter of the coil into which the tubing is bent.

In 1959, Ito [28] summarized his experimental data together with the experimental results of previous investigators and presented the following empirical equations

$$Re_{crit} = 420[Re(d/D)^{0.5}]^{0.39} \tag{1.6}$$

and

$$Re_{crit} = 20{,}000(d/D)^{0.32}. \tag{1.7}$$

The second equation gives good agreement with experimental results in the range

$$15 < D/d < 860 .$$

For $D/d > 860$, the critical Reynolds number for a curved pipe practically coincides with that for a straight pipe. Later, in 1967, Mori and Nakayama [38,39] theoretically confirmed Ito's empirical equations. But Ito's equation is not strictly valid since it does not yield $Re_{crit} = 2100$ for a straight tube when $d/D = 0$. This pitfall was corrected by Srinivasan(1970) [49] with the empirical equation

$$Re_{crit} = 2100[1+12(d/D)^{0.5}] \tag{1.8}$$

which agrees well with his experimental results, Ito's, and others.

Therefore, the use of equation (1.8) is preferred for single phase flow inside curved pipes and helically coiled tubes.

For a fluid flowing in a spiral coil, the fluid does not have a single critical Reynolds number because the curvature ratio varies along the axis of the spiral flow channel. In terms of equation (1.8), Srinivasan [49] presented the following equations for spiral coils:

$$(Re_{crit})_{min} = 2100[1+12(d/D_{max})^{0.5}] \tag{1.9a}$$

and

$$(Re_{crit})_{max} = 2100[1+12(d/D_{min})^{0.5}]. \tag{1.9b}$$

Equation (1.9a) gives the critical Reynolds number below which the flow in a spiral is completely laminar, while equation (1.9b) gives the critical Reynolds number above which the flow is completely turbulent. However, Equations (1.9a) and (1.9b) fit the experimental data obtained by Srinivasan [49] only very approximately.

Frictional Pressure Drop

As a result of secondary flow, the pressure drop along a coiled tube is larger than that in a straight tube at the same flow conditions. The pressure drop in the coils can be obtained from the equation for fluid flow through a straight tube after replacing the Fanning friction factor f by f_c, as follows:

$$\Delta P = 4f_c \frac{L}{d} \frac{1}{2g_c} \rho v^2 \tag{1.10}$$

1) Helical Coil

Laminar Flow

For laminar flow through bends and helically coiled tubes a number of both experimentally and theoretically based equations have been introduced in the literature [28,37,38,49] to calculate the value of the friction factor f_c. They all are in good agreement with the experiment data obtained but have at least one of the following disadvantages:

— the formulae are only applicable in a limited range of Dean numbers,

— they do not satisfy the boundary condition $f_c \rightarrow f_s$ if $De \rightarrow 0$.

Hart et al (1988) [26] proposed the following empirical correlation, which does not have the above two limitations and is in good agreement with the correlations of the previous researchers:

$$f_c = f_s\{1 + [0.090De^{1.5}/(70 + De)]\} \qquad (1.11)$$

where $f_s = 16/Re$. This correlation covers the whole domain $0 < Re < Re_{crit}$ in which Re_{crit} can be obtained from eq. (1.8). When $Re > Re_{crit}$, turbulent flow occurs.

From eq. (1.11) we can see that for laminar flow the ratio f_c/f_s of the friction factor is only a function of the Dean number, De.

Turbulent Flow

For turbulent flow, a correlation which is valid for all values of De and $Re \geq Re_{crit}$ does not appear to have been seen in the literature to date. Five of the correlations that are often used for curved tubes or helical coils are from:

— White (1932) [61]:

$$f_c = f_s + 0.01(d/D)^{1/2} \qquad (1.12)$$

for $Re_{crit} < Re < 2\times10^5$ and

$$f_s = 0.07725/[\log_{10}(Re/7)]^2 \quad (1.12a)$$

— Ito (1959) [28]:

$$4f_c(D/d)^{1/2} = 0.029 + 0.304[Re(d/D)^2]^{-0.25} \quad (1.13)$$

for $0.034 < Re(d/D)^2 < 300$. And

$$f_c/f_s = 1.00[Re(d/D)^2]^{1/20} \quad (1.14)$$

for $Re(d/D)^2 > 6$, where

$$f_s = 0.079Re^{-0.25}. \quad (1.14a)$$

Below 0.034 the friction factor f_c practically coincides with f_s.

— Srinivasan (1970) [49]:

$$f_c = 0.084/[Re(D/d)^{0.5}]^{0.2} \quad (1.15)$$

for $De_{crit} < De < 14{,}000$ and $0.0097 < d/D < 0.135$, in which $De_{crit} = Re_{crit}(d/D)^{1/2}$ from eqn.(1.8).

— Mishra (1979) [37]:

$$f_c = f_s + 0.0075(r/R_c)^{1/2} \quad (1.16)$$

for $4{,}500 < Re < 10^5$, $0.00289 < d/D < 0.15$, and $0 < p/D < 25.4$. The value of f_s in eqn.(1.16) can be calculated from eqn.(1.14a). R_c is the modified coil radius due to the effect of pitch in the helical coil (see the following eqn. (1.17)).

The above correlations all give good agreement with large numbers of experimental data in their applicable range. Furthermore, they yield very similar results [49]. Thus, each can be used in its applicable range.

It is interesting to notice that eqn.(1.16), obtained by Mishra [37] in 1979, is merely the same as eqn.(1.12) which White [61] presented nearly 50 years ago. Equation (1.16) is the only correlation covering a wide range of coil pitches for helically coiled tubes.

It should be mentioned that, unlike the case for the laminar flow region, f_c/f_s for the turbulent region is <u>not</u> a function of Dean number only, but is also a complicated function of Reynolds number Re and the curvature ration d/D. Also, f_c/f_s in the turbulent region is much less than f_c/f_s in the laminar region, which means that for single phase flow secondary flow has less effect on pressure drop when flow is turbulent than when flow is laminar.

Friction Factor Chart

By combining their equation (1.11) for the laminar domain and White's equation for the turbulent domain, Hart et al (1988) [26] introduced a friction chart for single-phase fluid flow through curved tubes or helical coils, which is presented as Figure 1.7.

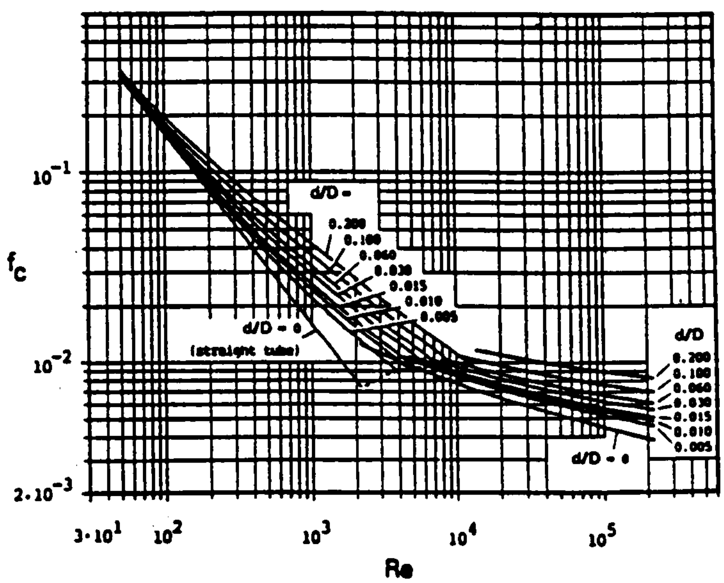

Figure 1.7 Friction factor chart for straight tubes and curved or helically coiled tubes

The value of the friction factor has been plotted as a function of the Reynolds number with d/D as a parameter. The graph is valid for $0 \le d/D < 0.2$ and $0 \le Re \le 2\times10^5$. The dotted line in Figure 1.7 represents values of f_c where $Re = Re_{crit}$ (Eqs. (1.8) and (1.11)).

Effect of Helix Pitch

When a helical coil has a finite pitch, its coil radius R is not the true radius of curvature. The derivation of the expression for the radius of curvature of a helix is presented by Thomas (1964) [52]. However, Mishra (1979) [37] found out, from his experimental study, that the pitch has a negligible effect on pressure drop if it is less than the diameter of the coil. He suggested that as long as the pitch is small with respect to helix circumference, the increase in radius of curvature due to finite pitch may be compensated to a high degree of approximation by replacing the radius of the coil R by R_c, where

$$R_c = R[1 + (p/2\pi R)^2] \tag{1.17}$$

Thus, the preceding equations for helical coils are valid when the pitch is small compared to the coil diameter. When helical coils have appreciable pitches they can be still valid by replacing the coil radius R by the radius of curvature of coil R_c.

2) Spiral Coil

Although the friction factors in curved tubes and helical coils have been widely studied, the study of friction factors in spiral coils is very limited.

A *spiral* can be considered as a two-dimensional helix with the coil diameter varying from point to point. This contrasts with a helical coil, which has a constant curvature and can be considered as a single 360 degree bend for each coil. Using this concept of a two-dimensional helix Srinivasan et al [49] integrated their empirical friction factor correlations for helical coils over the spiral coil diameter from D_{min} to D_{max}, and obtained the following empirical equations to predict friction factors in spiral coils:

$$f_c = a(n_2^{\,b} - n_1^{\,b})^c/[Re(2p/d)^{0.5}]^e \quad (1.18)$$

where $n_1 = D_{min}/2p$, $n_2 = D_{max}/2p$, and *a, b, c,* and *e* are given in Table 1.1.

Table 1.1 Constants in empirical equation (1.18) of friction factor in spiral coils by Srinivasan [49]

Region	Laminar	Transition	Turbulent
a	.31	.26	.0037
b	0.7	.75	0.9
c	2.0	1.0	1.5
e	0.6	0.5	0.2
$Re(2p/d)^{0.5}$, (limits)	500-20,000	20,000-40,000	40,000-150,000
2p/d, (limits)	7.3 - 15.5	7.3 - 15.5	7.3 - 15.5
Deviations, Max./Mean	9.0 % / 1.8 %	3.0 % / 1.1 %	2.0 % / .84 %

The dimensionless number, $Re(2p/d)^{0.5}$, in eqn.(1.18) is not as significant for determination of the friction factor f_c in spiral coils as is the dimensionless number, De, for f_c/f_s in helices, as may be seen, when plotting the experimental data of Srinivasan et al [49]. Establishing an appropriate dimensionless number for single phase flow friction factors in spirals is a task that must yet to be accomplished.

Entrance Region

Usually a straight pipe is joined to the inlet of a curved pipe or coil. Ito [28] reported that the influence of curvature extends upstream in a straight pipe thirty diameters from the curved pipe inlet. Also, he observed that the pressure drops in the curved pipe section become proportional to pipe length when

$$L \geq 4.7(d \times R)^{1/2} \tag{1.19}$$

where L is the axial length measured from the inlet of a curved pipe. These facts may be interpreted as evidence that (1) a secondary flow begins to develop fairly far upstream before the inlet of a curved pipe and (2) the secondary flow tends to accelerate development of the flow and temperature fields by its mixing effect. This greatly shortens the entrance length from the curved pipe inlet to the beginning of the fully developed region. Therefore, in the case of a pipe coiled several times, the influence of the entrance region on flow resistance and heat transfer is negligibly small [40]. In such cases, the preceding formulae can be used along almost the entire length of a coiled pipe.

1.2.2 Two-Phase Flow in Coils

Even not considering the secondary flow effects caused by the curvature of a flow channel, two-phase flow, even in a straight tube, has its inherent and complicated flow characteristics, evidenced by the diverse spatial configurations of the two phases (known as *flow patterns* or *flow regimes*). It should be mentioned that the term "flow pattern" rather than "flow regime" is used in the present study since "flow regime" is usually associated with the presence or absence of turbulence. Thus, in developing their two-phase friction multiplier, Lockhart & Martinelli (1949) [33] designated four two-phase flow regimes depending on whether none, one or both phases were turbulent. These flow regimes had no direct relation to the actual flow pattern.

Flow Behaviors Associated with Coil-Induced Centrifugal Forces

Obviously, the coil-induced centrifugal forces in two-phase flow will not result in a unique secondary flow pattern as in single phase flow. It may vary with different two-phase flow patterns.

Researchers working with annular two-phase flow in helically coiled tubes hypothesized that induced centrifugal forces should force the liquid onto the outside wall, as shown in Figure 1.8(b), rather than allowing it to flow in an annular fashion. The investigation of Owhadi et al [42] revealed that this hypothesis was inaccurate since they obtained higher dryout qualities with the coiled tubes than those normally found in straight tubes. Based on these findings Owhadi et al [42], Banerjee et al [3] and Crain [20] hypothesized that secondary flow similar to that shown in Figure 1.8(c) should exist in the gas core of two-phase mixtures flowing annularly inside helically coiled tubes. No investigations of the effects of centrifugal forces and secondary flow have yet been reported for flow patterns other than for the annular flow pattern.

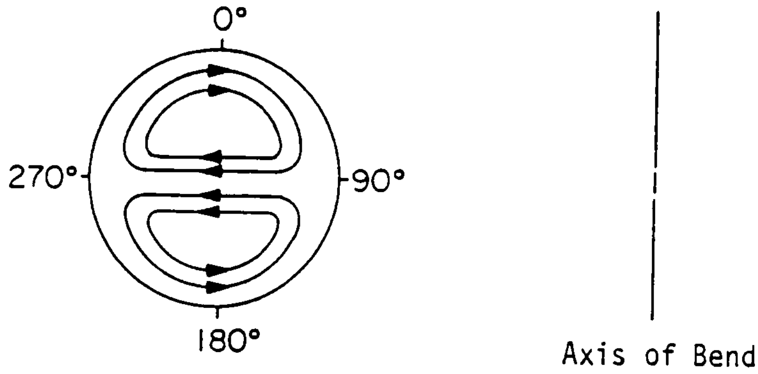

(a) Secondary Flow in Single Phase Fluid Flow

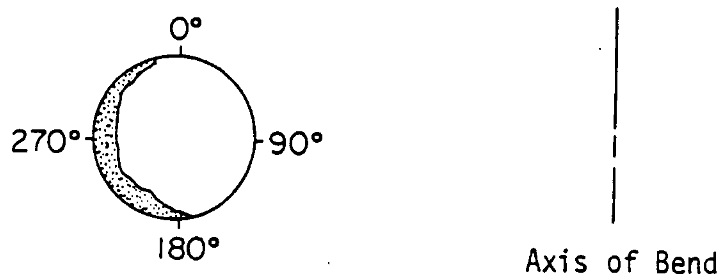

(b) Liquid Centrifuging in Two Phase Fluid Flow

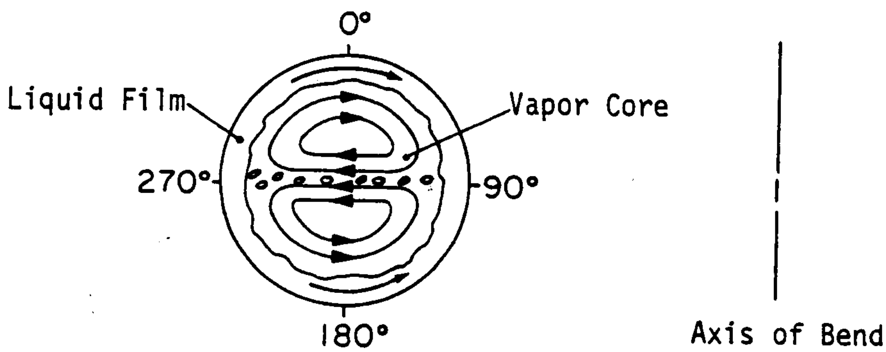

(c) Secondary Flow in Two Phase Annular Flow

Figure 1.8 Secondary Flow in Coiled Tubes

For some high quality flows in helically coiled tubes, a new phenomenon was reported by Banerjee *et al* (1967) [3]. In contrast to the hypothesis of many researchers, that induced centrifugal forces should force the liquid onto the outside wall, as shown in Figure 1.8(b), he found that at low liquid flow rates but high gas flow rates, the liquid phase travels along the inside of the tube wall facing the coil axis. In his experiments, at a constant, fairly low, water flow rate and low gas flow rates the liquid film in upward cocurrent flow in a helical coil was located mainly on the outside of the tube wall. However, as the gas velocity was further increased, the liquid film moved from this position, first into the neutral position and then into the inverted position (see Figure 1.9). As the gas velocity continued to increase, the film moved further and further

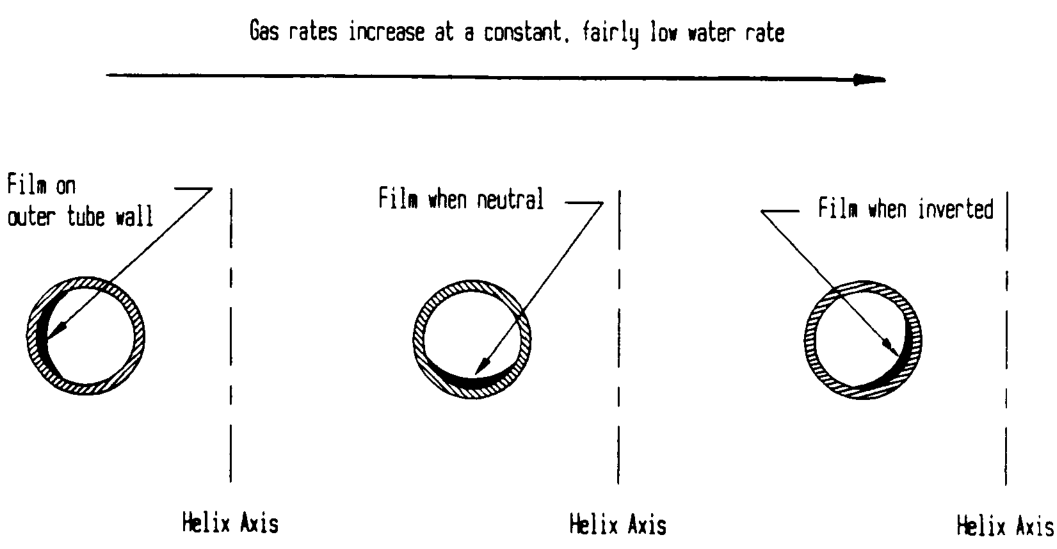

Figure 1.9 Film Inversion Phenomenon

up the inner wall of the tube. He called this phenomenon "*film inversion*". He attributed it to the fact that the magnitude of the slip velocity between the gas and liquid phases is so large that a much greater centrifugal force acts on the gas phase, in spite of its much lower density, and cause it to flow on the outer wall. Crain and Bell [20], on the other hand, have noted that the secondary flow in the gas core also helps in shearing the liquid from the outer wall to the inside wall of tube. Hart (1988) [26] studied this film inversion phenomenon experimentally and theoretically. Using a lumped system for each phase, and applying the conservation of momentum under steady-state conditions, while neglecting secondary flow, he obtained a semi-empirical equation to calculate the "inversion" angle for small liquid holdup values ($\epsilon_1 \leq 0.03$), which could be used to predict the film inversion when the value of the calculated angle is negative. However, it should be pointed out that this film inversion phenomenon only occurs at certain conditions, that is, at fairly low liquid flow rates and high gas flow rates, in which case the magnitude of the slip velocity makes film inversion possible. Otherwise, film inversion will not occur. For example, in some tests of Banerjee [3] at high gas flow rates but moderate liquid flow rates film inversion was not observed. For such liquid/vapor flow rates in the mist flow region, either no film inversion was apparent or an inversion point was difficult to observe, since the water film appeared to be continually broken and replenished at random positions and with high frequencies.

In summary, the combination of various two-phase flow patterns with the secondary flow phenomenon associated with coil-induced centrifugal forces makes it extremely difficult to perform a flow field analysis of two-phase flow in coiled tubes. A great amount of study is needed in order to understand the flow dynamics for two-phase flows in coiled tubes.

Flow Patterns and Flow Maps

Studies of flow patterns and flow maps have been of fundamental interest for investigators in the field of two-phase flow. One method of predicting a flow pattern is to use a specially developed *flow pattern map*, or simply, a *flow map*. A *flow map* is a two dimensional representation of the flow pattern existence domains. These domains are separated by their boundaries, which are called *transition lines* between two different flow patterns on each of its sides and are usually determined by empirical or semi-empirical methods.

1) Flow Patterns and Flow Maps in Straight Tubes:

In straight tubes, flow patterns are categorized according to the orientation of the tube, i.e. horizontal, vertical, or inclined.

Rouhani and Sohal(1983) [44] summarized two-phase flow pattern studies very well. Following are their summaries of the most commonly observed cocurrent two-phase flow patterns in channels with different orientations.

Horizontal Flow: Cocurrent flow of gas and liquid in horizontal channels may assume one or a fluctuating combination of the patterns depicted in Figure 1.10 [44]. In general most of flow patterns in horizontal channels show a non-symmetric pattern, which is due to the effect of gravity on fluids with different densities. Starting at the top in Figure 1.10, *stratified smooth flow* is usually observed at relatively low flow rates of both gas and liquid. As the vapor or gas flow rate is increased, the smooth interface of the liquid will become rippled and wavy. This pattern is referred to by many researchers as *stratified wavy flow.* If the liquid

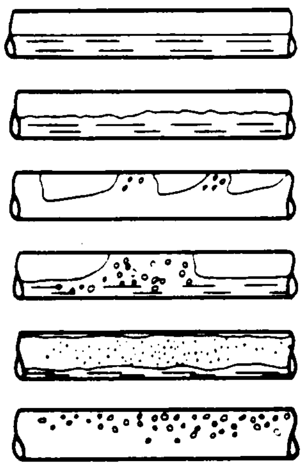

Figure 1.10 Schematics of horizontal flow patterns [44]

flow rate is increased, while the gas flow is maintained low, an intermittent flow pattern will develop in which gas pockets or plugs are entrapped in the main liquid flow. This is termed *plug flow.* If the flow rates of gas and liquid are increased together, a so-called *slug flow* pattern will develop. The main distinction between slug flow and plug flow is in the more pronounced nature of intermittent liquid masses separated by a larger gas bubble. As more clearly described by Choe et al [16], plug flow is used to describe the condition where elongated bubbles (plugs) of gas move through a tube filled with liquid; Slug flow describes the situation where packets of liquid (slugs) periodically move through an upper gas layer. With further increase in the gas flow rate alone the state of *annular flow* will develop in which the liquid flow occurs mostly within an annular zone, like a thick layer on the channel walls, while the gas flow will be confined to the central portion of the channel area. The semi-annular or annular mist pattern is a noticeable deviation from the intermittent natures of plug and slug flow patterns. The gas flow in the core of an annular flow may entrain a portion of the liquid phase in the form of droplets and, in some cases, the liquid film may also entrain some small bubbles. At relatively large liquid flow rates, with little gas flow, one would observe the so called *dispersed bubble flow pattern* in which the liquid is continuous, while the gas is in the dispersed form of scattered bubbles.

Another flow pattern classification has been suggested by several researchers [16] from a frictional pressure drop viewpoint. Their primary and secondary flow classifications are listed as follows:

(a) Homogeneous Flow

- Dispersed Flow

(b) Separated Flow

- Stratified Smooth Flow
- Stratified Wavy Flow

(c) Intermittent Flow

- Slug Flow
- Plug Flow

(d) Annular Flow

- Semi-annular Flow
- Mist-annular Flow

Vertical Upward Flow: In vertical upward flow, one may observe a variety of flow patterns which have similarities with those described for horizontal flow, with the exception of stratified flow. A flow pattern appearing in upward flow that is absent in horizontal flows is churn-turbulent flow. Generally speaking vertical two-phase flow patterns are more axisymmetrical for the obvious reason of the effect of gravity being parallel to the flow direction. Figure 1.11 [44] shows some of the most commonly observed two-phase flow patterns in vertical channels. At the left of Figure 1.11 is shown *bubble flow*, which will occur when a relatively small quantity of gas is mixed with moderate flow rate of liquid. Increasing the gas flow rate would lead to *plug flow*, which some observers call *Taylor bubble flow*. With a further increase in gas flow, or at higher elevations above the inlet to the vertical channel, where plug flow is generated, one may observe

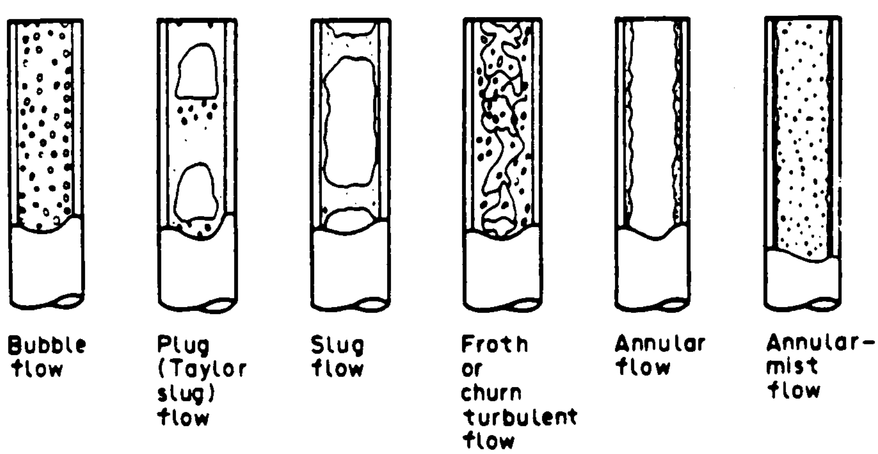

Figure 1.11 Schematics of vertical flow patterns [44]

slug flow, which consists of a regular train of very large bubbles. Each of these "slug" bubbles occupy almost the whole channel cross section except for a thin liquid layer on the wall; Their length is several times the channel diameter. An increase in both gas and liquid flows will lead to a frothy flow pattern that is called *churn-turbulent flow*. Relatively high gas flow rate with low liquid flow rate results in a *annular flow* pattern in which both gas and liquid flows are continuous. Very high gas flow rates or a high density gas flow will cause some of the liquid flow to be entrained as droplets carried with the continuous gas phase. This is called *annular-mist flow*.

Vertical Downward Flow: All of the flow patterns of upward flow may also appear in the downward flow situations.

Inclined Flow: Studies of flow patterns in inclined channels have been reported by some investigators [5,27]. The flow patterns for inclined flows seem to have the same patterns as in <u>vertical flow</u> except for the limitation or total suppression of the churn turbulent flow patterns [44].

For two-phase flows in straight tubes, numerous flow pattern maps have been presented in the literature over several decades that propose to predict the types of two-phase flow patterns that will exist in a flow channel given the individual flow rates of the phases. Weisman (1979) [58] summarized these studies very well. Among them, the Baker map [2], Taitel & Dukler [50] map, and Choe et al map [16] are the most widely used ones. It should be mentioned that although there are many flow pattern transition lines in a flow map, the transition to an annular flow pattern is of most interest and importance because of the good heat transfer rates and lesser instability in annular flow.

2) Flow Patterns and Flow Maps in Coiled Tubes:

While there have been extensive flow pattern studies for two-phase flow in straight tubes [6,16,27,50,51,58], the study of flow patterns in helical or spiral coils has, by contrast, been very limited both experimentally and theoretically.

Helical Coil Vertical Up- and Down-Flow: Visual studies by several investigators [3,8,13,43,46] have shown that the flow patterns observed in helical coil vertical up- and down-flow are similar to those observed in horizontal or near horizontal straight tubes, but with some minor modifications, such as the effect of the centrifugal forces on fluids. Boyce and Collier (1963) [8] attempted to predict the air-water two-phase flow patterns in helical coil vertical up-flow using Baker's flow map [2], but comparisons of their predictions with the experimental results were not good. An experimental investigation has been performed by Uddin (1988) [53], who developed a semi-empirical model (flow map) for air-water flow in *vertical upflow* helically coiled circular tubes. Chen et al(1987) [13] presented a semi-empirical flow map for helical vertical down-flow in a circular tube based, on their air-water experimental data. So far, they appear to be the only flow maps developed for helical coil vertical up- and down-flows, respectively.

Helical Coil Horizontal Flow: For two-phase flow in horizontal helical coils, only Guo et al(1988) [25] experimentally studied flow dynamics in horizontal helical coils for air-water two-phase flow. The flow patterns they observed are: unstable pulsed flow, intermittent flow, annular flow, and dispersed bubble flow. They proposed two semi-empirical correlations for the transitions of intermittent-to-annular flow and intermittent-to-dispersed bubble flow. However, the flow map and correlations they obtained were based only on their experimental data and were not modified for more general use. A need exists for developing a more general flow map for two-phase flow in horizontal helical coiled tubes.

The preceding flow maps for helical coiled tubes were all obtained for air-water two-phase flows; No flow map exists for other two-phase fluid mixtures in helically coiled tubes, nor for the flow in other cross-section flow channel shapes.

Spiral Coil: No publication was found in the literature for two-phase flow patterns and resulting flow maps for spiral tubes so far.

Two-Phase Frictional Pressure Drop

1) Two-Phase Frictional Pressure Drop in Straight Tubes:

Although there were numerous studies on this subject because of its practical value, the most commonly used correlations of two-phase frictional pressure drop by researchers are still the classical ones, such as Lockhart-Martinelli correlation and homogeneous model.

2) Two-Phase Frictional Pressure Drop in Coiled Tubes:

Helical Coil Vertical Up- and Down-Flow: In 1967 Banerjee [3] experimentally compared the pressure drop in vertical upward helical air-water flow with that in the upstream horizontal section of the same length and flow rates. The flow patterns were stratified and annular flow, the latter occurring at high gas flow rates. He found out that the pressure drop in a helical coil is about the same as in an equivalent horizontal section. Hence, he speculated that secondary flow is probably unimportant in increasing the pressure drop in vertical upward helical coil two-phase cocurrent flow. Boyce et al(1963) [8], Owhadi et al(1968) [42], Akagawa et al(1971) [1], and Kasturi et al (1972) [32] tried to use the straight tube Lockhart-Martinelli pressure drop model to predict the experimental pressure drop for air-water, steam-water, and air-water+solutions systems in helical vertical up-flow. However, the predictions for their test data were very approximate.

Hart et al (1988) [26] have generated curves for friction factors for use in pressure drop calculations in helical coiled tubes, for conditions of a small liquid holdup range($\epsilon_l \leq .003$), which almost extends within the dispersed droplet flow region. His experimental results of air-water and air-water+glycol(25 w%) systems shows that the increase(in comparison with single-phase flow) in the pressure gradient(about 30%) of a gas-liquid flow($\epsilon_l \leq .003$) in a vertical up-flow helically coiled tube is much lower than the increase in the pressure gradient value measured in a gas-liquid flow in a horizontally straight pipe(about 70%). Much additional similar work needs to be done to study more flow pattern regions, and especially for the annular flow region.

Helical Coil Horizontal Flow: Concerning the systematic investigation of two-phase pressure drop in helical coil horizontal flow, no report has been published to the author's knowledge.

Spiral Coil: Niggemann et al (1985) [41] obtained experimental data of temperatures and pressure drop in their square tube (.5"x.5") spiral coil heat exchanger with R-114 liquid/vapor mixture and compared with their pressure drop data with Chisholm's [15] two-phase annular flow frictional pressure drop correlation in bends, which under-predicted their test results. No other experimental or analytical studies on two-phase frictional pressure drop in spiral coils appear in the literature to the writer's knowledge.

Based on a survey of literature published from 1962 to 1990, the status of two-phase flow patterns and frictional pressure drop study in helical and spiral coils could be summarized as follows:

- Flow patterns, flow behaviors, and flow transitions in different helical coil flow and spiral coil flow situations have not been investigated systematically. Experimental studies are needed to obtain such understanding.
- No flow map has been proposed for helical and spiral coils, except for Uddin's and Chen et al's semi-empirical maps for helical coil vertical upward and downward flows in circular tubes, respectively, which apply only to a limited range of flow conditions of air-water two-phase system.
- Because of the lack of experimental data, satisfactory correlations to predict frictional pressure drop in helical and spiral coils have not been seen in the literature. Both experimental and analytical studies are needed.
- No literature was found dealing with two-phase flow in helical coils with non-circular cross sections.
- No reports were found dealing with flow pattern and pressure drop studies on two-phase fluids systems other than air-water, steam-water, and air-water+solution systems.

1.3 Objectives and Scope of Study

As seen in the previous literature review, there is limited information available dealing with the behavior of two-phase flow in coils, especially the flow field associated with secondary flow phenomenon. Flow pattern studies are in an early stage and experimental pressure drop data are few and limited for some specific conditions. Theoretical analyses have not been made due to the difficulties in describing the flow field. Because of the very limited studies in coiled tubes, experimental studies are very much needed to obtain both flow pattern and pressure drop data. The present study is intended to develop a better understanding of two-phase flow behavior in helical and spiral coils, and specifically, to study flow patterns, their transitions and pressure drop characteristics in such coils.

This study is an experimental investigation of two-phase gas-liquid flow in both helical and spiral coiled tubes. The general intent is to develop criteria for establishing the nature of the flow dynamics (flow pattern) with special emphasis on annular flow. In addition, the study is to determine the magnitude of the pressure drop in such configurations over a range of flow rates and fluid properties.

In practical systems of interest, the working fluids are likely to be refrigerants 12 and 114 [11]. In the study proposed here, the working fluids are an air-water mixture and refrigerant 113. The use of air-water and R-113 fluids is of value in that the fluid viscosities, liquid surface tension and liquid/vapor densities span a range of conditions that can be valuable in developing more generalized predictions of flow patterns and two-phase pressure drop. Furthermore, the properties of R-113 are reasonably close to those of R-12 and R-114. Thus, while the earlier argon-flourinent studies [17] simulated the latter refrigerants, it was nevertheless a two-component two-phase flow, rather than the flow of a liquid and its own vapor.

Five test sections, namely, helical coils having a circular cross-section and three with rectangular cross-sections of different aspect ratios, along with a circular cross-section spiral tube, are tested using air-water and R-113 fluids over a range of liquid flow rates and qualities. Three configurations of horizontal, vertical-upward and vertical-downward flow for helical coils are tested, and direct visual observation and video photography are used so as to permit flow pattern identification over a range of flow conditions. Measurements of temperature, pressure, flow rates and pressure drop are made.

Data relative to flow pattern identification as a function of flow rates, fluid properties, channel geometry and channel curvature are plotted and compared with some existing flow pattern maps, as in [11]. The determination of how fluid properties, channel cross-section and test section orientation affect the flow dynamics is studied. Of practical interest is the establishment of conditions under which the transition to annular flow occurs, accounting for the range of fluid dynamics, fluid properties and channel geometries.

Pressure drop measurements are compared with predictions of several models appearing in the literature, as in [11,12]. An attempt is made to utilize the measured results to develop an annular flow model for predicting pressure drop in coiled geometries.

CHAPTER 2

EXPERIMENTAL PROGRAM

2.1 Description of Experimental Apparatus

2.1.1 Description of Test Sections

Five test sections were utilized in this study. Four helically coiled flow channels, each of different cross-section, and one spiral coil test section of circular cross-section were studied.

The first helical coil test section (No. 0) was made of a circular glass tube (0.325" I.D.), while the remaining three helical coil test sections (No.1-3), were of rectangular cross-section flow channels and were fabricated from plexiglass. The rectangular cross-section channels were machined into the outer surface of a solid plexiglass cylinder of 3.325" diameter. Each cylinder was then covered with a snug-fit outer plexiglass tube of 4-1/4" outside diameter. The hydraulic diameter of these three rectangular cross-section channels were designed to be the same as that of the circular cross-section glass tube, which is 0.325". Therefore, it is possible to make comparisons on the basis of equal hydraulic diameters. Their aspect ratios, H/W, were approximately 0.677, 1, and 1.5 respectively. In all of the three rectangular cross-section helical coil channels, a short circular cross-section tube was inserted into the test piece body, so that a short transition section existed between the circular cross-section insert and the rectangular cross-section helical coil flow channel. The coiled test sections were then able to be connected into the remainder of the experimental test loop through these short circular connection tubes. All of the four helical coils had the same pitch of 1" and a helix-angle of 8°. The detailed dimensions of the four helical coil test sections (No.0-3) are illustrated in Figure 2.1(a) and Table 2.1.

The spiral coil test section (No.4) was made of circular cross-section glass tubing with the same inner diameter (0.325") as the helical coil circular cross-section test section. The coil pitch of the spiral coil was almost constant, such as in an Archimedean spiral. The dimensions of this spiral coil test section are illustrated in Figure 2.1(b) and Table 2.1. At the inlet and the outlet ends of the coiled tube are short, straight lengths of straight tube, tangent to each end of the coil and inclined out of the coil plane, which permitted the connection of the spiral coil to the main circulation loop.

Photographs of the various test sections are shown in Figure 2.2, along with a reference scale to give the reader a better concept of the size of test sections investigated.

2.1.2 Working Fluids

In potential practical applications (heat exchangers), the working fluids are likely to be refrigerant fluids. For the present study, two kinds of two-phase working fluids, an air-water mixture and refrigerant 113 (R-113) liquid/vapor mixture, were tested in two different experimental apparatus. In this way, one can compare how fluid properties influence the behavior of flow dynamics and two-phase pressure drop in helical and

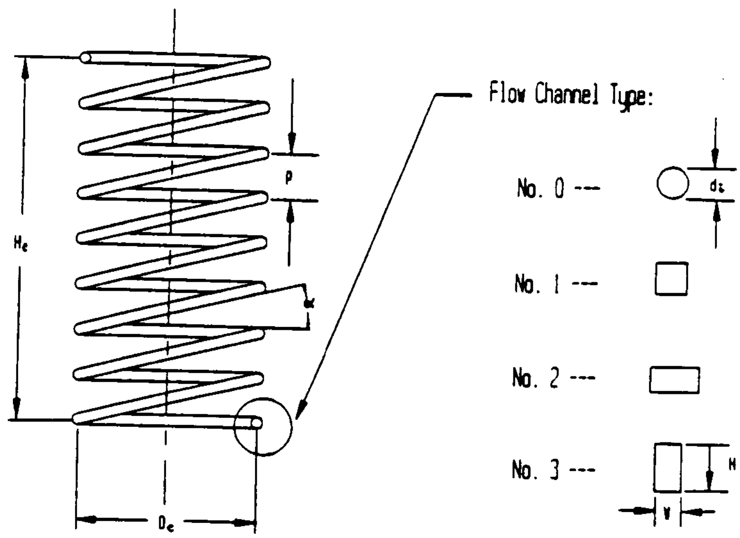

(a) Helical Coil Test Sections

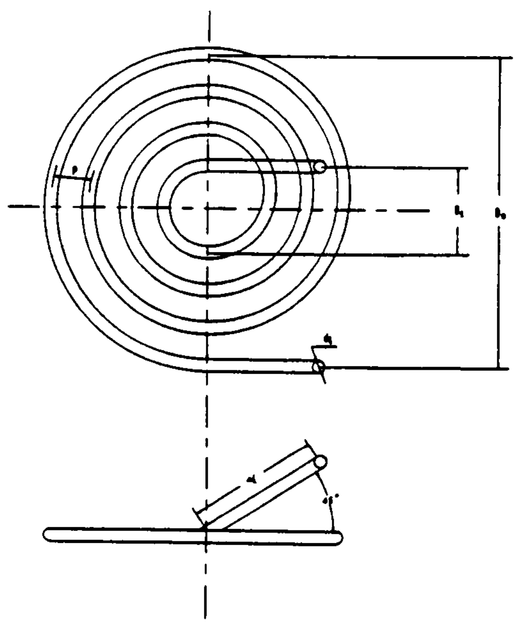

(b) Spiral Coil Test Section

Figure 2.1 Schematic Diagram of Test Sections

Table 2.1 Dimensions of Five Test Sections

Coil Type	Helical			
Test Section ID No.	No. 0	No. 1	No. 2	No. 3
Tube Cross-Section Shape	Circular	Rectangular		
Tube Inner Dia., d_i (or hydraulic d_h)	0.325" (8.255mm)	0.3416" (8.677mm)	0.325"	0.325"
Rect. Cross-Section Aspect Ratio H/W, Height H, Width W		H/W ≈ 1.0 H= 0.36" W= 0.325"	H/W=0.667 H= 0.271" W= 0.406"	H/W=1.5 H=0.406" W=0.271"
Tube Length, L_c	1.590 m (5.216 ft)	2.0101 m (6.595 ft)	2.0358 m (6.6791 ft)	2.2754 m (7.4652 ft)
Coil Diameter, D_c	7.5 cm	7.6 cm	7.2 cm	7.8 cm
Helical Dia. Ratio, D/d_i (or D/d_h)	9.085	8.759	8.722	9.449
Helixangle, α	8^o	8^o	8^o	8^o
Helix height, H_c	16 cm	21.3 cm	22.5 cm	23.2 cm
Helix Pitch, p	1"	1"	1"	1"
Coil Type	Spiral			
Test Section ID No.	No. 4			
Tube Cross-Section Shape	Circular			
Tube Inner Dia., d_i	0.325" (8.255 mm)			
Tube Length, L_c	1.49 m (4.8885 ft)			
Inner Coil Dia., D_1	5.5 cm			
Outer Coil Dia., D_2	16.0 cm			
Length of Straight Inlet/Outlet Section, ΔL_0	6 cm			

(a) Helical Coil Test Sections

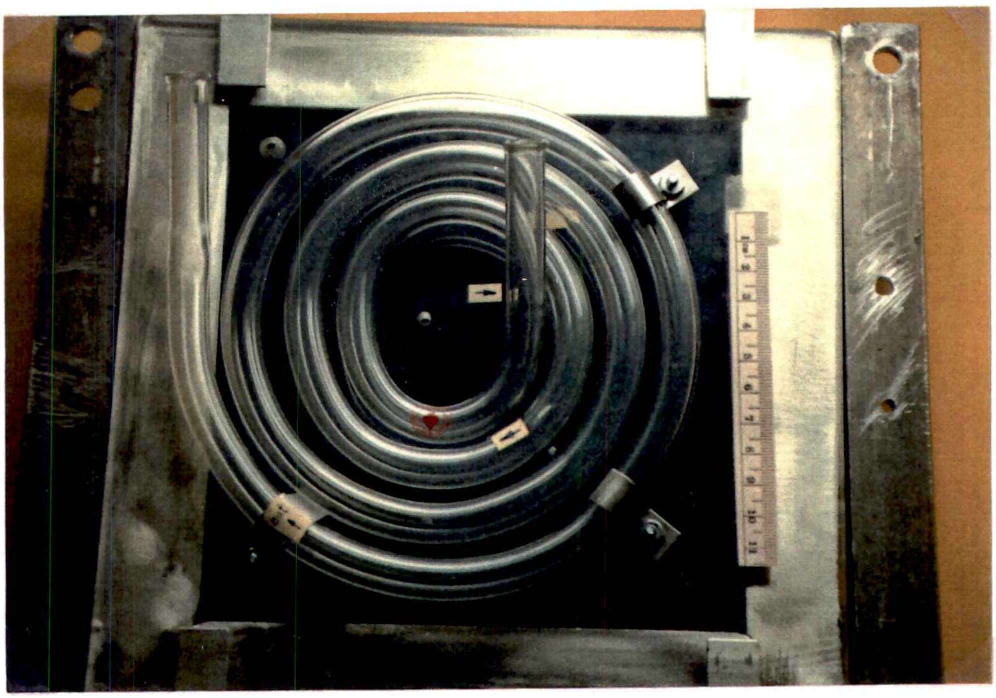

(b) Spiral Coil Test Section

Figure 2.2 Photo Illustration of Test Sections spiral coils.

2.1.3 Experimental Loops

In order to test two kinds of working fluids, two sets of experimental apparatus were used. An existing two-phase flow loop, in one of the Mechanical and Aerospace Engineering Department laboratories, was used to generate a refrigerant-113 (R-113) liquid/vapor two-phase flow over a range of thermodynamic qualities, as input to the helical or spiral coiled test sections. An apparatus for generating an air-water two-phase flow was provided by the Sundstrand Corporation and was located in the same laboratory.

(1) Air-Water Two-Phase Flow Experiment Loop

The air-water two-phase flow apparatus consisted of an air supply line, a water circulating loop, a mixing tee, a two-phase line along with the coil test section, remote flow control valves, and temperature and pressure sensors. A schematic diagram of the apparatus is depicted in Figure 2.3.

Air was taken from the laboratory compressed air supply line through a pressure regulator. The flow rate of air was measured by a venturi meter before the mixing tee. Water was pumped from a reservoir tank and filtered before entering the mixing tee. Its flow rate was measured by a turbine flow meter before being mixed with the air flow. A short transparent tube was added in the water line before the mixing tee to assure that no air bubbles existed in the water line, in order to insure obtaining accurate water flow rates. Within the mixing tee, air was mixed

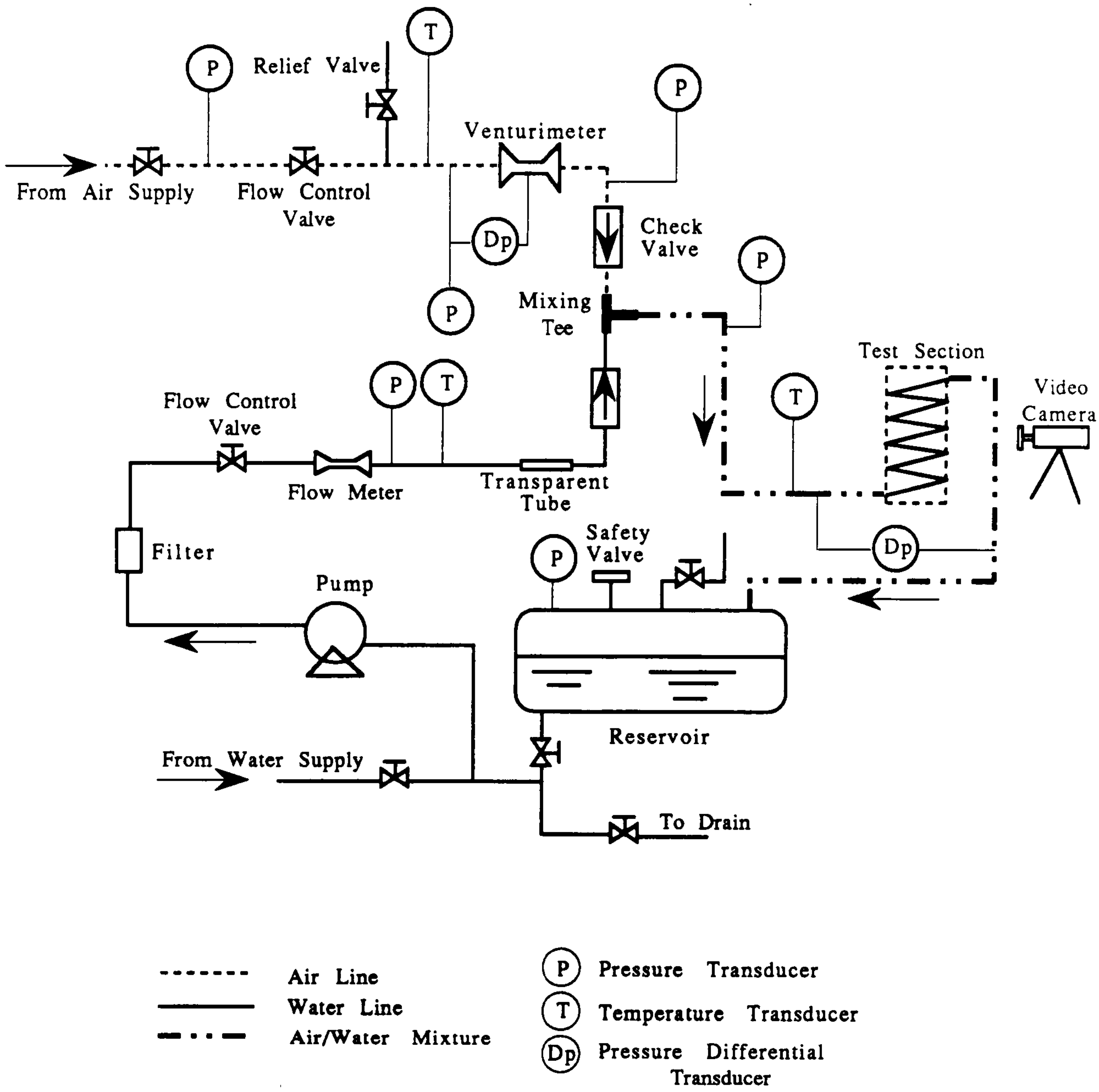

Figure 2.3 Schematic Diagram of Air-Water Two-Phase Flow Experimental Loop

with water to form the air-water two-phase mixture entering the test section. The total pressure drop across the test section was measured by a differential pressure transducer. The pressure and temperature of the two-phase flow were also recorded before entering the test sections. After the test section the two-phase mixture was released into a reservoir, where air was released into the atmosphere, while the water was recirculated by a pump into the water inlet line again. The air and water flows were controlled and regulated by two Fuji Koki electronic linear control valves to maintain different air and water flow rate combinations for the different test conditions.

All the measurement output signals were connected to a 3497A model Hewlett Packard data acquisition and control unit, except for the frequency of the water turbine flow meter, which was entered by hand. An HP desk top computer, connected to this data acquisition unit, was also used to write a BASIC computer program to obtain these measurements. All instruments were calibrated by the Sundstrand Corporation and were checked for selected points before each test.

(2) R-113 Two-Phase Flow Experiment Loop

A schematic diagram of the test loop is depicted in Figure 2.4. The working fluid, refrigerant-113, was circulated by a belt-driven six-vane positive pump, operated at 200 rpm. To heat the R-113 to its saturation temperature and different qualities, a 6 ft long, 1" inner diameter horizontal stainless steel tube was electrically heated with a 25 KVA adjustable DC power supply. To cool the working fluid to its original temperature, the test loop employs a single pass vertical shell and tube

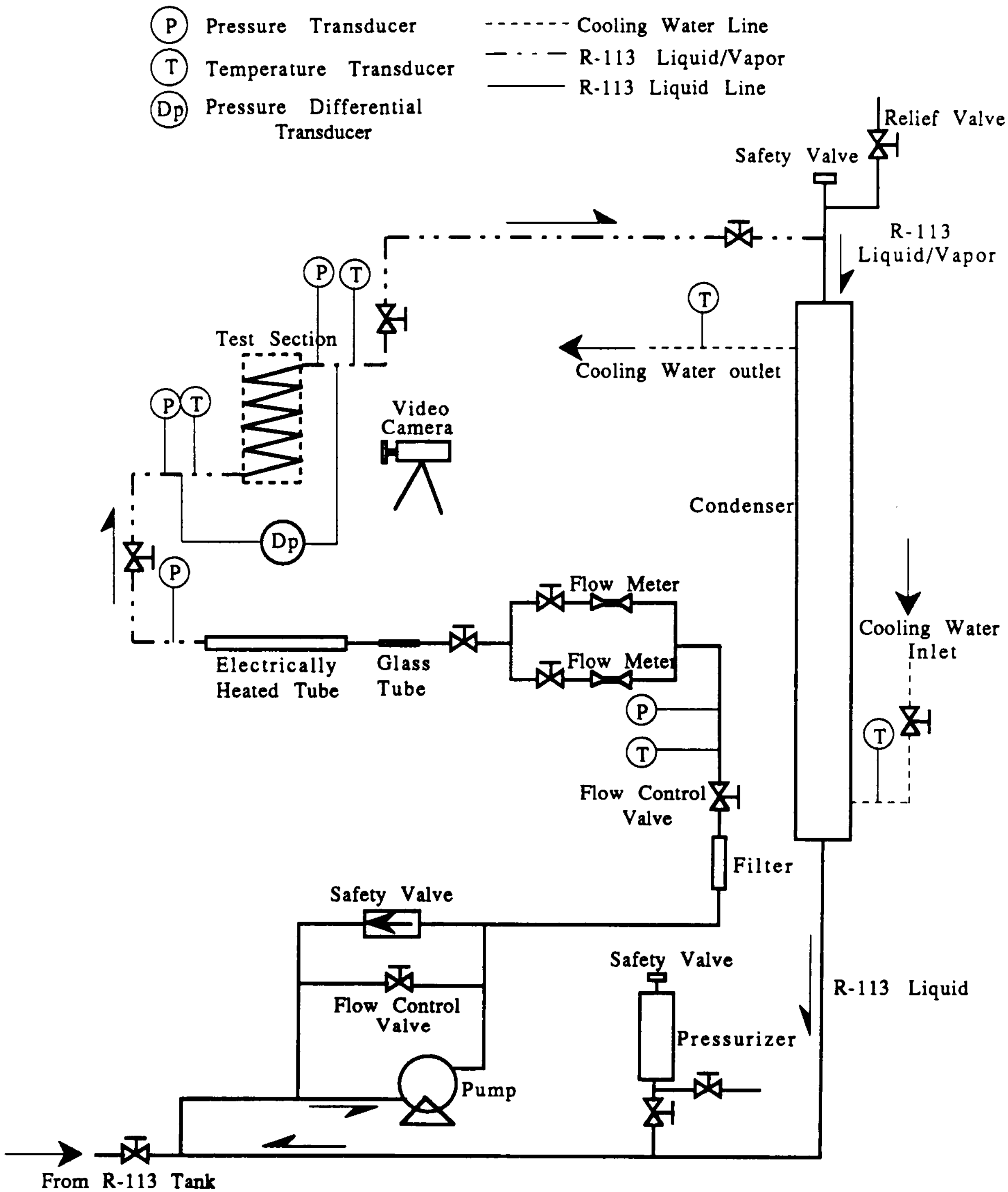

Figure 2.4 Schematic Diagram of R-113 Two-Phase Flow Experimental Loop

condenser, which used tap water as the cooling water supply.

In order to obtain accurate measurements of vapor phase quality, a sight glass tube was added to the loop just before the stainless steel heating tube. In this way, it was able to observe if any uncondensed vapor bubbles were present beyond the condenser that would enter the stainless steel resistance heater tube and cause inaccurate calculations of vapor quality. The loop was insulated from the beginning of the electrical heater to a point far beyond the outlet of the test section, except for a small window area in the test section itself, intended for video camera recordings. This insulation provided a quasi-adiabatic condition for the R-113 saturated two-phase mixture (generated along the electric heater tube length) flowing from just beyond the electrically heated tube to the outlet of the test section. The test data showed that for most of the data the temperature drop from inlet to the outlet of the test sections was less than 1 ^{o}F. In only a few cases temperature differences of about 2 ^{o}F were measured. From a sample calculation of the test data, the saturation temperature drop across the test section due to a typical value of pressure drop occurring across the test section is in the 1 ^{o}F range (1.34 ^{o}F). Therefore, it can be assumed that the two-phase flow in the test section was essentially adiabatic and that the two-phase quality calculated from an energy balance on the electric heater was maintained essentially constant (unchanged) throughout the test section.

There were two flow meters in the test loop, a Fisher Porter turbine flow meter for high flow rates of 1.6 - 24 gpm and a Foxboro turbine flowmeter for low flow rates of .23 - 2 gpm. In the present study, only the Foxboro turbine flowmeter was used since the flow rates which occurred were within its measurement range.

The same HP data acquisition and computer units as for the air-water tests were used to obtain all the measurement data output except the liquid phase flow rate. The liquid flow rate was measured by its frequency output. This frequency value was then input into the computer by hand, which then converted this value into a corresponding flow rate.

2.2 Methodology and Procedures

2.2.1 Air-Water Two-Phase Flow Test

The apparatus depicted schematically in Figure 2.3 was first filled with water and circulated about the loop to flush out any contaminants before draining, refilling the loop and repeating the process until the loop was clean.

After this flushing/cleaning procedure, water was circulated at a predetermined, constant mass flow rate. The air flow rate was adjusted so as to create a slug flow condition within the coiled test section that was determined to be slightly below the onset of an annular flow condition. After making videotapes and pressure drop measurements of this flow condition, the gas flow was increased carefully up to the point at which it was judged that a hydrodynamically defined annular flow just existed (a continuous liquid film existing about the entire tube periphery). This was designated as the transition condition from the slug to annular flow.

The air flow was increased again to a level somewhat above this transition condition, which assured a definite annular flow condition. Additional operating conditions spanning the highest and lowest operating points (in terms of gas quality) were attained, where additional measurements of pressure differential and flow observations were made.

The air flow was then stopped, the liquid flow rate adjusted to the next higher predesignated flow rate, and a range of air flow rates was spanned so as to define the transition condition at that flow rate. Pressure drop data was obtained over the range of gas phase qualities experienced.

These procedures were repeated for each of the five test sections and their selected orientations and flow directions.

2.2.2 R-113 Two-Phase Flow Test

For the refrigerant tests the general procedure was similar to that of the air-water tests. However, the vapor phase flow was generated by means of an electrically heated circular tube preceding the coiled test section(s), as depicted in the schematic diagram of Figure 2.4. At the beginning of a test run, the flow loop was completely filled with R-113 liquid, and circulated through it. Power was applied to the electrically heated tube, generating vapor. Vapor was vented through a release valve at the uppermost part of the loop to insure that any trapped air would be eventually discharged from the system. After so evacuating air from the system, the R-113 liquid flow was adjusted to a fixed preset flow rate (total flow rate of the R-113 two-phase mixture when exiting the electric heater), and power applied to generate a predetermined vapor quality, resulting in a slug flow condition, just below an annular flow condition.

Procedures similar to those in the air-water tests were followed so as to generate measurements and observations over a predetermined span of test conditions. Instead of maintaining a preset liquid flow rate for each range of gas flow rates, as in the air-water tests, in the R-113 tests the total flow rate was kept at a preset value and was maintained constant over a range of qualities.

It should be noted that at each test condition equilibrium conditions were attained before taking data, i.e. the liquid saturation temperature was required to be at the saturation temperature of the refrigerant corresponding to the measured system pressure. Additional attention was given to the condenser cooling water adjustment in order to assure that the circulated refrigerant was entering in the liquid phase as it passed through the glass tube before entering the stainless steel preheating section.

The achievement of steady state condition was required for every data point taken. During any test, steady state conditions were considered to be reached when the R-113 average temperature reached the saturation temperature and the readings of thermocouples along the wall of the heater remained unchanged during a relatively long time period, say 4 — 5 minutes. Because of the slow time response of the test loop to step changes in the power input to the stainless steel heater, the time interval between the sets of equilibrium data points was about 20 to 30 minutes. For each steady state and equilibrium condition, two or more records of the measurements were taken to assure the repeatability of the measurements at that point.

2.3 Experimental Results and Data Reduction

2.3.1 Experimental Results

A total of 15 test conditions were studied. These conditions included two combinations of working fluids, five coil test sections, and three different flow orientations. A total of 609 data points were taken, together with the accompanying visual observations and video tape records. Part of these test data will be discussed in detail in the following chapters. The experiment parameter ranges for the 15 tests are:

For air-water data

1. Helical Coil Vertical Up-Flow

(a) circular tube:

Q_l = .04 - .1238 GPM

W_g = .2592 - 205.5 lb_m/hr

x = .0073 - .9113

(b) rectangular tube, aspect ratio = 1.1:

Q_l = .040 - .2229 GPM

W_g = 1.08 - 36.0 lb_m/hr

x = .0107 - .463

(c) rectangular tube, aspect ratio = .667:

Q_l = .040 - .2229 GPM

W_g = 1.08 - 21.24 lb_m/hr

$x = .0106 - .3909$

(d) rectangular tube, aspect ratio = 1.5:

$Q_l = .040 - .2524$ GPM

$W_g = .72 - 32.76\ lb_m/hr$

$x = .0048 - .2833$

2. Helical Coil Vertical Down-Flow

(a) circular tube:

$Q_l = .0271 - .2473$ GPM

$W_g = .36 - 118.4\ lb_m/hr$

$x = .0035 - .6938$

3. Helical Coil Horizontal Flow

(a) circular tube:

$Q_l = .0352 - .2542$ GPM

$W_g = 1.08 - 21.96\ lb_m/hr$

$x = .0154 - .450$

(b) rectangular tube, aspect ratio = 1.1:

$Q_l = .040 - .2524$ GPM

$W_g = .72 - 16.92\ lb_m/hr$

$x = .0064 - .3061$

(c) rectangular tube, aspect ratio = .667:

$Q_l = .040 - .2229$ GPM

$W_g = .0936 - 36.36\ lb_m/hr$

$x = .0013 - .2824$

(d) rectangular tube, aspect ratio = 1.5:

$Q_l = .0707 - .2229$ GPM

$W_g = .2556 - 13.72\ lb_m/hr$

$x = .0023 - .2124$

4. Spiral Coil Horizontal Outward Flow

   (a) circular tube:

   $Q_l = .040 - .2524$ GPM

   $W_g = .216 - 15.48$ lb_m/hr

   $x = .0017 - .3449$

<u>For R-113 liquid/vapor data</u>

1. Helical Coil Vertical Up-Flow

   (a) circular tube:

   $W_{tot,tp} = 90.11 - 191.65$ lb_m/hr

   $W_g = .83 - 30.5$ lb_m/hr

   $x = .0062 - .2723$

   (b) rectangular tube, aspect ratio = 1.1:

   $W_{tot,tp} = 89.77 - 189.97$ lb_m/hr

   $W_g = 1.77 - 22.7$ lb_m/hr

   $x = .01 - .253$

   (c) rectangular tube, aspect ratio = .667:

   $W_{tot,tp} = 88.94 - 192.33$ lb_m/hr

   $W_g = .889 - 16.17$ lb_m/hr

   $x = .0046 - .1532$

   (d) rectangular tube, aspect ratio = 1.5:

   $W_{tot,tp} = 89.02 - 191.23$ lb_m/hr

   $W_g = .3274 - 27.54$ lb_m/hr

   $x = .0023 - .3070$

2. Spiral Coil Horizontal Outward Flow

   (a) circular tube:

$W_{tot,tp}$ = 91.90 - 185.78 lb_m/hr

W_g = .668 - 20.86 lb_m/hr

x = .004 - .1577

2.3.2 Data Reduction

1. Air-Water Test Data

The parameters Q_l, W_g, $DP_{measured}$, and x are the primary data for the experimental study.

- Q_l (in GPM) is the directly measured reading from the turbine flow meter. The maximum turbine frequency fluctuation is less than 10 HZ (0.003 GPM). The uncertainty of Q_l gives a standard deviation of 0.00252 GPM. For detailed information concerning the uncertainty of any other quantity refer to Appendix A.
- W_g (in lb_m/sec) is the directly measured reading from the venturi meter.
- $DP_{measured}$ (in psi) is the directly measured reading from the differential pressure drop transducer across the entire test section, including the straight lengths of inlet and exit tubing connected to the coiled test section and the gravitational pressure drop differences of the transducer measuring lines. The corrections for obtaining the frictional pressure drop in the coiled tube will be discussed in the following Chapter 4.
- x is the quality of the two-phase mixture and is calculated by:

$$x = W_g \ / \ (W_g + \rho_l Q_l) \tag{2.1}$$

2. R-113 Liquid/Vapor Test Data

As for the air-water test data, the parameters Q_{tot}, W_g, $DP_{measured}$, and x are the primary quantities measured in the experimental study.

- $W_{tot,tp}$ (in lb_m/hr), the total mass flow rate of the R-113 two-phase mixture, is equal to the loop inlet liquid R-113 volumetric flow rate (Q_{tot}, directly measured reading from the turbine flow meter) times the liquid R-113 density. The maximum frequency fluctuation of turbine flow meter is less than 10 HZ (0.003 GPM).

$$W_{tot,tp} = \rho_{l,R\text{-}113} * Q_{tot} \tag{2.2}$$

- x, the equilibrium two-phase quality of R-113 mixture, is calculated from the measured readings of the power to the stainless steel tube heater (P), the estimated (calculated) heat losses of the heater to the room (Q_{loss}), the total mass flow rate ($W_{tot,tp}$), and the fluid temperatures at the inlet and outlet of the heater (T_{in},T_{out}) by:

$$x = (1/h_{lgo}) * [(P-Q_{loss})/W_{tot,tp} - (h_{l\text{-}out}-h_{l\text{-}in})] \tag{2.3}$$

where, ρ_l is the saturated liquid density of R-113 at T_{out}, h_{lgo} is the latent heat of vaporization at the outlet of heater (a function of T_{out} & P_{out}), $h_{l\text{-}out}$ is the saturated liquid enthalpy of R-113 at outlet of heater (a function of T_{out}), and $h_{l\text{-}in}$ is the liquid enthalpy of R-113 at inlet of heater (a function of T_{in} & P_{in}).

- W_g (in lb_m/hr) is the mass flow rate calculated from $W_{tot,tp}$ and x by:

$$W_g = x * W_{tot,tp} \tag{2.4}$$

where, ρ_l is the liquid density of R-113 at the inlet of the heater.

- $DP_{measured}$ (in psi) is the directly measured reading from the differential pressure transducer across the entire test section, including the straight lengths of inlet and exit tubing connected to the coiled test section and the gravitational pressure drop differences of the transducer measuring lines. The corrections for obtaining the frictional pressure drop in the coiled tube will be discussed in Chapter 4.

CHAPTER 3

PRESENTATION AND DISCUSSION OF FLOW PATTERN RESULTS

For two-phase flow inside tubes, the heat transfer and pressure drop are strongly affected by the flow pattern because different two-phase structures yield different momentum and heat transfer characteristics. Models of pressure drop that are not flow pattern-dependent are generally only valid in the limited range of conditions where their empirical data was obtained. To accurately predict pressure drop and heat transfer, the flow patterns of the mixture must be known. Because of the unstable, and periodic characteristics of slug flow, it should be avoided in practical heater exchanger operations. An annular flow condition is usually the desired condition [17].

One of major objectives of the present study was to observe and develop a fundamental understanding of the flow patterns, and to establish the conditions under which the transition to annular flow occurs in helical and spiral coils.

In this study, direct visual observations were made of two-phase flow patterns for each of 15 experimental conditions (listed in Section 2.3 of Chapter 2) associated with different test sections, flow channel cross-sections, flow directions, test section orientations, and two-phase working fluids. The flow patterns were video-recorded for every set of steady flow conditions, with a fast shutter speed of 1/1000 of a second. With the combination of observation with the naked eye and a frame by frame playback of recorded video tape, the flow pattern for each flow condition could be described and identified quite clearly.

It was observed that for different combinations of flow directions and test section orientations -- for example, vertical flow vs. horizontal flow for the helical test sections -- the flow dynamics and flow patterns were quite different. All the possible combinations are summarized in Figure 1.3 of Chapter 1. Table 3.1 lists the four combinations employed in the present study. Following sections analyzed helical coil vertical upflow and spiral coil horizontal outward flow and left the other two conditions for future investigation.

Table 3.1 Combinations of Flow Direction & Test Section Orientation in the Present Study

Test Section	Flow Direction & Test Section Orientation
Helical Coil	Vertical Upward Flow
Helical Coil	Vertical Downward Flow
Helical Coil	Horizontal Flow
Spiral Coil	Horizontal Outward Flow

3.1 Flow Patterns of Vertical Up-Flow in Helically Coiled Tubes

For helical vertical up-flow in a helical coil, the flow is similar to that in a horizontal straight tube, despite the differences of: (1) the tube being curved, and (2) the tube being slightly inclined.

3.1.1 Flow Pattern Observations

For vertical up-flow of two-phase mixtures in helical coils, air-water and R-113 liquid/vapor in the present study, the flow patterns observed in either the circular or rectangular cross-sectional coils of the same hydraulic diameters, are similar. The flow patterns are depicted in Figure 3.1 and are described as follows:

PLUG FLOW: Elongated plugs (bubbles) of the gas phase moving through the continuous liquid phase which wets the entire periphery the tube. The plugs and bubbles travel preferentially along the top of the tube.

SLUG FLOW: In this flow pattern, packets of liquid slugs or liquid bridges contact the upper channel wall, and periodically move down the flow channel between regions of gas/liquid flow, with the gas phase at the top and liquid phase at the bottom generally.

TRANSITION: The transition flow condition is considered to be that condition between slug flow and annular flow patterns, i.e. the liquid slug has just started to break away from touching the upper flow channel wall.

ANNULAR FLOW: Annular flow in general is defined as a flow when a continuous liquid film exists around the entire tube circumference and a

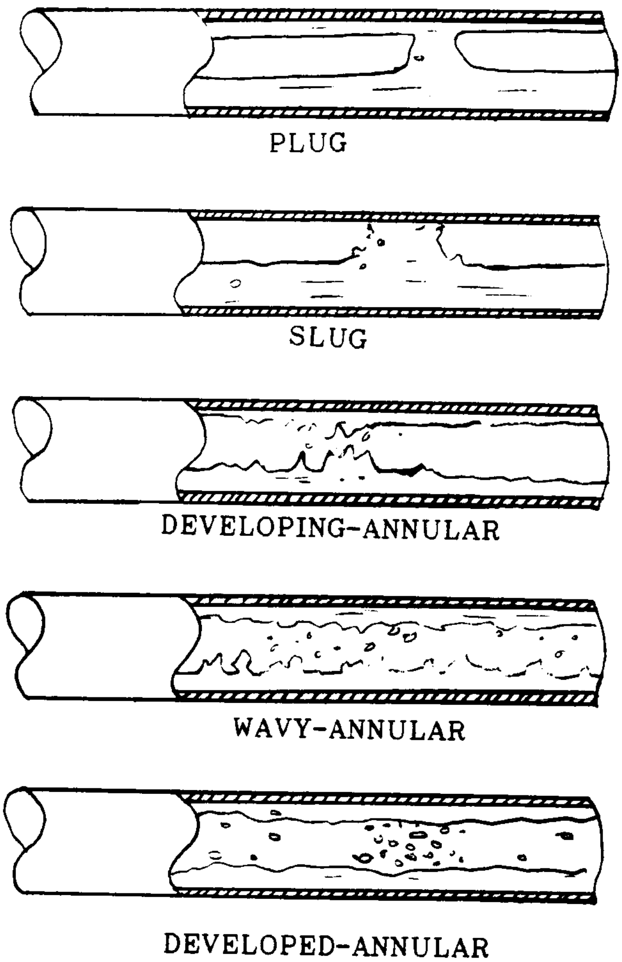

Figure 3.1 Flow patterns observed in helical coil vertical up-flow

continuous gas passage way exists in the center. However, with different qualities, this flow pattern can yield different flow sub-patterns, each of which has its own flow dynamic characteristics. The following annular flow sub-patterns were observed in the helical coil vertical up-flow.

ASYMMETRIC-ANNULAR or DEVELOPING-ANNULAR FLOW: This flow pattern is the onset annular flow pattern after transition from slug flow, when a continuous liquid film exists around the entire tube circumference. Periodic pulsating bridges of liquid are still seen, but they no longer touch the upper tube wall, and are therefore appropriately described as pulsating wave peak surges within the lower liquid film.

WAVY-ANNULAR FLOW: If the gas flow rate continues to increase, the pulsating liquid wave peaks within the lower liquid film will start to break out. This results in the liquid/gas interface's becoming very wavy and irregular.

ANNULAR or FULLY DEVELOPED ANNULAR FLOW: In this flow pattern, the pulsating wave - peak surges of the liquid film at the channel bottom are greatly smoothed, such that a transformation occurs in which a symmetric annular flow pattern is formed. In addition, a lump of liquid droplets which are produced by the breakage of pulsating liquid slugs flows periodically through the continuous central gas core.

It should be noted that unlike the two-phase flow patterns observed in a straight horizontal tube, stratified flow patterns were not observed in the helical coils within the range of test conditions examined herein. This occurs because the helical coil tubes have an inclination angle of 8^{o} from the horizontal, which is apparently large enough to prevent stratified flow from existing, while still allowing the rest of the similar horizontal-characteristic flow patterns to exist. This behavior was also observed at angles from 1° to 30° by Taitel, Dukler and Barnea [5], 1987 and from 1/2° to 7° by Weisman [58], 1979, for flows in straight tubes. Furthermore, the small tube diameter (.325") of the test section used in the present study may be another factor that prevents the maintenance of a stratified flow pattern (see Choe, Weinberg & Weisman [16], 1978).

No bubbly flow pattern data points were recorded in the range of test conditions of interest for the present study. However, a bubbly flow pattern did occur at some very low gas flow rates.

In conclusion, the flow patterns observed in the studied range for helical vertical up-flow with two kinds of two-phase working fluids (air-water and R-113 liquid/vapor mixtures) in both circular and rectangular cross-section flow channels were similar to those observed in horizontal straight flow channels (except for the absence of a stratified flow pattern, believed to be due to small flow channel inclination of 8°). The stratified flow pattern appears to be replaced by the slug flow pattern.

Additional Flow Regime Observations

In the slug flow condition it was observed that due to the inclination of the helically coiled tube, the liquid film at the channel bottom, together with its entrained bubbles, sometimes moved in a backward direction between each slug, until the following slug surge pushed it forward again. This intermittent phenomenon disappeared when the liquid flow rates were high. This observation also confirms the same observation reported first time by Saxena et al [46] (1990) in their study of air-water two-phase flow in vertical oriented helical coils.

In all flow ranges some degree of periodic, pulsating flow occurred

— even in vigorous symmetric annular flow, in which case a glob of droplets surged periodically through the central gas core.

3.1.2 Comparison with Existing Flow Maps

Both air-water and R-113 two-phase flows were observed in the circular cross-section helically coiled tubes. Two-phase R-113 flow was additionally observed in the helically coiled tube of nearly square cross-section.

The flow pattern observations were compared with the predictions of four flow pattern maps. The four maps used are those by: (1) Baker [2], (2) Taitel-Dukler [50], (3) Choe, Weinberg and Weisman [16], and (4) Uddin [53]. The first three were developed for two-phase flows in horizontal straight tubes. These were chosen because it was believed that the vertical up-flow condition in helical coils with a small helix angle (about 8^o in this study) would be similar to that in horizontal straight tubes. The fourth map by Uddin [53] was an empirically developed map for air-water two-phase upward flow in helical coils, for coil-diameter to tube-diameter ratios from 20 to 25.

A. MODIFIED BAKER FLOW MAP

The original Baker map [2] (1954), one of the earliest and most widely used flow maps, was empirically derived for horizontal flow of air-water and some oil and gas two-phase mixtures. This map was modified later to account for property effects in order to extend its application range. The experimental results of the three test conditions of the present investigation were plotted on the modified Baker flow map in Figures 3.2, 3.3, and 3.4.

In Figure 3.2, for air-water two-phase flow in the circular cross-section helically coiled tube test section, almost all operating conditions fell in the stratified regime, even though such a flow pattern was not even observed for this range of flow conditions. Even in the case of the R-113 flow conditions, which are seen to be shifted from the stratified regime to the slug and annular regimes according to the map (see figures 3.3 & 3.4), the predicted transition lines from slug to annular flow were too high for the flows in the circular cross-section tube, and too low in the rectangular cross-section tube. Therefore, we can conclude that the modified Baker map can not be used to predict the flow patterns in helically coiled tubes.

B. TAITEL & DUKLER FLOW MAP

The Taitel & Dukler map was also developed for horizontal flow in straight tubes. The experimental data of three test conditions were plotted on a Taitel & Dukler flow map, as illustrated in Figures 3.5, 3.6, and 3.7. As shown in these three figures, it is obvious that this flow map is no better than the modified Baker map, and therefore its use is not recommended for two-phase vertical upward flow in helically coiled tubes.

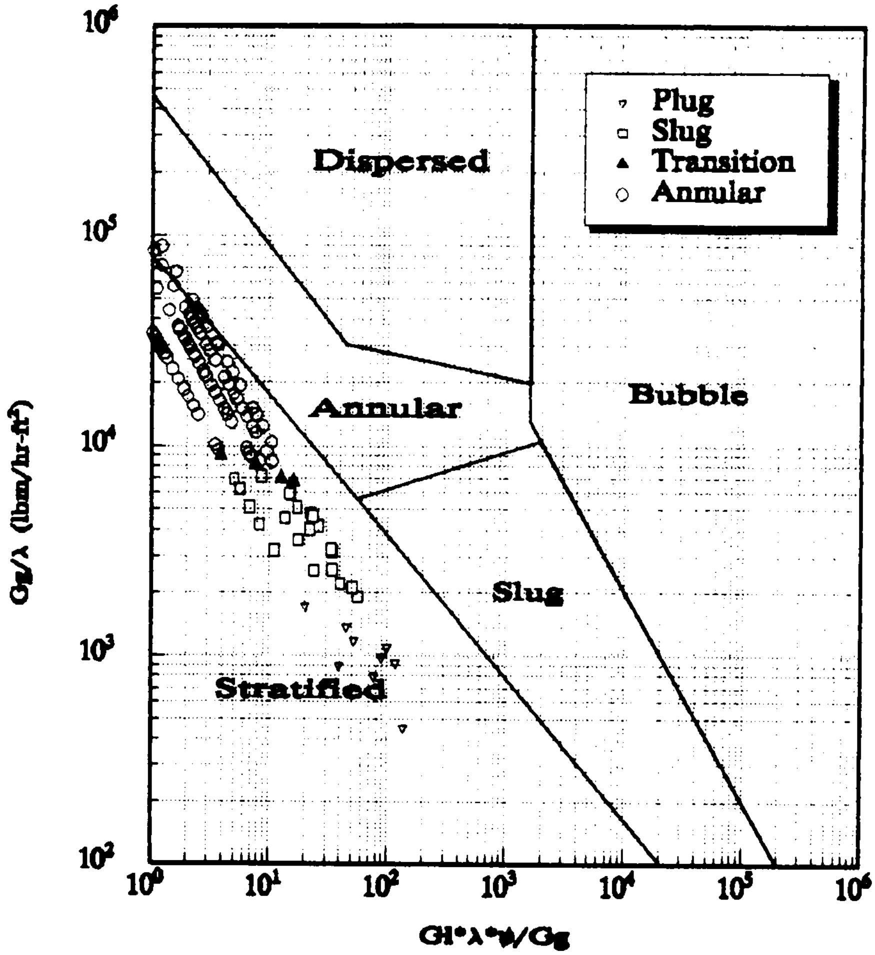

Figure 3.2 Modified Baker Horizontal Flow Map (Helical Coil Vertical Up-Flow, Circular Tube, Air-Water)

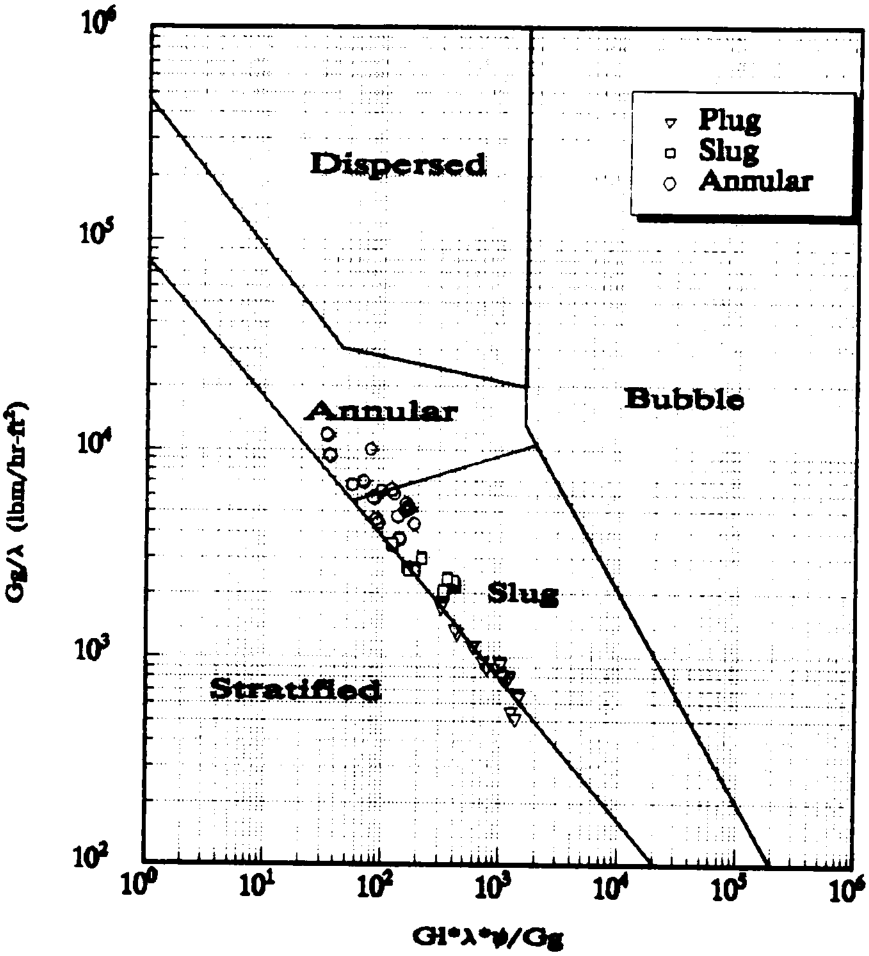

Figure 3.3 Modified Baker Horizontal Flow Map (Helical Coil Vertical Up-Flow, Circular Tube, R-113 Liquid/Vapor)

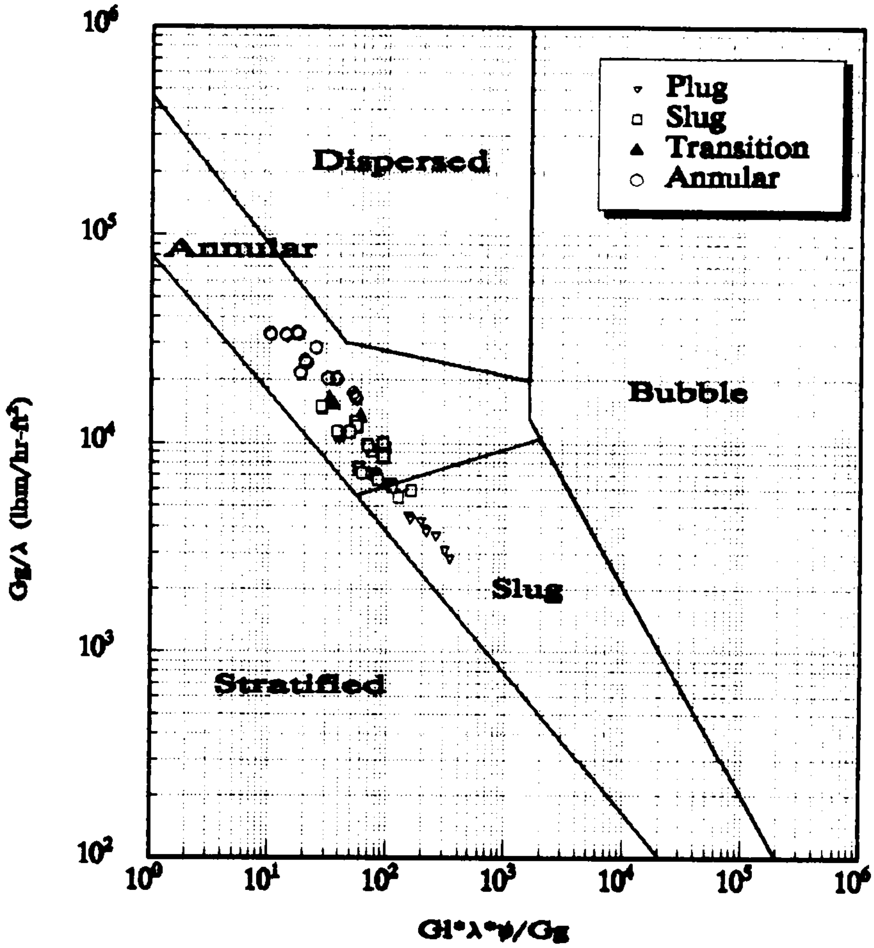

Figure 3.4 Modified Baker Horizontal Flow Map (Helical Coil Vertical Up-Flow, #1 Rectangular Tube, H/W=1.1, R-113 Liquid/Vapor)

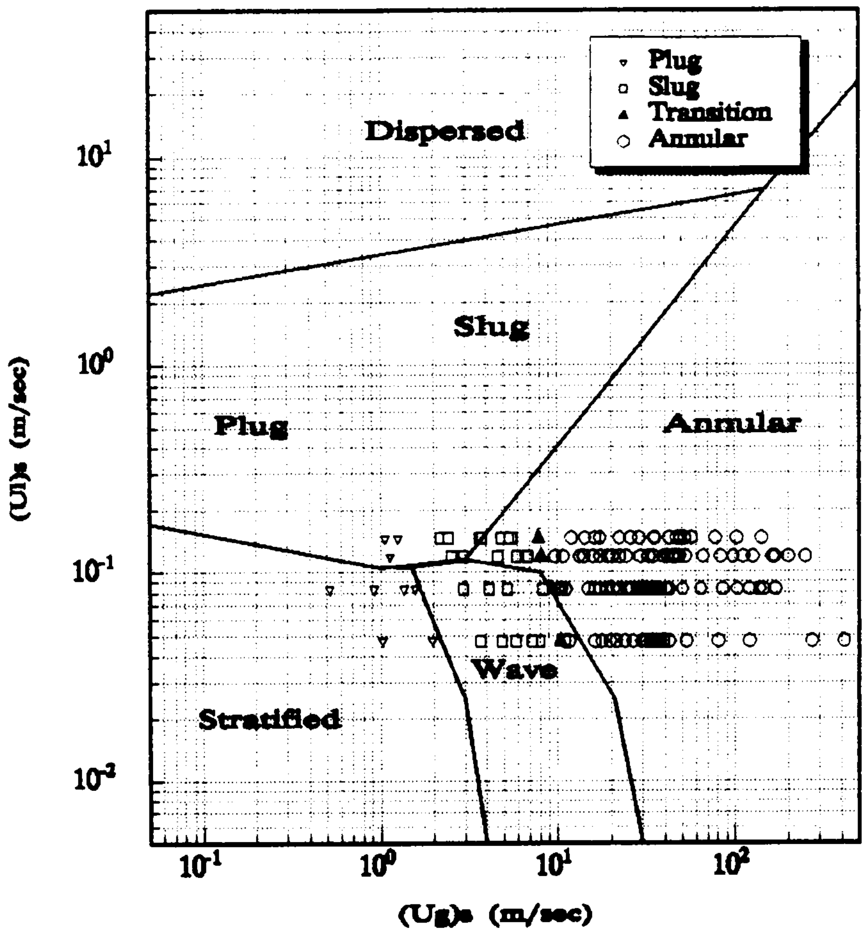

Figure 3.5 Taitel & Dukler Horizontal Flow Map (Helical Coil Vertical Up-Flow, Circular Tube, Air-Water)

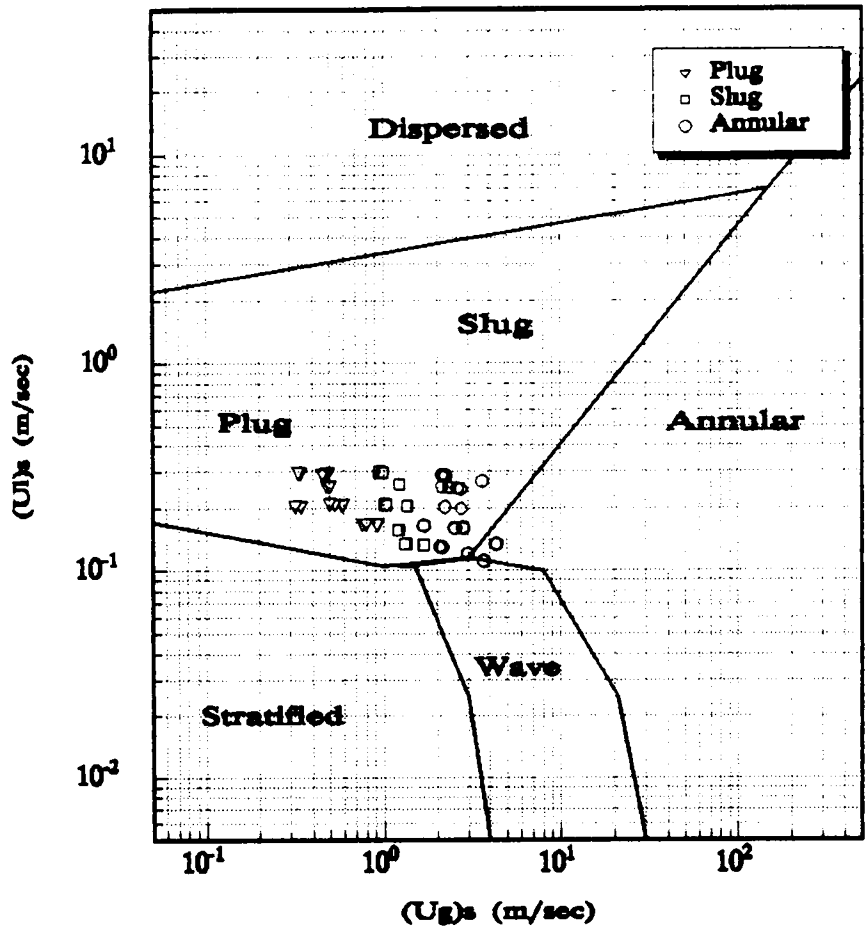

Figure 3.6 Taitel & Dukler Horizontal Flow Map (Helical Coil Vertical Up-Flow, Circular Tube, R-113 Liquid/Vapor)

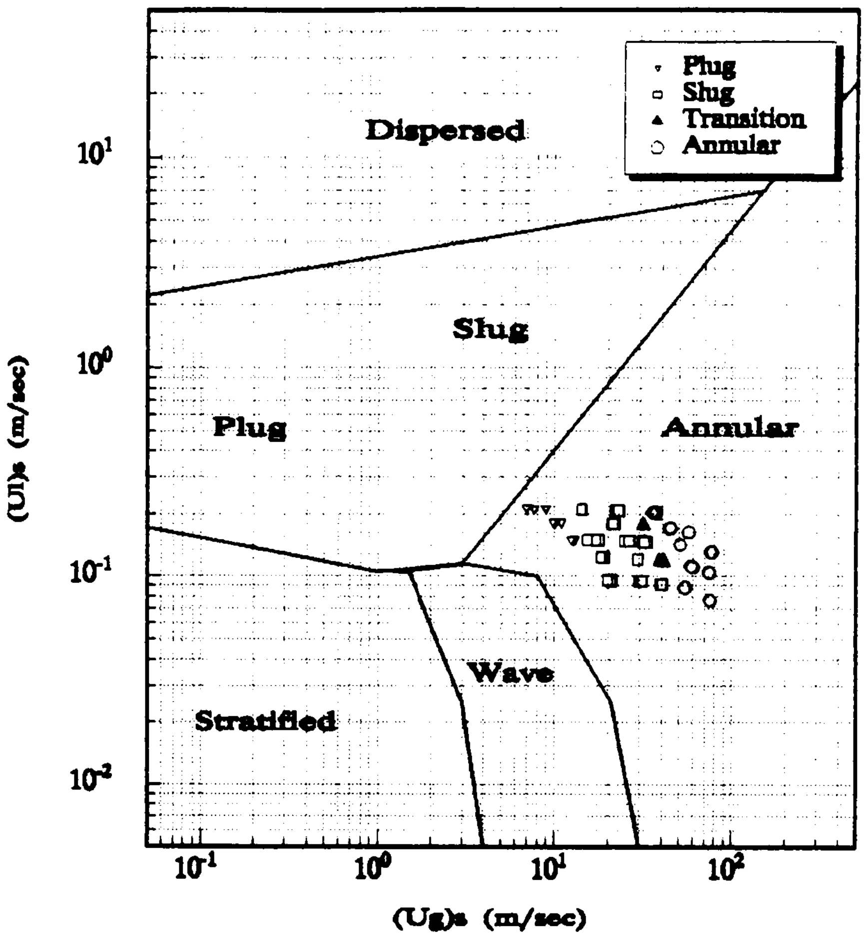

Figure 3.7 Taitel & Dukler Horizontal Flow Map (Helical Coil Vertical Up-Flow, #1 Rectangular Tube, H/W=1.1, R-113 Liquid/Vapor)

C. UDDIN FLOW MAP

The test data were also plotted on the Uddin map in Figures 3.8, 3.9, and 3.10. The Uddin flow map is the only flow map empirically developed for air-water vertical upward flow in helically coiled tubes. However, examination of Figures 3.8 - 3.10 indicates that it does not predict the present air-water experimentally observed flow patterns of vertical up-flow in helically coiled tube. The main reason for this inadequacy is that in his map there is no transition line between annular flow and slug flow. Yet, this was the major transition occurring for the present experimental data. The lack of a slug-annular transition may be due to the relatively large tube diameter of Uddin's helical test section, although no absolute magnitude of the tube diameter was presented in his article. The larger coil-diameter to tube-diameter ratios of 20 to 25 in his test sections are much larger than the 9.08 used in the present study. This may imply a significant difference in tube diameter between his and the present test sections. Figures 3.8 clearly illustrates that for air-water vertical up-flow in helically coiled circular tubes of .325" diameter and D_c/d_i of 9.08, the Uddin map does not provide a good prediction of the observed flow patterns.

For the R-113 experimental data, the transition line fell into the stratified and plug regimes of the Uddin map for the data of the circular cross-section tube (see Figures 3.9), while the transition and all the data fell into the annular mist regime of the Uddin map for the data in near square cross-section tube (see Figure 3.10). This showed that the Uddin flow map can likewise not be used for predictions of R-113 flow patterns

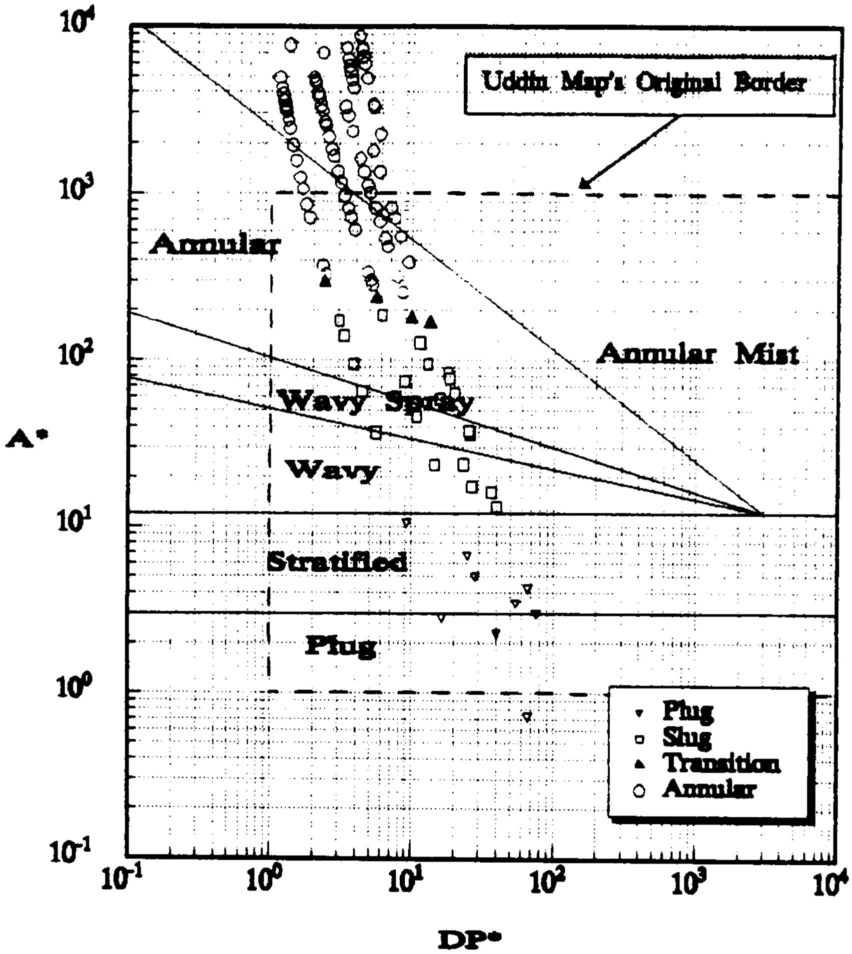

Figure 3.8 Uddin Flow Map (Helical Coil Vertical Up-Flow, Circular Tube, Air-Water)

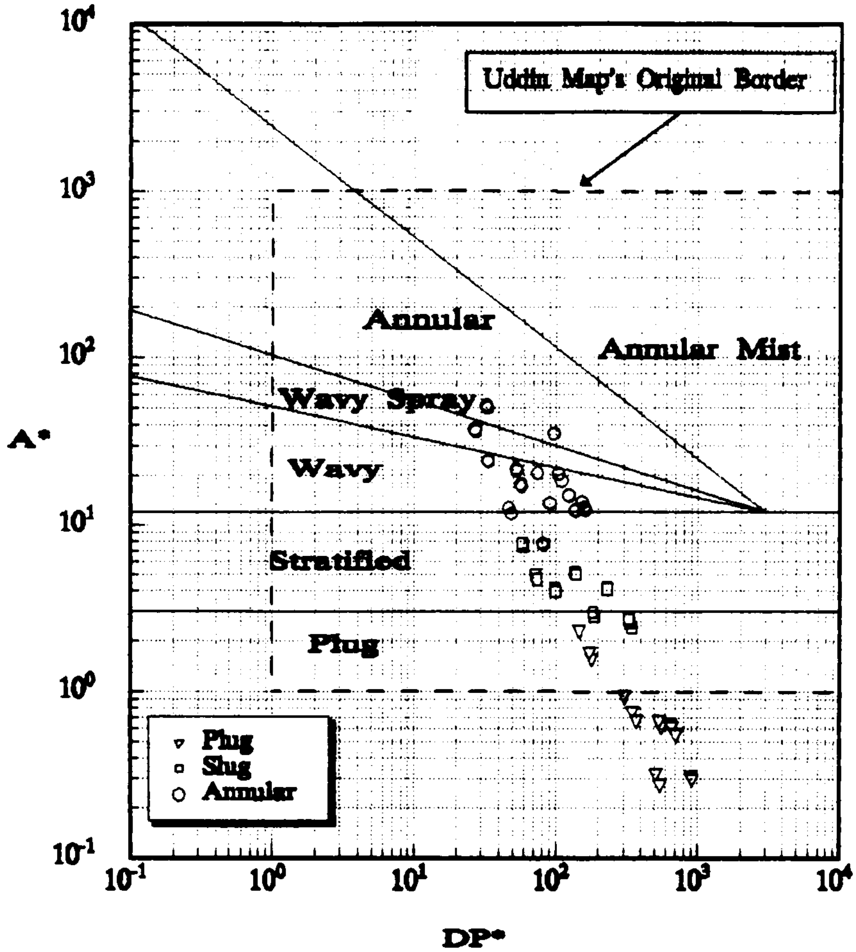

Figure 3.9 Uddin Flow Map (Helical Coil Vertical Up-Flow, Circular Tube, R-113 Liquid/Vapor)

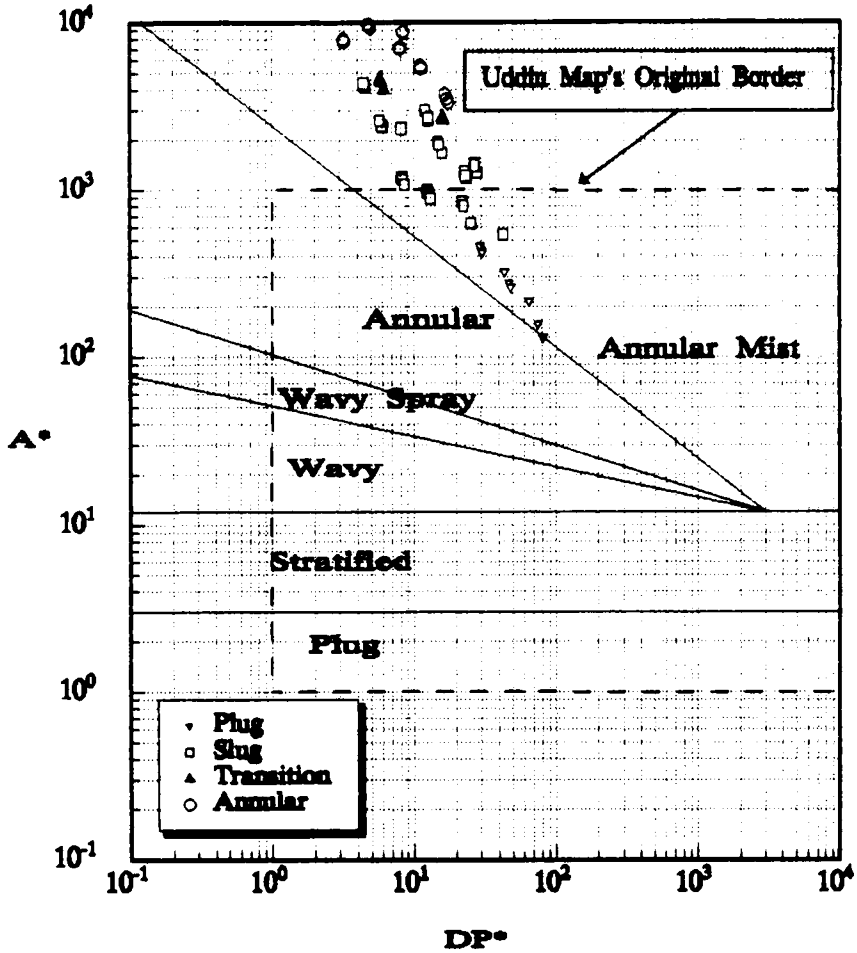

Figure 3.10 Uddin Flow Map (Helical Coil Vertical Up-Flow, #1 Rectangular Tube, H/W=1.1, R-113 Liquid/Vapor)

and their transitions perhaps because the map was based only upon his limited air-water experimental data.

D. CHOE, WEINBERG & WEISMAN FLOW MAP (CHOE MAP)

Finally, the three sets of test data were compared with the Choe map in Figures 3.11, 3.12, and 3.13. In the Choe map, plug and slug flows are considered as "intermittent flow" and stratified and wavy stratified flows as "separate flow". It should be noticed that even though the Choe map was developed for horizontal straight tubes, it would predict the slug-annular transition line of the present air-water data in the helically coiled circular cross-section tube quite well if the separated regime were replaced by an intermittent regime. The replacement of the separated regime by an intermittent regime is necessary to account for the inclination effect of the helical tube (see Figure 3.11).

In the circular cross-section coil, the experimental slug-annular transition line for the R-113 two-phase mixture was somewhat higher than that of the air-water two-phase mixture (see figures 3.11 and 3.12). For the R-113 two-phase mixture, the experimental slug-annular transition line in the near square cross-section coil was only slightly lower than for the circular cross-section coil (see figures 3.12 and 3.13).

In conclusion, none of the four flow maps predicted flow patterns well for the helical coil test data obtained here. Among them, the Choe map provided the most reasonable transition line if the separated regime is replaced by an intermittent regime. This map would appear to provide

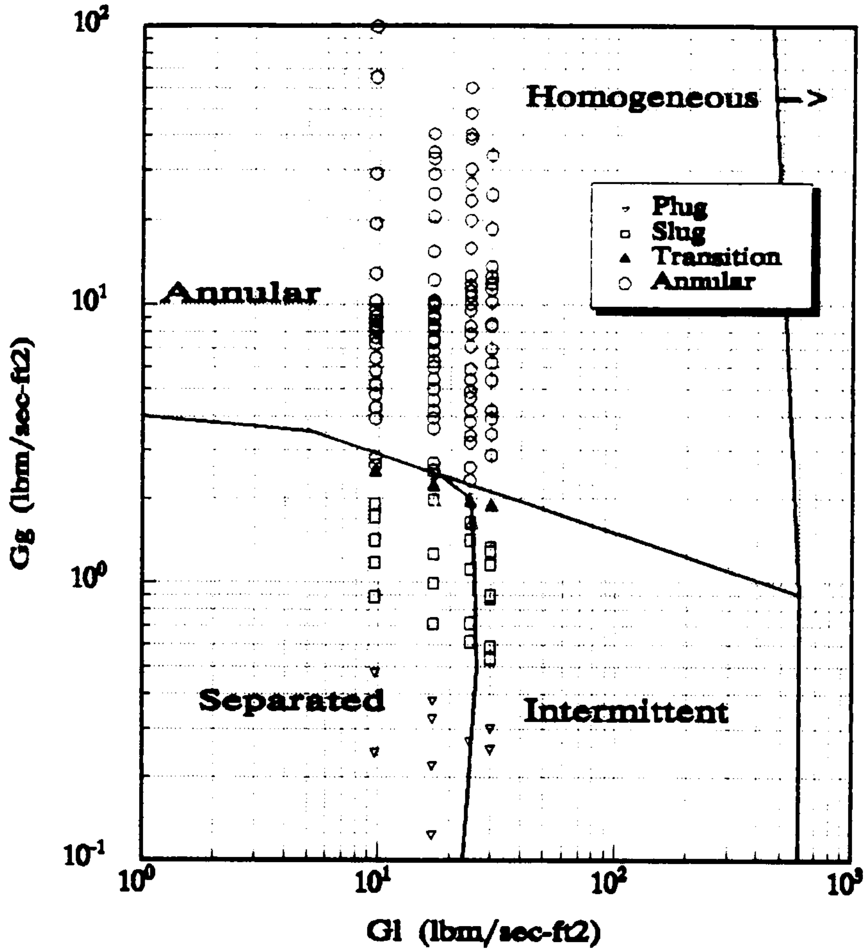

Figure 3.11 Choe, Weinberg & Weisman Horizontal Flow Map (Helical Coil Vertical Up-Flow, Circular Tube, Air-Water)

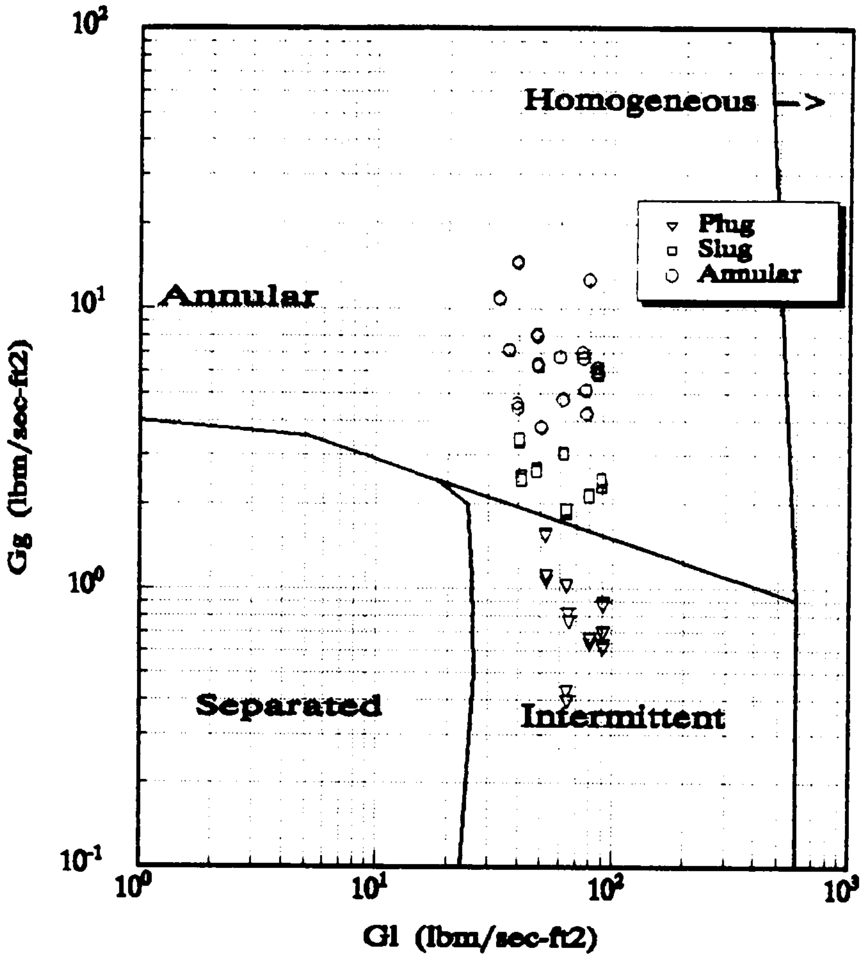

Figure 3.12 Choe, Weinberg & Weisman Horizontal Flow Map (Helical Coil Vertical Up-Flow, Circular Tube, R-113 Liquid/Vapor)

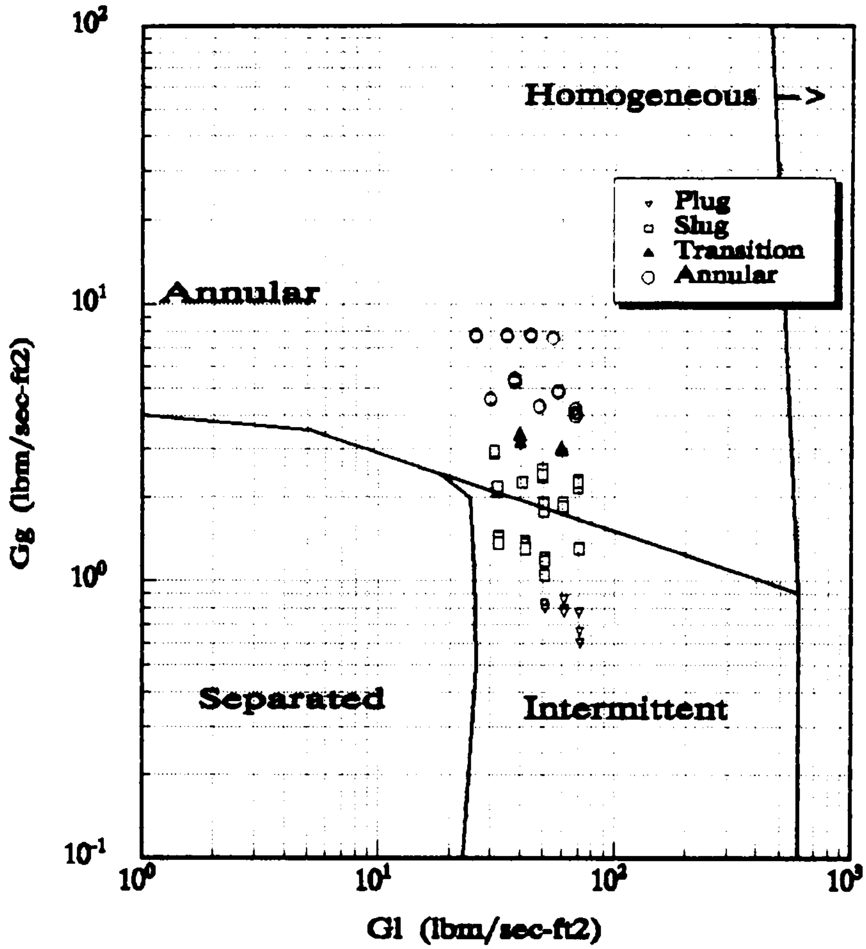

Figure 3.13 Choe, Weinberg & Weisman Horizontal Flow Map (Helical Coil Vertical Up-Flow, #1 Rectangular Tube, H/W=1.1, R-113 Liquid/Vapor)

a good starting point for predicting the slug-annular transition for two-phase vertical up-flow in helical coils.

3.1.3 Modified Correlation for Slug-Annular Transition in Helical Coil Vertical Up-Flow

In the flow conditions of interest being studied here, the transition to annular flow appeared to be a slug-annular transition, or more generally speaking, an intermittent-annular transition.

The two most widely used semi-theoretical correlations for intermittent-annular flow transition in horizontal straight tubes are those of Choe, Weisman et al(1978) [16] and Taitel & Dukler(1976) [50]. Choe et al used wave theory as the theoretical basis for the intermittent-annular transition. Their map has been shown, by many different investigators, to predict the flow patterns in horizontal straight tubes quite well. For the present study, as demonstrated in the previous section, the Choe map provides the best prediction for the three sets of test data for vertical up-flow in helical coil flow channels among the four flow maps used for comparison. Taitel and Dukler have used a semi-theoretical basis for slug-annular transition in terms of the ratio of equilibrium liquid level in the pipe, h_l, to pipe diameter d_i, which reflects the force balance of liquid gravity and viscosity in liquid slug. However, their assumption is in disagreement with the data reported by Choe et al(1978), Simpson et al (1977), Spedding and Nguyen(1976), and Weisman et al(1979). As shown in the previous Section 3.1.2, the Taitel and Dukler map does not predict the helical vertical up-flow data of the present study either.

As a result of the inadequacies of existing flow pattern maps when applied to vertically oriented helical coils, the semi-empirical correlation for the intermittent-annular transition in the Choe map was investigated and modified to predict the slug-annular transition in helical coil vertical up-flow.

Choe et al (1978) suggested that the transition from intermittent flow to annular flow is due to periodic slugs or pulses which splashed liquid to the top of the tube. When the pulses are so frequent that the liquid is unable to drain before the next pulse or slug, annular flow begins. By using air-water slug frequency data, they concluded that the transition to annular flow could be correlated by:

$$G_g = 10\ (G_l)^{-0.285}\ (d_i/d_{ref})^{0.38} \tag{3.1}$$

where, G_g and G_l have the units of lb_m/ft^2-sec, d_i is the pipe diameter in inches, and d_{ref} = 1.5 inches.

For the present air-water test data in helical coil vertical up-flow, the slug-annular transition line is very close to that predicted by Choe's correlation if the separated flow pattern is replaced by a slug flow pattern (see Figure 3.11). As seen in Figure 3.11, the air-water slug-annular transition line for the helically coiled tube is somewhat lower than for a straight tube, as predicted by the Choe map. This is reasonable because the secondary flow effect in a helically coiled tube can enhance the splashing of the liquid slug in an additional direction -- perpendicular to the flow direction -- and hence, cause the transition to an annular flow pattern to occur earlier. Equation (3.1) was therefore modified to attempt to take into account this curvature effect of the helically coil tube, based upon the air-water test data obtained in the circular cross-section helical coil, as follows:

$$G_g = 10 \left(1 - (d_i/D_c)^{0.88} \right) (G_l)^{-0.285} (d_i/d_{ref})^{0.38} \qquad (3.2)$$

where, D_c is the helical coil diameter. Equation (3.2) is plotted in Figure 3.14 compared with the air-water test data together with Choe's correlation.

It is noticed that Equation (3.3) for helical coil vertical up-flow will coincide with the Choe's correlation (Equation (3.1)) for straight tube horizontal flow, if the $D_c \rightarrow \infty$.

A further effort was made to correlate the effects of R-113 properties into Equation (3.2). Because only a few experimental results of flow patterns of air-water helical coil vertical up-flow has been reported in the literature, the effects of the fluid properties of each phase on the slug-annular transition in helical coil are unclear. However, the situation is not as bad as it may first appear, because of the similarity of the flow patterns and the slug-annular transition observed with the helical coil vertical up-flow results to the horizontal and near horizontal straight tubes. This similarity could provide the certain starting point for the present study.

Weisman [58] (1979) summarized the results of previous researchers in horizontal and near horizontal straight tubes, and concluded that for the intermittent-annular transition the effect of gas density is significant, while the effects of liquid density, liquid viscosity, and surface tension are very small. These conclusions can also be qualitatively confirmed by the

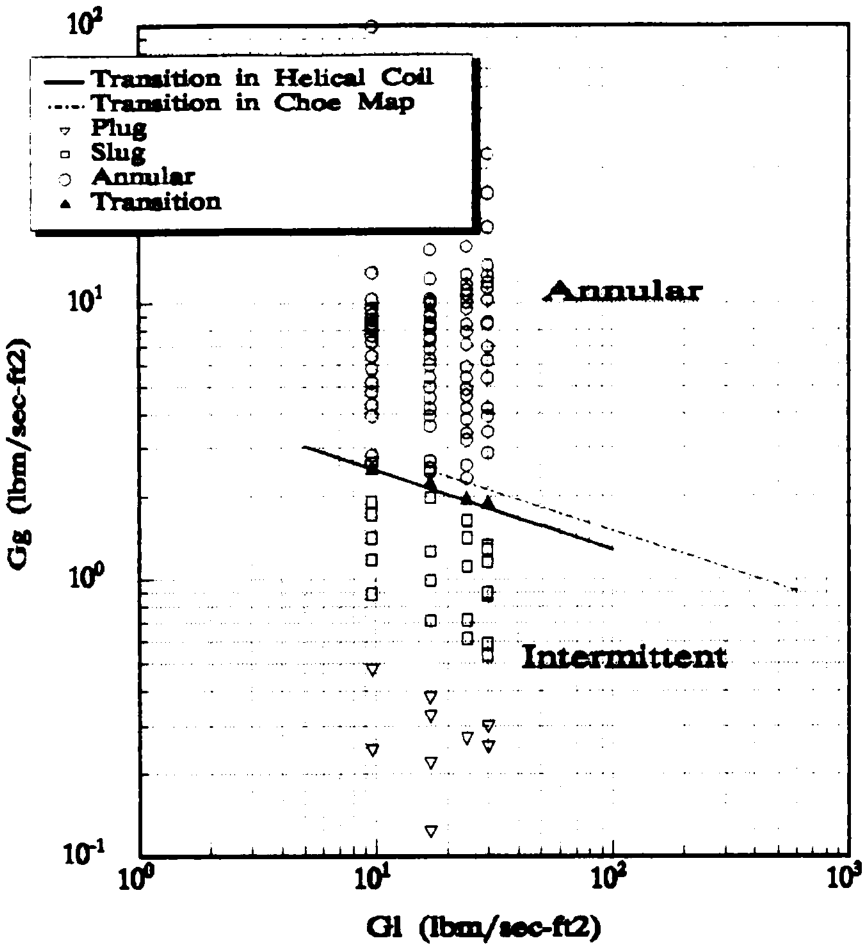

Figure 3.14 Modified Correlation to Predict Slug-Annular Transition for Helical Coil Vertical Up-Flow (Air-Water, Circular Tube)

results of the Choe and Taitel & Dukler flow map comparison for the present helical vertical up-flow data, because the disagreement of the slug-annular transition of the present data with the Taitel & Dukler map prediction may imply a small effect of liquid density and liquid viscosity, since both of these quantities reflect the theoretical basis (balance of equilibrium liquid level, h_l) for the slug-annular transition of the Taitel & Dukler map. However, the relatively good prediction of transition provided by the Choe map for the present helical coil test data may suggest that the gas density and density difference of the two phases could have a significant influence on the slug-annular transition, since the theoretical basis of this map is the frequency behavior of slug pulsing. Therefore, with this indirect evidence, the incorporation of property effects on the slug-annular transition proposed by Weisman [58] for horizontal straight tube was adopted for helical coil vertical up-flow in the present study.

The R-113 test data in the circular cross-section coil was used here as the basis for the following empirical slug-annular transition correlation, which includes property effects:

$$G_g = 10\left[1-\left(\frac{d_i}{D_c}\right)^{.88}\right]\left[\frac{\rho_g/(\Delta\rho_{g,l}\sigma)^{1/2}}{\rho_a/(\Delta\rho_{a,w}\sigma_w)^{1/2}}\right]^{.34} G_l^{-.285}\left(\frac{d_i}{d_{ref}}\right)^{.38} \qquad (3.3)$$

where, $\Delta\rho_{w,a} = (\rho_w - \rho_a)$, in which ρ_a = .0745 lb_m/ft^3 (1 atm, 70 °F) and ρ_w = 62.31 lb_m/ft^3 (1 atm, 70 °F). The water surface tension, σ_w, is taken to be that at 70 °F, which is .0644 N/m. Equation (3.3) was plotted with the test data in Figure 3.15. Good agreement is shown. Further study is needed to verify this method of incorporating property effects in the slug-annular transition developed for horizontal straight tube flow, by Weisman, so as

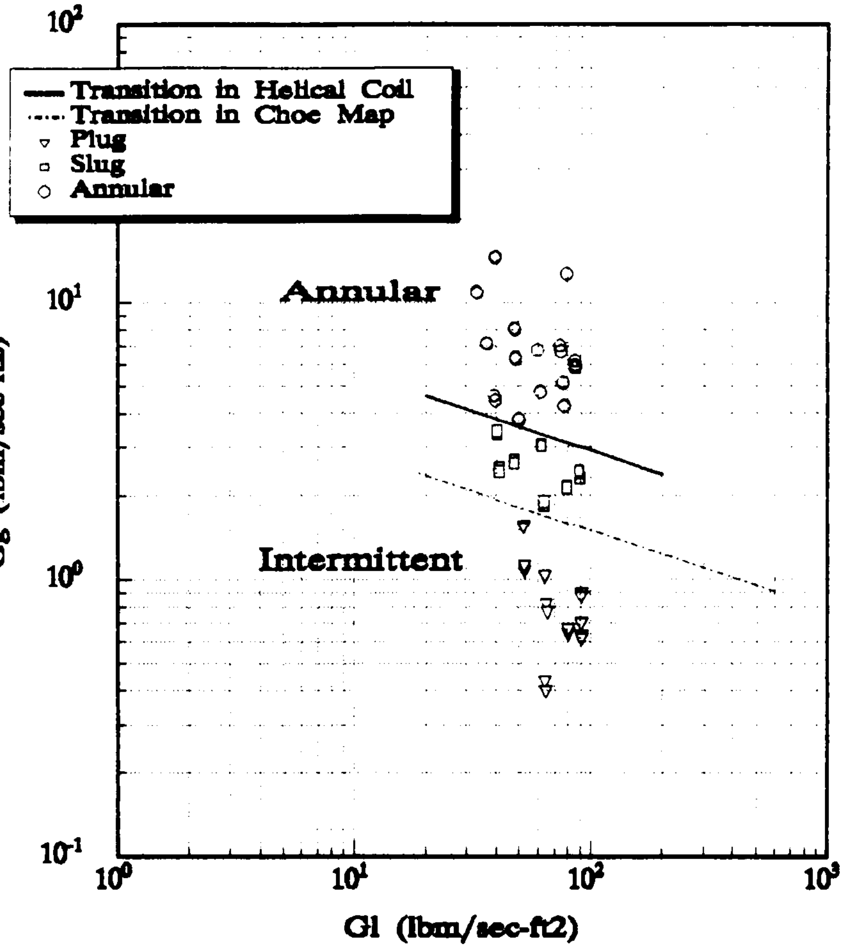

Figure 3.15 Modified Correlation to Predict Slug-Annular Transition for Helical Coil Vertical Up-Flow (R-113 Liquid/Vapor, Circular Tube)

to be applied to vertical up-flow in helical coils.

Finally, comparing the transitions of the R-113 test data between circular tube flow channel and rectangular cross-section flow channel (Figures 3.12 and 3.13), the transition to annular flow in near rectangular cross-section flow channel occurs slightly earlier than in circular cross-section flow channel. This is believed due to the influence of the upper corners of the rectangular cross-section flow channel, which have the tendency to retain liquid (i.e. prevent draining) due to the liquid surface tension and wetting characteristics.

Since no study has been seen so far in the literature on for two-phase flow in helical coils with rectangular cross-sections, a correlation is proposed here to take into account the effect of the rectangular cross-section by modifying Equation (3.3) as follow:

$$G_g = 10\left[1-\left(\frac{d_h}{D_c}\right)^{.88}\right]\left(\frac{H}{W}\right)^{-1.71}\left[\frac{\rho_g/(\Delta\rho_{g,l}\sigma)^{1/2}}{\rho_a/(\Delta\rho_{a,w}\sigma_w)^{1/2}}\right]^{.34} G_l^{-.285}\left(\frac{d_h}{d_{ref}}\right)^{.38} \qquad (3.4)$$

where, H and W are the height and width of the rectangular cross-section, respectively, and d_h is the hydraulic diameter of the rectangular cross-section flow channel. The term $(H/W)^{-1.71}$ in Equation (3.4) can be considered to be the shape factor of the rectangular cross-section flow channel. It is noticed that the exponent of the aspect ratio (H/W) in Equation (3.4) is negative, which implies that the larger the aspect ratio the earlier the transition from slug flow to annular flow will occur. It is reasonable since if the height of the flow channel cross-section were very small it would be very difficult for the liquid slug to break away from the top to form a continuous gas flow passage. It would be easier for a liquid slug to separate from the top surface if the height of the flow channel cross-section were relative high. In any situation, the centrifugal force effect could still maintain a continuous liquid film at the tube top, preventing a liquid film at the upper surface from draining down. Experimental data for R-113 flow in the #1 rectangular tube channel for vertical up-flow are plotted and compared with the predictions of Equation (3.4) and Choe's correlation in Figure 3.16.

The slug-annular transition in helical vertical up-flow for the present study can be summarized as follows:

- The slug-annular transition for air-water and R-113 up-flow in a circular cross-section vertical helical coil is described by Equation (3.3). The transition for flows in rectangular cross-section channels is described by Equation (3.4). Applicability to other coil geometries and fluids must be established.
- Using the data obtained as a guide, it appears that the curvature effect (centrifugal force) in a coil geometry causes the transition from slug to annular flow to occur earlier as compared with straight channels. This applies to both circular and rectangular cross-section flow channels.
- The effect of properties of R-113 liquid/vapor upon the flow patterns and transition observed, as compared with those of air-water, is significant. The transition to annular flow for R-113 liquid/vapor is much higher than for air-water.

Among the preceding effects, the effect of properties is largest, while the effects of tube curvature (vs. straight tube) and

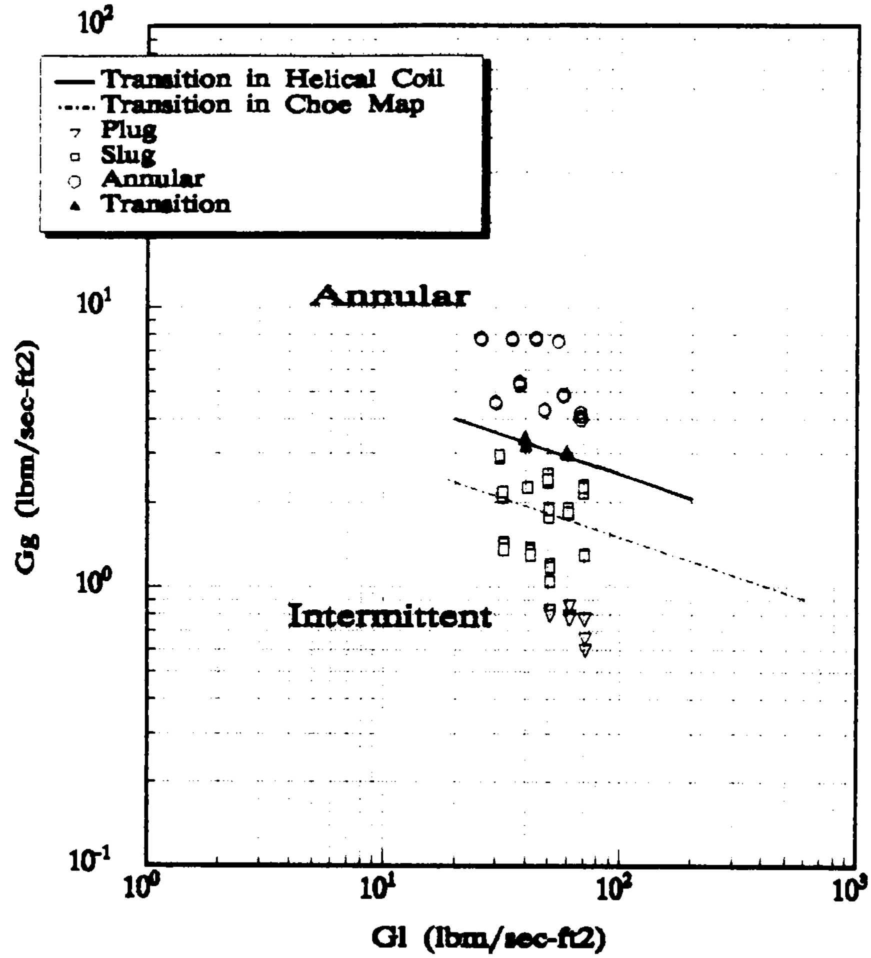

Figure 3.16 Modified Correlation to Predict Slug-Annular Transition for Helical Coil Vertical Up-Flow (R-113 Liquid/Vapor, #1 Rectangular Tube H/W=1.1)

rectangular cross-section (vs. circular cross-section) are relatively small. Since the hydraulic diameter of the studied #1 rectangular cross-section helical coil flow channel is about the same as that of the compared circular cross-section helical coil, the small difference on transition to annular flow between the two may imply that the hydraulic diameter is the factor of significance in the transition criteria, rather than the channel shape. Further studies need to be done concerning this implication.

3.2 Flow Patterns of Horizontal Outward Flow in Spiral Coils

For flows in a spiral coil oriented within a horizontal plane, the flow is similar to that in a horizontal straight channel, except for the channel curvature. Therefore, the flow channel in a spiral coil horizontal outward flow may be expected to be similar to the helical coil vertical upflows described earlier, except for the small inclination of the coil passages. Additionally, it should be noted that the curvature is not constant in a spiral coil, as it is in a helical coil.

3.2.1 Flow Pattern Observation

Experimental observations were made for the spiral coil test section of circular cross-section in horizontal outwardly spiraled flow for air-water and R-113 liquid/vapor flows. The flow patterns observed in the spiral coil geometry proved to be similar to those in helical coil vertical up-flow. The transition to annular flow was also observed to be a slug-annular type of transition. Because the curvature of a spiral coil changes along the flow channel -- i.e. the coil curvature decreases for outward flow as the coil diameter increases -- this transition was observed, for a certain gas flow rate, to occur first in the upstream portion of the channel where the smallest coil diameter (largest curvature) occurred. Then, this transition will develop downstream towards a larger coil diameter if the gas flow rate increases under the same liquid flow rate. This is consistent with the observation in helical coil vertical up-flow that the centrifugal force caused by the flow channel curvature tends to cause slug-annular transition to occur earlier for the same flow condition and same flow channel tube diameter. The transition identified for each test condition conducted in the present study is that flow condition for which annular flow exists along the entire length of the spiral coiled flow channel. At this transition condition, in accordance with the preceding argument, the transition should occur in the region having the largest coil diameter, i.e. just before exiting from the test section.

An additional observation of interest that was made is that the periodic backward motion of the liquid film at the channel bottom between slug surges that was observed in the helical coil vertical upflows was not observed in the spiral coil horizontal outward flow. This is probably due to the absence of any inclination in the flow channel.

3.2.2 Comparison with Existing Flow Maps

Like the analysis for the helical coil data, the observed flow patterns in spiral coil tests were compared with four flow maps, the Baker modified flow map, Taitel & Dukler map, Choe et al map and Uddin map, in Figures 3.17 — 3.24. As shown in Figures 3.17 — 3.22, the Baker map, Taitel & Dukler map, and Uddin map all show disagreement with the present air-water and R-113 test data. However, the Choe map gives a good prediction of intermittent-annular transition for the air-water data if the separated flow pattern were replaced by intermittent flow pattern (see Figure 3.23). As seen in Figure 3.24, the slug-annular transition for R-113 test data is much higher than the transition line predicted in the Choe map for air-water, but if it were shifted upward, it could predict the R-113 data quite well. These results are similar to those for helical coil vertical up-flows.

3.2.3 Modified Correlation to Predict Slug-Annular Transition in Spiral Coil Horizontal Outward Flow

Because no study on flow pattern transitions in spiral coils has been seen in the literature and there is a similarity of flow pattern behaviors in spiral coil horizontal outward flow to that in helical coil vertical up-flow, the previously developed correlation herein for slug-annular transition in helical coil vertical up-flow is also used here to predict the slug-annular transition in spiral coil horizontal outward flow. An additional modification is made, however, to take into account the changing curvature of the coil along the flow channel. Instead of giving a transition line as in a helical

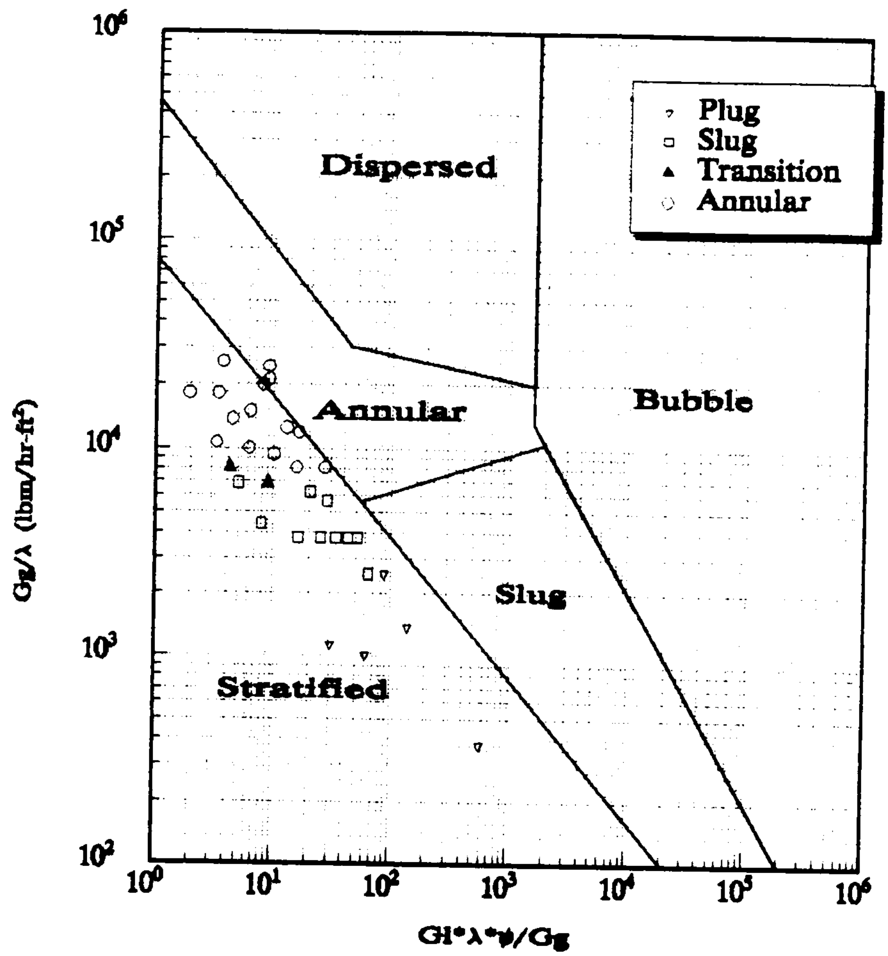

Figure 3.17 Modified Baker map, air-water, circular tube, spiral coil horizontal outward flow

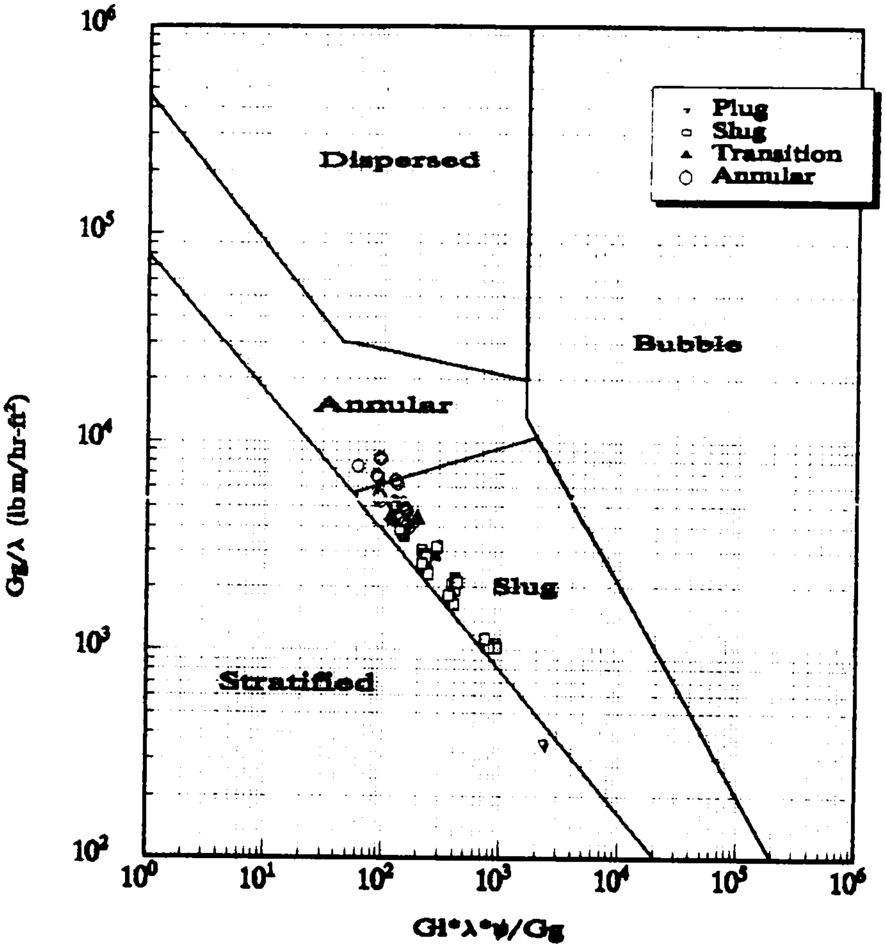

Figure 3.18 Modified Baker map, R-113 liquid/vapor, circular tube, spiral coil horizontal outward flow

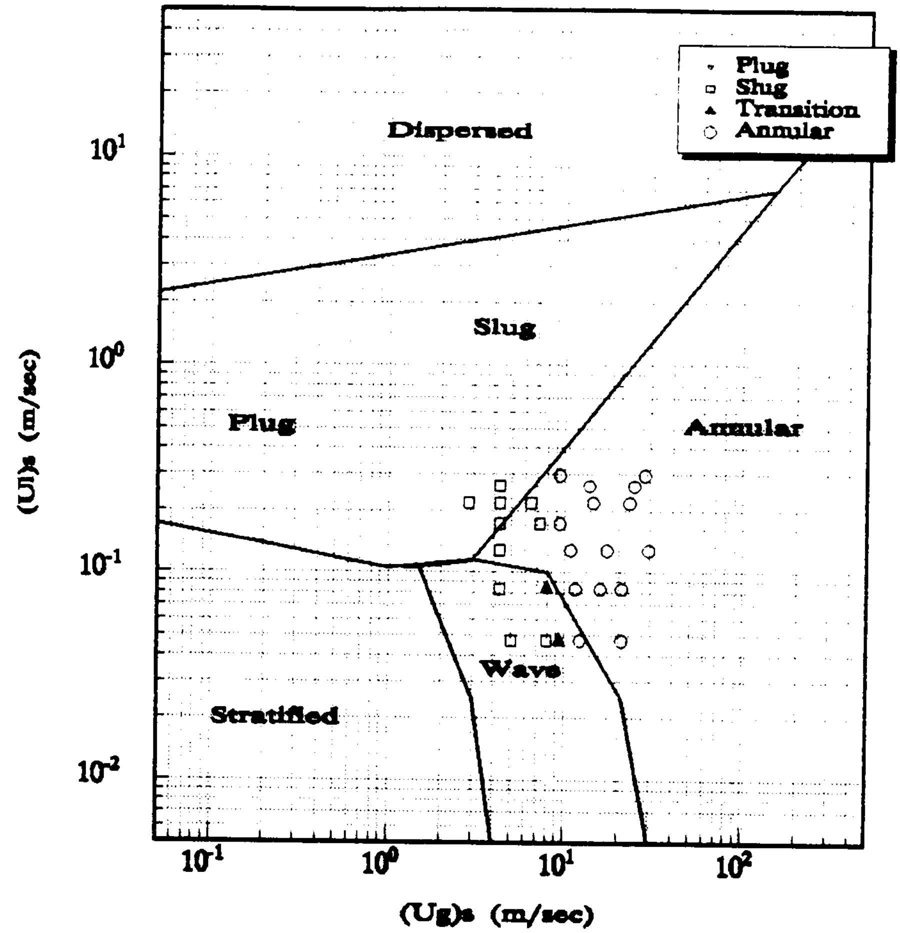

Figure 3.19 Taitel and Dukler map, air-water, circular tube, spiral coil horizontal outward flow

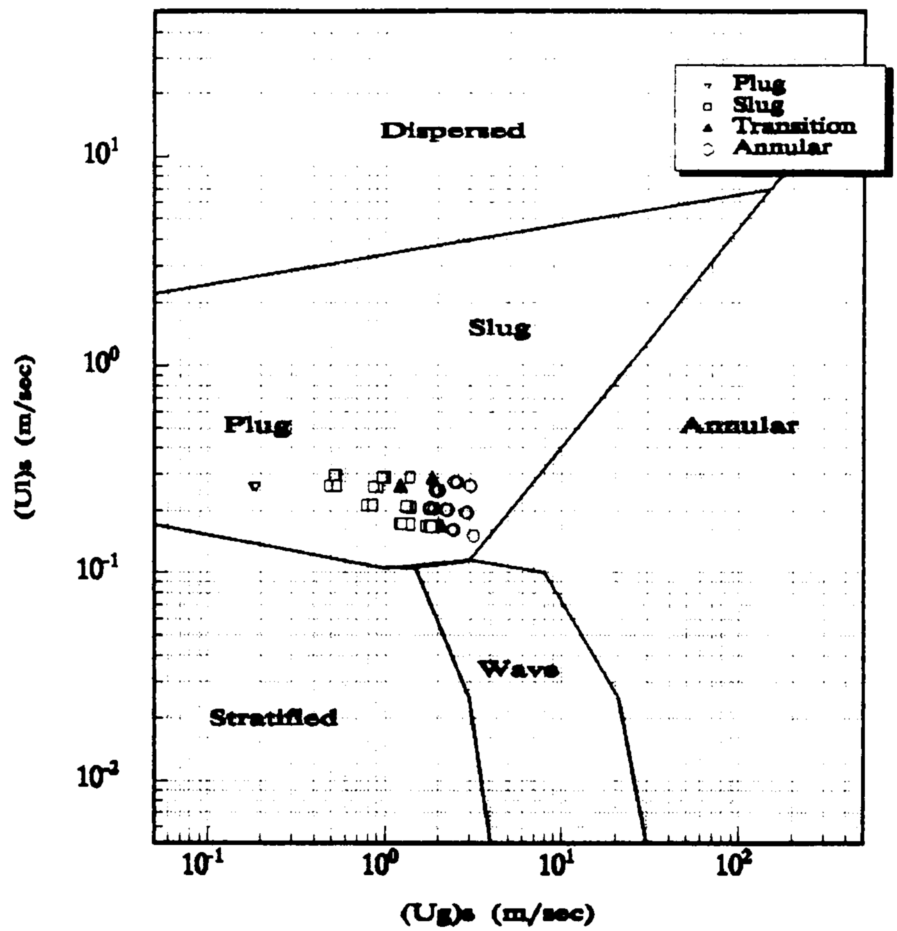

Figure 3.20 Taitel and Dukler map, R-113 liquid/vapor, circular tube, spiral coil horizontal outward flow

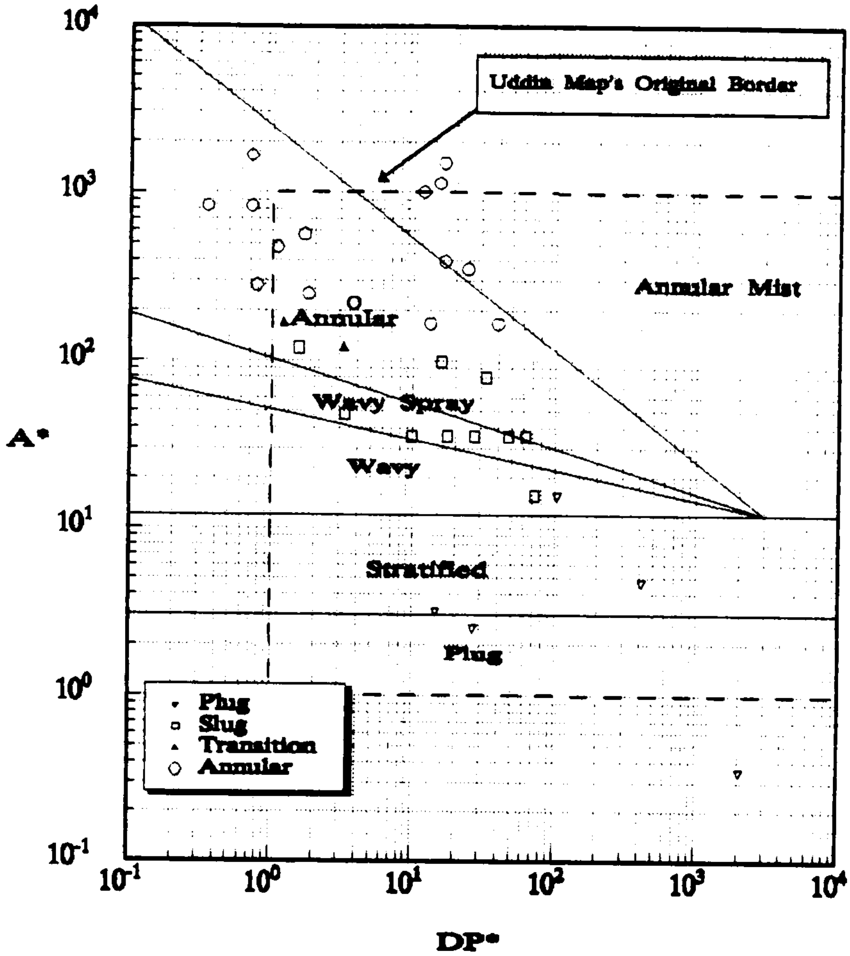

Figure 3.21 Uddin flow map, air-water, circular tube, spiral coil horizontal outward flow

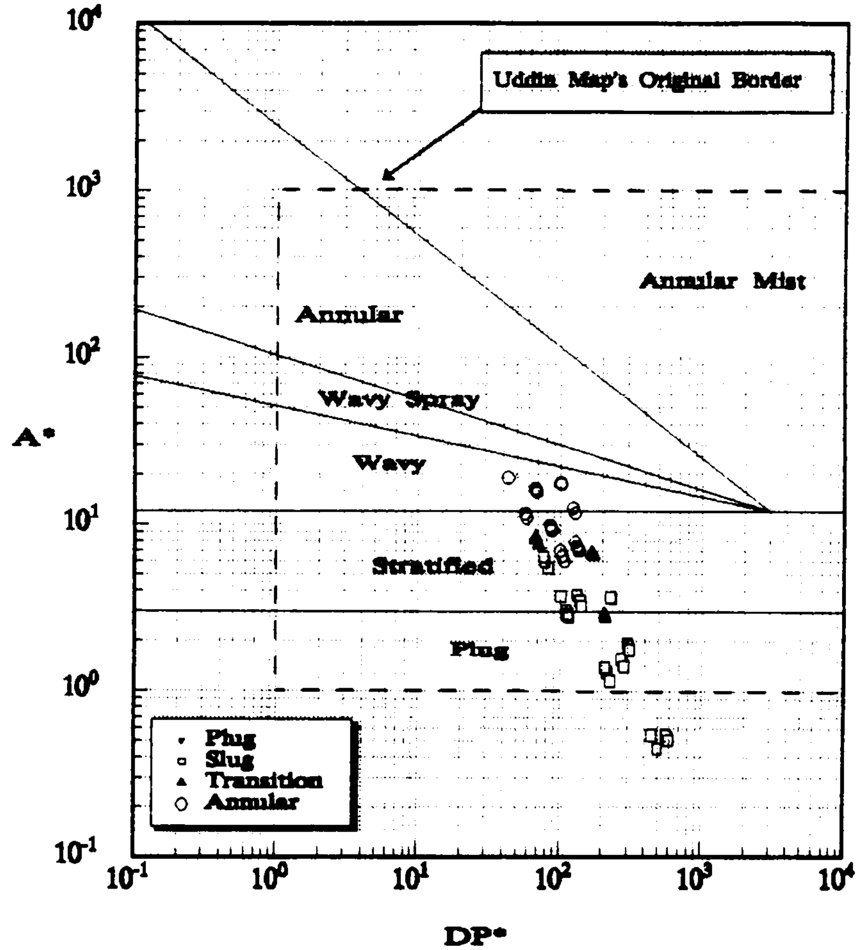

Figure 3.22 Uddin flow map, R-113 liquid/vapor, circular tube, spiral coil horizontal outward flow

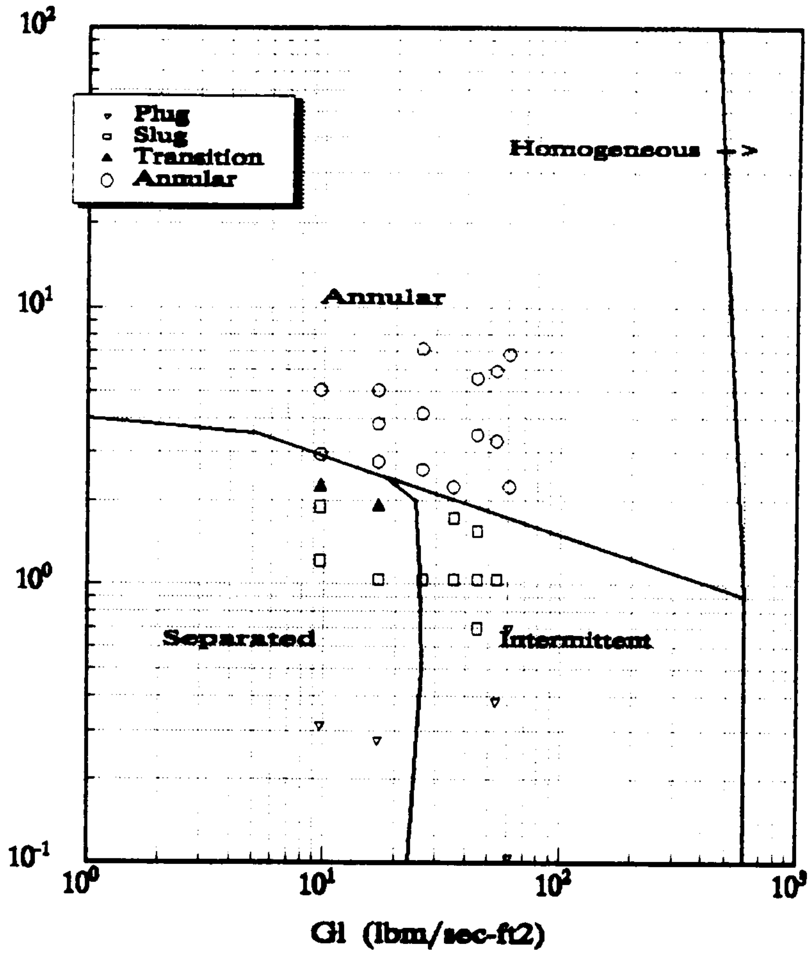

Figure 3.23 Choe, Weinberg, & Weisman map, air-water, circular tube, spiral coil horizontal outward flow

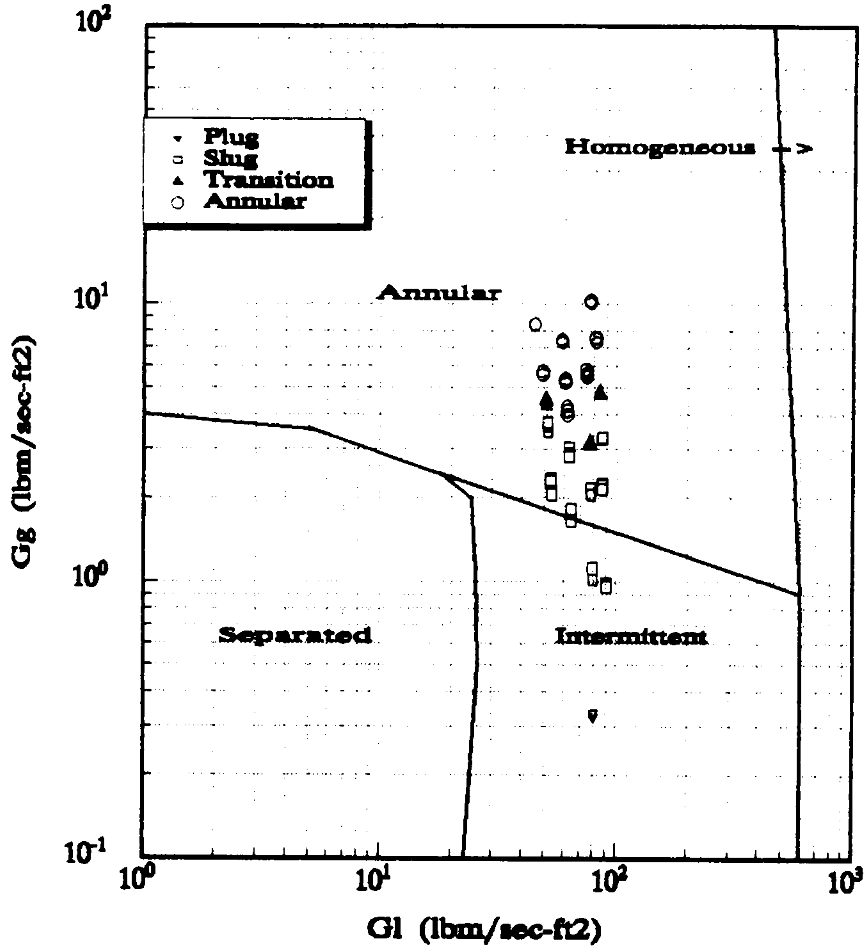

Figure 3.24 Choe, Weinberg, & Weisman map, R-113 liquid/vapor, circular tube, spiral coil horizontal outward flow

coil system with a constant coil diameter, the transition in the spiral coil geometry is identified as a band bounded by upper and lower transition lines which correspond to the largest and smallest coil diameters of the spiral coil. The upper and lower slug-annuler transition lines for circular tube spiral coil horizontal outward flow are given as follows:

$$G_{g,lower} = 10\ [1-(\frac{d_i}{D_{c,min}})^{.88}]\ [\frac{\rho_g/(\Delta\rho_{g,l}\sigma)^{1/2}}{\rho_a/(\Delta\rho_{a,w}\sigma_w)^{1/2}}]^{.34}\ G_{l,lower}^{-.285}(\frac{d_i}{d_{ref}})^{.38} \quad (3.5)$$

$$G_{g,upper} = 10\ [1-(\frac{d_i}{D_{c,max}})^{.88}]\ [\frac{\rho_g/(\Delta\rho_{g,l}\sigma)^{1/2}}{\rho_a/(\Delta\rho_{a,w}\sigma_w)^{1/2}}]^{.34}\ G_{l,upper}^{-.285}(\frac{d_i}{d_{ref}})^{.38} \quad (3.6)$$

where, $\Delta\rho_{w,a} = (\rho_w - \rho_a)$, in which ρ_a = .0745 lb_m/ft^3 (1 atm, 70 °F) and ρ_w = 62.31 lb_m/ft^3 (1 atm, 70 °F); d_{ref} = 1.5 inches. The water surface tension, σ_w, is taken to be that at 70 °F, which is .0644 N/m.

In Figures 3.25 and 3.26, the test data for air-water and R-113 liquid/vapor flow in the circular cross-section spiral coil are compared with the proposed correlations (Equations (3.5) & (3.6)), together with the Choe map intermittent-annular transition line. Good agreement is shown for air-water data. Fairly good agreement is shown for the R-113 data with some fluctuation occurring in the vicinity of the transition band. These results suggest that the same transition criteria can be used in the spiral coil horizontal outward flow as in the helical coil vertical upward flow for the coil geometries of the present study. The transition band for the spiral coil, instead of a transition line as in the case of a helical coil, reflects the characteristics of the variation of the coil curvature of a spiral coil upon

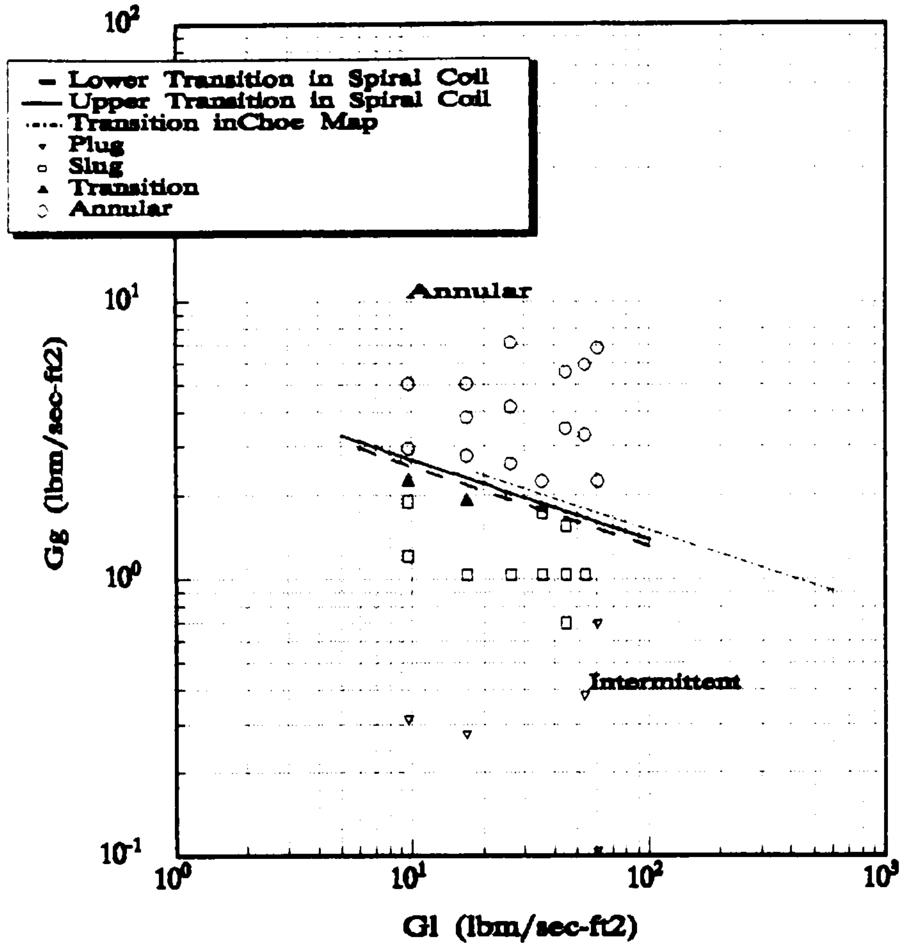

Figure 3.25 Modified correlation for slug-annular transition for spiral coil horizontal outward flow in circular tube, air-water

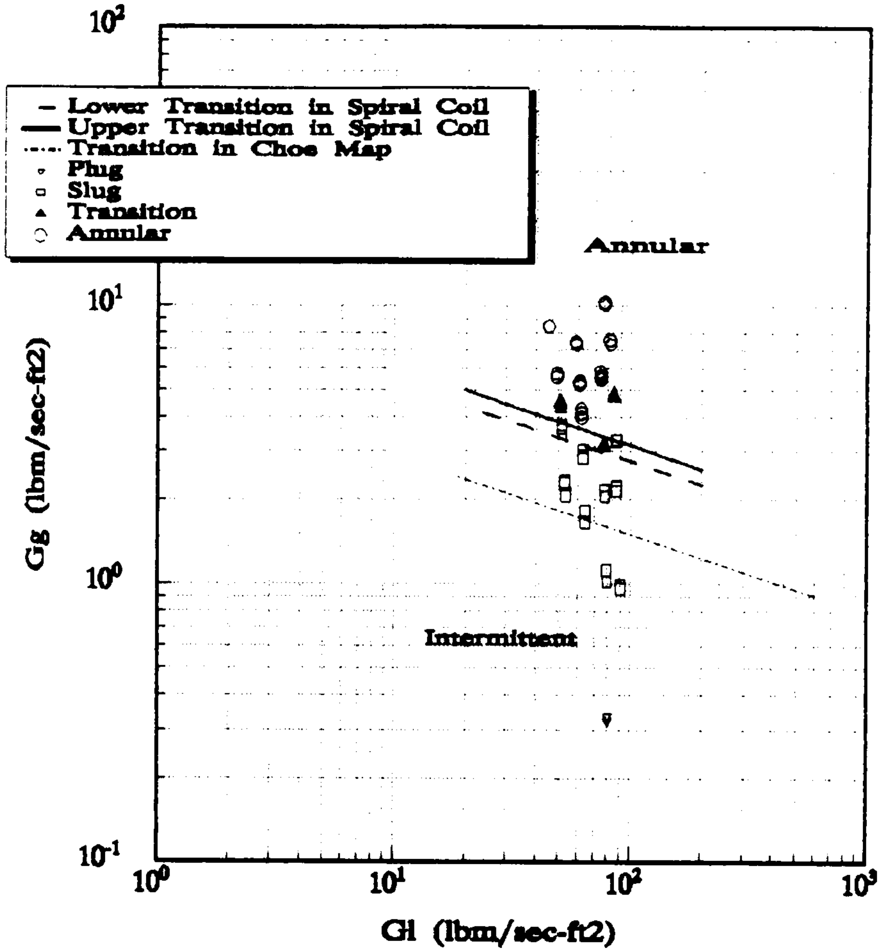

Figure 3.26 Modified correlation for slug-annular transition for spiral coil horizontal outward flow in circular tube, R-113 liquid/vapor

the flow pattern transition. However, as seen in Figures 3.25 & 3.26, when the curvature ratio D/d changes from 6.7 (D_{min}/d_i) to 19.4 (D_{max}/d_i) the transition line does not shift much. The small curvature effect compared with the property effects, is in agreement with the conclusion made earlier for helical coil vertical upflow conditions. Also, the successful use of the slug-annular transition correlation developed here for helical coil vertical up-flow gives credits to the conclusion by Hasan (1988) [27] that in straight tubes the small pipe inclination does not affect the flow pattern and its transition, except for shrinking the existence of a stratified flow pattern. Apparently, a similar conclusion can be drawn for flows in coiled tubes.

The fairly good agreement of the slug-annular transition prediction in spiral coils by using the empirical correlation developed herein from helical coil data provides additional support for its application -- predicting the slug-annular transition in horizontal and near horizontal coiled tubes.

3.3 Summary

Helical Coil Vertical Up-Flow

- The flow patterns observed in helical coil vertical-up flow were similar to those observed in horizontal straight tube. They are:
    - Bubble

· Plug

· Slug

· Annular

The stratified flow pattern was not observed as might be expected in a horizontal straight tube, but was replaced by a slug flow pattern in the same flow range. This is apparently due to the slight inclination of the flow channel, and has been confirmed by other investigators [27,58] for flows in straight channels with small angles of inclination. A backward motion of the liquid film at the channel bottom, between slug surges, was observed for helical coil vertical up-flow conditions at some low gas flow rates. This also appears to be due to the pipe inclination and has also been reported by other earlier investigators [46].

• The observed transition to an annular flow pattern occurs from a slug flow pattern.

• It was concluded that the tube curvature, fluid properties, and flow channel cross-section have an influence upon the slug-annular transition. Among them the properties effect is the most dominant one.

• Three sets of experimental data of air-water and R-113 liquid/vapor in a circular tube, and R-113 liquid/vapor in a near square cross-section helical coil test section with vertical up-flow, are compared with four flow maps. They are the modified Baker flow map, Taitel & Dukler map, Choe et al map, and the Uddin flow map. None of these maps was able to adequately predict the present helical vertical up-flow test data. However, the Choe map gives the closest prediction for the transition to annular flow.

• An empirical correlation of the slug-annular flow pattern transition for circular cross-section helical coil vertical up-flow is developed. It gives good agreement with the air-water and R-113 test data.

• With a shape factor correction, an empirical correlation of slug-annular transition in rectangular cross-section channels for helical coil vertical up-flow is proposed.

Spiral Horizontal Outward Flow

• The flow patterns observed for horizontal outward flow in a spiral coil were similar to those observed in helical coil vertical up-flow. Even though there is no flow channel inclination in a horizontal spiral coil orientation, the stratified flow pattern was still not observed. The backward motion of the liquid film at the channel bottom between slug surges, at some low gas flow rates, was not observed simply because the flow channel has no inclination in this situation. The observed transition to the annular flow pattern in the test ranges studied is also a slug-annular type transition.

• Two sets of the test data in spiral coil horizontal outward flow of air-water and R-113 in circular tube were compared with the same four flow maps as for helical coil data. Similar results as for the helical coils were obtained.

• The transition between the slug and annular flow patterns in spiral coil horizontal outward flow are about the same as in helical coil vertical up-flows. The difference to be noted is that the transition line in spiral coils is not as clearly defined as in helical coils because of the variation of coil diameter along the flow channel. Instead, for the spiral coil, the transition from slug to annular flow was designated by a band which reflects the largest and smallest curvature ratios throughout the entire spiral coil flow channel. The overlapped slug-annular transition line/band between helical and spiral coils suggests that the small flow channel inclination does not appreciably affect the flow pattern transition in coiled tubes. Correlations to predict the upper and lower slug-annular transition lines for circular tube spiral coil horizontal outward flow are proposed.

CHAPTER 4

PRESENTATION AND DISCUSSION OF PRESSURE DROP RESULTS

4.1 INTRODUCTION

For two-phase flows, the pressure drop is strongly affected by the flow pattern because the momentum characteristics of the flow are dependent on the spatial configuration formed by the two phases. The pressure drop for two-phase flow inside a coiled flow channel can be divided into three components: gravitational pressure drop, accelerational pressure drop, and frictional pressure drop, just as for two-phase flow in straight tubes, i.e.,

$$\Delta P_{TP} = \Delta P_g + \Delta P_a + \Delta P_f \tag{4.1}$$

or, it can be expressed in the form of pressure gradients,

$$\left(\frac{dp}{dz}\right)_{TP} = \left(\frac{dp}{dz}\right)_g + \left(\frac{dp}{dz}\right)_a + \left(\frac{dp}{dz}\right)_f \tag{4.2}$$

Therefore, to obtain the two-phase frictional pressure drop from the measured pressure drop values in the present study one may subtract the accelerational and gravitational pressure drop components from the total measured pressure drop.

1. Gravitational Pressure Drop

The gravitational pressure drop in two-phase flow can be expressed as

$$\Delta P_g = \rho_{TP} \frac{g}{g_c} \Delta z \tag{4.3}$$

where, ρ_{TP} is the two-phase mixture density, g is the gravitational acceleration, g_c is the gravitational conversion factor, and Δz is the elevation in the gravity direction. Two methods are used to estimate the two-phase mixture density. One method uses mass quality, while the other uses the void fraction.

A. Mass Quality Method

$$\frac{1}{\rho_{TP}} = \frac{x}{\rho_g} + \frac{(1 - x)}{\rho_l} \tag{4.4}$$

where, ρ_g and ρ_l are the density of gas and liquid, respectively, and x is the quality of the two-phase mixture.

B. Void Fraction Method

In this method, the two-phase void fraction may be calculated by

$$\alpha = \frac{1.0}{(1.0 + X^{0.8})^{0.378}} \tag{4.5}$$

where X is the Lockhart-Martinelli parameter. Equation (4.5) is Martinelli's empirical correlation for two-phase flows at low pressures [56]. The density of the two-phase mixture can then be estimated as

$$\rho_{TP} = \alpha\rho_g + (1 - \alpha)\rho_l \tag{4.6}$$

For the horizontally oriented helical coil and for a spiral coil oriented in a horizontal plane, the term ΔP_g will be negligible. In contrast, for a vertical helical coil orientation, particularly at low void fractions, this term can account for the major part of the total pressure drop. In the present study, Equation (4.4) will be used if using a homogeneous method to analyze two-phase flow pressure drops but Equations (4.5) and (4.6) will be used if using Lockhart-Martinelli model to analyze two-phase flow pressure drops. However, as will be seen later in the analysis, the results are close for the two methods in calculating two-phase mixture average density in the studied ranges herein.

2. Accelerational Pressure Drop

The accelerational pressure drop in a flow arises from the momentum change between the two-phases, which could occur as a result of evaporation and/or expansion of the two-phase flow. In the present tests, the tubes were of uniform cross section, and the data were collected under essentially adiabatic, steady-state conditions. Thus, this term is assumed to be negligible.

3. Frictional Pressure Drop

One of the principal objectives of the present study is to obtain the two-phase frictional pressure drop in coils. Therefore, the following sections will primarily discuss the frictional pressure drop. Since for the present test conditions the accelerational pressure drop is negligible, the frictional pressure drop will be obtained by subtracting only the gravitational pressure drop from the total pressure drop.

4.2 TEST DATA

1. CORRECTION OF ELEVATION HEAD IN ΔP TRANSDUCER MEASUREMENT

The measured values of pressure drop contain the hydrostatic head within the pressure drop measuring lines of the transducer. Therefore, the following steps were taken to exclude this gravitational pressure drop from the measured data to obtain the frictional pressure drop component.

The actual connection of the pressure drop transducer taps across a coil test section is shown in Figure 4.1. As seen in the figure, the measured pressure drop from the Δp transducer is,

$$\begin{aligned} \Delta P_{measured} &= P_{A'} - P_{D'} \\ &= P_A - (P_D + \rho_{l\text{-}room}(g/g_c)(z_2 - z_1)) \\ &= (P_A - P_D) - \rho_{l\text{-}room}(g/g_c)\Delta z. \qquad (4.7) \end{aligned}$$

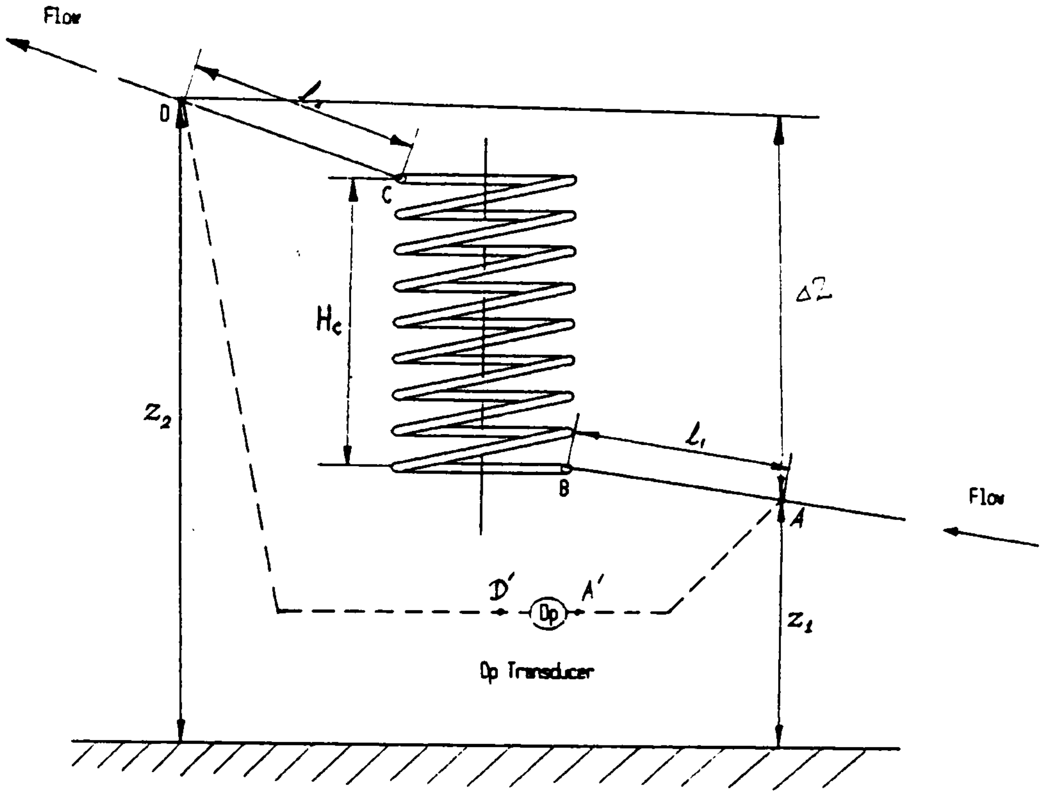

Figure 4.1 Pressure Drop Transducer Measurement Connection

The measured two-phase total pressure drop from point A to point D can be obtained by modifying this equation as follows:

$$(P_A - P_D) = \Delta P_{measured} + \rho_{l\text{-}room}(g/g_c)\Delta z. \tag{4.8}$$

For each test condition of the different coil test sections, flow orientations or fluids, the connection of the Δp transducer varied. The following Table 4.1 listed the actual Δp transducer connection dimensions for the three test conditions for which pressure drop measurements were analyzed in the present study.

2. CORRECTION OF GRAVITATIONAL PRESSURE DROP

According to equations (4.1) and (4.3), the total two-phase pressure drop along the flow channel from point A to D (see Figure 4.1) can be written as

$$(P_A - P_D) = \Delta P_{f\text{-}total} + \rho_{TP}(g/g_c)\Delta z \tag{4.9}$$

where $\Delta P_{f\text{-}total}$ is the total two-phase frictional pressure drop between A and D, and Δz is the elevation difference between A and D. Therefore, combining equations (4.8) and (4.9), the measured total two-phase frictional pressure drop from transducer taps A to D can be obtained by

$$\Delta P_{f\text{-}total\text{-}measured} = \Delta P_{measured} + (\rho_{l\text{-}room} - \rho_{TP})(g/g_c)\Delta z. \tag{4.10}$$

Table 4.1 ΔP Transducer Measurement Connections For Each Test Condition

Test Section	Test Condition Description		
Helical Coil	Table 11 Air/Water Circular Tube Vertical Up-Flow	Table R0 R-113 Liq/Vapor Circular Tube Vertical Up-Flow	Table R1 R-113 Liq/Vapor #1 Rec. Tube (Near Square) Vertical Up-Flow
Coil Dia. D_c	2.953 in	2.953 in	2.992 in
Tube Dia. d_i	0.325 in	0.325 in	.360 in x .325 in (height x width) d_h = .3416 in
Total Length L_c	5.217 ft	5.217 ft	6.595 ft
Inlet & Exit Connection	Straight Tube Connections from Coil to ΔP Transducer Taps		
Inlet Length L_1	0.742 ft	0.755 ft	.820 ft
Exit Length L_2	0.968 ft	1.017 ft	1.083 ft
Total Length L_s	1.709 ft	1.772 ft	1.903 ft
Elevation Δz	Elevation between ΔP Transducer Taps		
$\Delta z = (z_1 - z_2)$	0.551 ft	0.525 ft	.650 ft

3. CORRECTION OF FRICTIONAL PRESSURE DROP ALONG INLET AND EXIT STRAIGHT TUBES

The total frictional pressure drop between A and D (see Figure 4.1) contains two portions, ΔP_{f-s}, the frictional pressure drop along the inlet and exit straight tubes, and ΔP_{f-c}, the frictional pressure drop along the coiled tube of the test section, that is,

$$\Delta P_{f-total} = \Delta P_{f-c} + \Delta P_{f-s}. \tag{4.11}$$

Therefore, the measured frictional pressure drop along the coil flow channel can be obtained by,

$$\Delta P_{f-c-measured} = \Delta P_{f-total-measured} - \Delta P_{f-s-calc.} \tag{4.12}$$

where $\Delta P_{f-total-measured}$ can be obtained from eq. (4.10), and $\Delta P_{f-s-calc.}$ is the calculated frictional pressure drop along the inlet and exit straight tube lengths obtained by applying two-phase frictional pressure drop correlations for two-phase flow in straight tubes. It should be noticed that the values obtained for $\Delta P_{f-c-measured}$ will have different values when using different straight tube two-phase frictional pressure drop correlations to calculate $\Delta P_{f-s-calc.}$.

It should be noted that the straight tube length is about 1/3 of the coil length, or about 1/4 of the total measured length in the present study.

4.3 SINGLE PHASE FRICTIONAL PRESSURE DROP IN HELICAL COILS FOR VERTICAL UP-FLOW

1. Test Results and Analytical Correlations

Single phase pressure drop data were taken for each tested liquid flow rate before the two-phase flow test measurements were made. The helical coil test sections were vertically oriented, with the two-phase mixture flowing upward. The measured pressure drop data were corrected from hydrostatic pressure drop (gravitational pressure drop inside the flow channel and inside the differential pressure transducer measuring lines, see equation (4.10)), and then compared with calculated results by frictional factor correlations with and without a correction factor accounting for coil curvature, respectively.

For flow in the circular cross-section coiled channel, the measured and calculated total frictional pressure drop results are plotted against Reynolds number in Figure 4.2 and 4.3 for both water and R-113 liquids, respectively. Also, the total frictional pressure drop of R-113 liquid in the near square cross-section flow channel is plotted in Figure 4.4. Shown in figures 4.2-4.4, are the measured total frictional pressure drop values between pressure drop transducer taps, which include two sections of straight flow channels and the coiled test section. The dashed lines are the calculated total frictional pressure drop using the following straight channel friction factor (f_s) correlations (equations (4.13) - (4.15)) for single phase flow in both straight and coiled tube lengths.

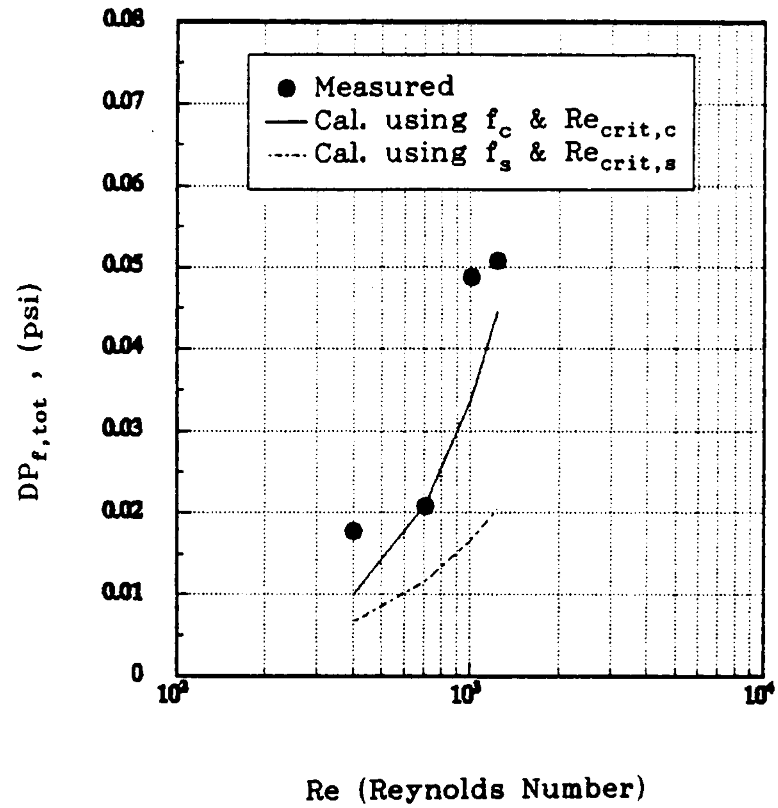

Figure 4.2 Total Frictional Pressure Drop For Water, Helical Coil, Vertical Up-Flow, Circular Tube

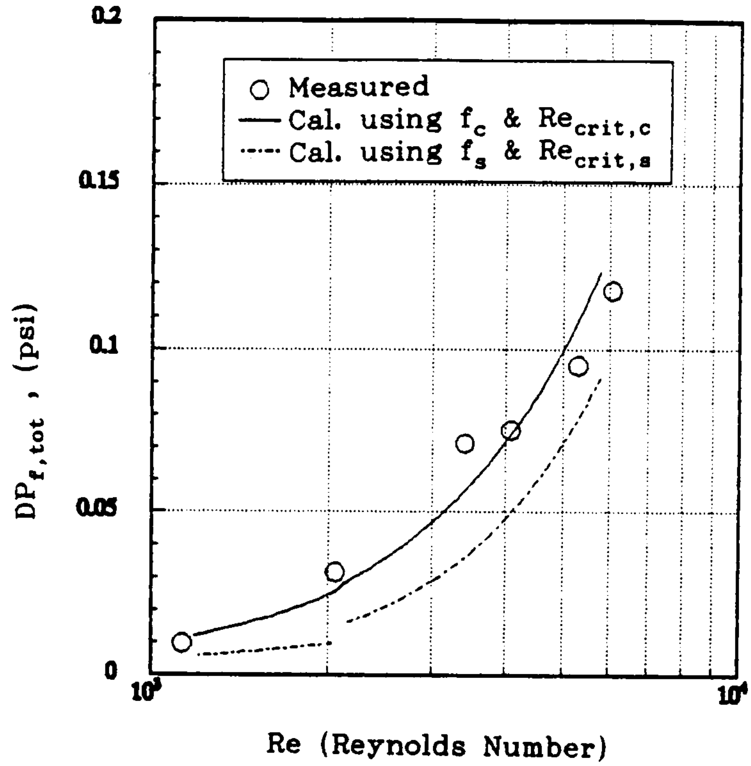

Figure 4.3 Total Frictional Pressure Drop for R-113 Liquid, Helical Coil, Vertical Up-Flow, Circular Tube

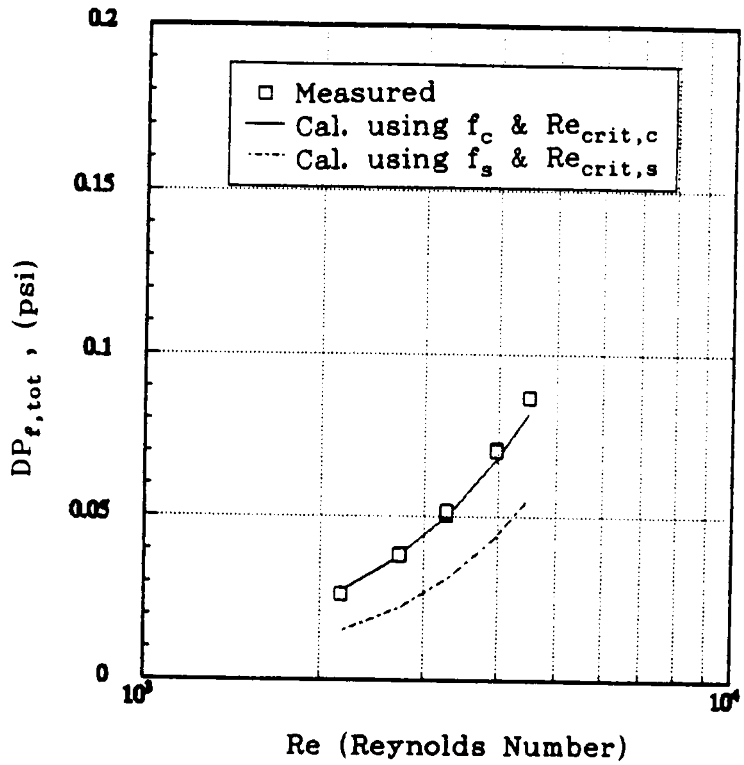

Figure 4.4 Total Frictional Pressure Drop for R-113 Liquid, Helical Coil Vertical Up-Flow, Near Square Tube

$$Re_{crit} = 2100, \quad (4.13)$$

$$f_s = 16/Re, \quad \text{if } Re < Re_{crit}, \quad (4.14)$$

$$f_s = 0.079\ Re^{-0.25}, \quad \text{if } Re > Re_{crit}. \quad (4.15)$$

The solid lines are the calculated total frictional pressure drop, in which, the frictional pressure drop in a straight tube was calculated using the above straight tube frictional factor (f_s) correlations, and the frictional pressure drop in the coiled tube length was calculated using the following correlations developed and proposed specifically to apply to flows in coiled geometries, which are the most recommended combinations of correlations as discussed previously in Chapter 1.

$$Re_{crit} = 2100\ [1 + 12\ (d/D)^{0.5}\ ], \text{ [Srinivasan]} \quad (4.16)$$

$$f_c = (16/Re)*\{1+[0.090De^{1.5}/(70+De)]\}, \text{ if } Re < Re_{crit}, \text{ [Hart]} \quad (4.17)$$

$$f_c = 0.079Re^{-0/25} + 0.0075(r/R_c)^{1/2}, \text{ if } Re > Re_{crit}, \text{ [Mishra]} \quad (4.18)$$

where $R_c = R[1 + (p/2\pi R)^2]$, is a correction for the pitch effect on coil curvature.

A good agreement was shown, for all three conditions, between the measured $\Delta P_{f\text{-}total}$ data and the calculated $\Delta P_{f\text{-}total}$ data with coil-corrected friction factors by Hart et al [28,26,37,49]. This good agreement also proved, to some extent, that the measurements obtained in the present tests are considered to be reliable.

The calculated frictional pressure drop curves using straight-tube friction factor correlations were far below the measured values. These results indicate that, because of the secondary flow effects, the friction loss in a coiled tube is greater than in an equal length of straight tube, and that laminar flow is maintained to higher Reynolds numbers in a coil geometry (see eq. (4.16)).

2. Frictional Pressure Drop Comparison Between Water and R-113 Liquid in Circular Tube For Helical Coil Vertical Up-Flow

The frictional pressure gradients of water and R-113 liquids flowing through a coiled tube in the vertical up-flow direction are plotted in Figure 4.5. From this plot, it is observed that water has a higher pressure gradient than R-113 liquid in coiled or straight tubes; This is likely due to the higher viscosity of water (At 25 °C, the viscosity of water is 2.1788 lb_m/ft-hr while that of R-113 liquid is 1.6449 lb_m/ft-hr).

3. Frictional Pressure Drop Comparison of R-113 Liquid in Circular and Near Square Tubes For Helical Coil Vertical Up-Flow

In order to compare the effect of the flow channel cross-sectional shape on the frictional pressure drop in coiled tubes, the friction factors in the coiled channels are plotted in Figure 4.6 for R-113 liquid in a circular and a near square channel cross-section helical coil test channel, respectively. The hydraulic diameter of the near square channel was 0.3416", about the same as the diameter of the circular tube, which is 0.325".

As shown in Figure 4.6, the friction factors in the tubes of both cross-sections are about the same. This suggests that, in helically coiled

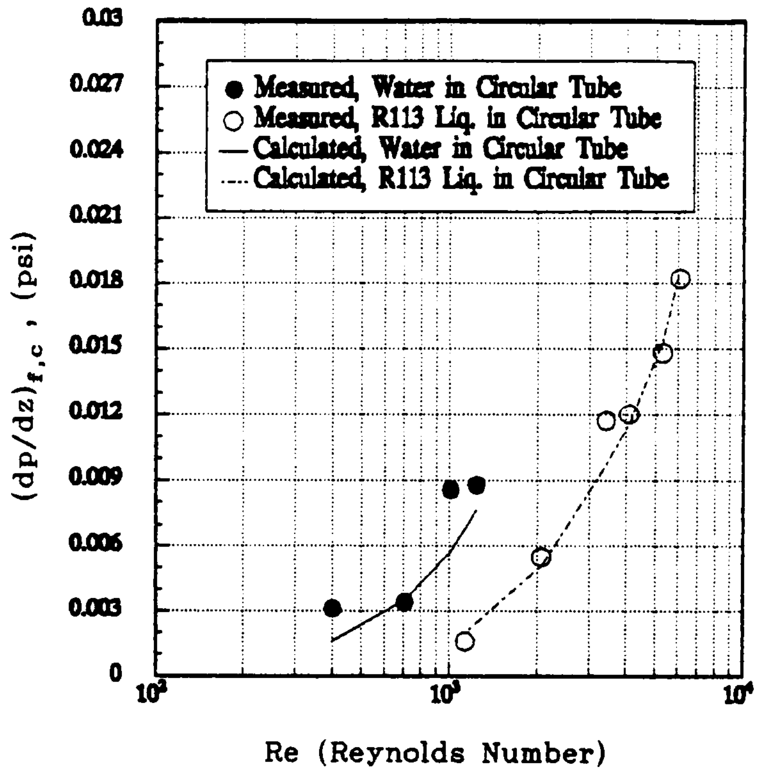

Figure 4.5 Frictional Pressure Gradient for Vertical Up-Flow in Helical Coil with Circular Tube For Water and R-113 Liquid

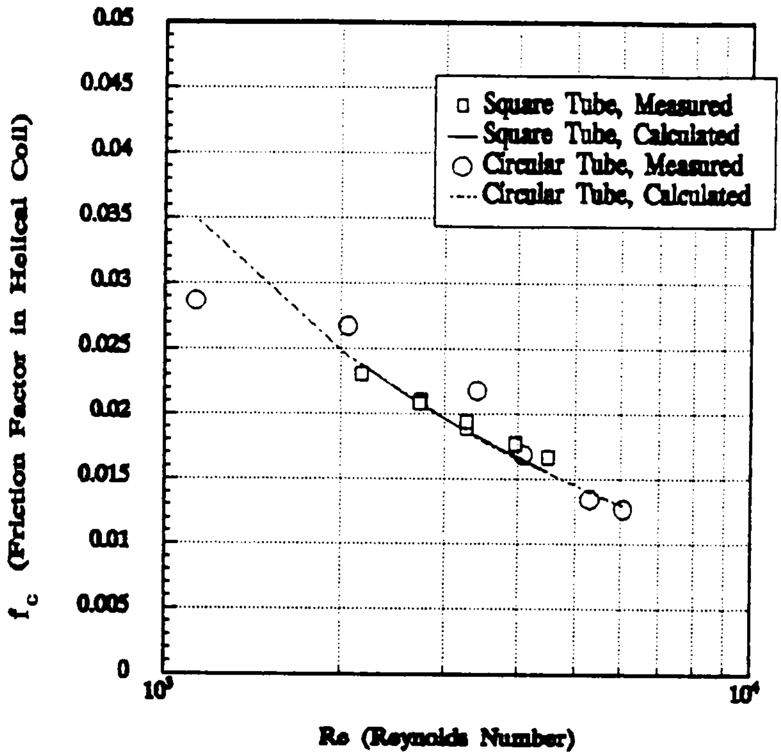

Figure 4.6 Comparison of Friction Factors of R-113 Liquid in Circular and Near Square Tubes for Helical Vertical Up-Flow

tubes, the friction factor through a circular cross-section channel is about the same as that in a channel of near square cross-section having a same hydraulic diameter. Because of the secondary flow occurring in the coil geometry, it may suppress the small shape effect of a square tube having the same hydraulic diameter as a circular tube.

4.4 Two-Phase Frictional Pressure Drop in Helical Coil Vertical Up-Flow

Three sets of test conditions were studied. They are (1) air-water helical coil vertical upflow in circular cross-section flow channel, (2) R-113 liquid/vapor helical coil vertical upflow in circular cross-section flow channel, and (3) R-113 liquid/vapor helical coil vertical upflow in #1 rectangular cross-section flow channel (aspect ratio equal to 1.1, and of the same hydraulic diameter as the circular tube).

4.4.1 General Observation and Analysis

Frictional Pressure Drop and Flow Pattern:

In order to investigate the effect of flow pattern on frictional pressure drop in helical coil vertical up-flows, a large number of observations and measurements of air-water flows were made. In particular, pressure drop data and the associated flow pattern identifications were obtained over a wide span of quality: 0.73% -- 91.13%. The total measured frictional pressure drop across the test section (which includes the straight sections that precede and follow the helical coil section) are plotted in Figure 4.7, together with the identified flow pattern areas. The experimental pressure drop data points in Figure 4.7 are connected by straight line segments.

As seen in Figure 4.7, a direct relationship appears to exist between the measured two-phase pressure drops in the helical coiled channels and the flow patterns, as in straight flow channels. Generally, pressure drop increases as liquid and/or gas flow rates increase. However, the slope of the pressure drop curve changes, depending on the kind of flow pattern that exists in the two-phase flow. It was observed that when the liquid and gas flow rates are both low the observed flow patterns are in the intermittent or developing-annular regions, as indicated in the figures, and the increase of pressure drop with flow rates are moderate. This may be explained as follows. In these types of flow patterns the periodic liquid slugs (in slug flow) or the big pulsating wave peaks within the lower liquid film (in developing-annular flow) largely block the central gas passage way, so that the gas velocity can not increase sharply with an increase of gas flow rate. This implies that in this regions (slug and developing-annular), the slip ratio (V_g/V_l) is close to 1 or the difference between the velocities of the gas and liquid phases is sufficiently small that pressure drop analyses based on homogeneous methods are reasonable.

Further, as seen in Figure 4.7, with increasing higher gas flow rate the increase in the frictional pressure drop starts to increase sharply with the quality. The flow pattern occurring in this region is wavy-annular, based upon the observations of flows in this region. This is an unstable or transient flow region between developing-annular and developed-annular

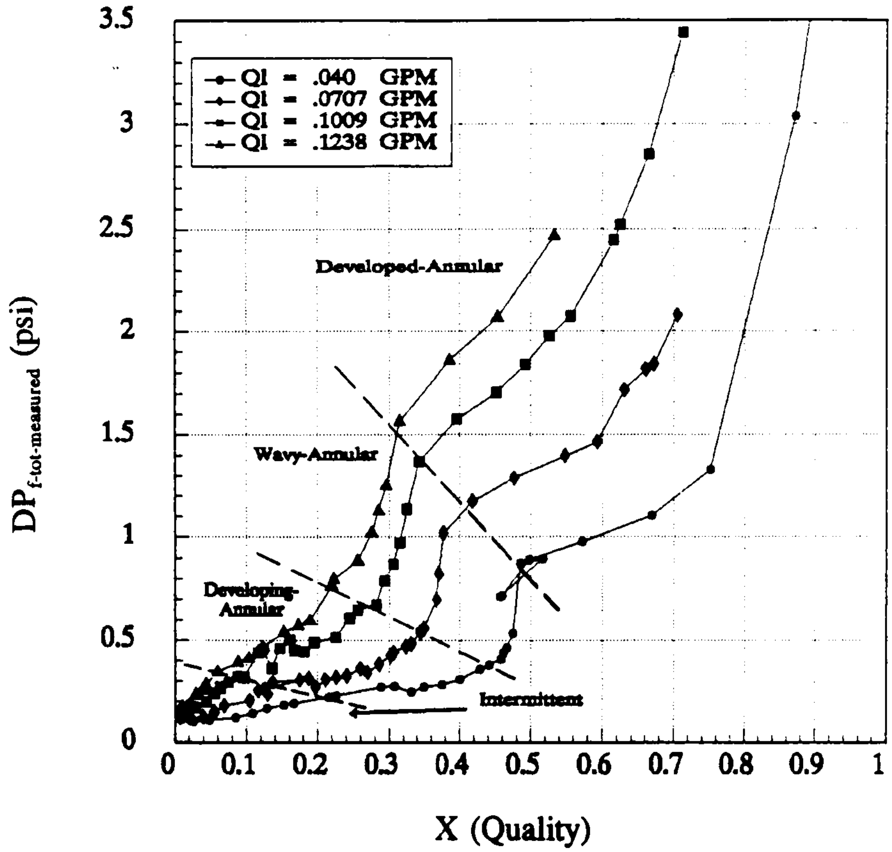

Figure 4.7 Measured Total Frictional Pressure Drop in Helical Coil Vertical Up-Flow, Air-Water, Circular Tube

flow regions. As described earlier in Chapter 3, in wavy-annular flow, the pulsating wave peak surges within the lower liquid film may be sheared away, causing the lower liquid film to become very irregularly, and causing large amount of liquid to be entrained into the central gas core. The sharp slope of pressure drop shown in this region suggests that when analyzing the frictional pressure drop in this region, additional pressure losses may need to be considered which could result from the breakage (entrainment) of wave peak surges of liquid film and from the irregularly wavy interfacial friction loss.

After the wavy-annular region, if the gas flow rate is further increased, the flow enters into the developed-annular flow region. In this region, as described earlier in Chapter 3, the wavy peak surges of the liquid film becomes greatly smoothed, and the annular pattern becomes more symmetric. As shown in Figure 4.7, the pressure drop in this region increases in an exponential manner with the gas quality which may suggest that a high slip ratio exists within this flow pattern. In this developed-annular flow region, the peripheral annular liquid film is more symmetric and has a smoother interface, which allows the gas velocity in the central gas core to increase faster than the liquid velocity in the annular liquid film around the tube periphery. Therefore, homogeneous method based models would be expected to be unsuccessful in predicting the pressure drop in this flow regime.

It is also observed from Figure 4.7, that the flow pattern transition from intermittent flow (slug flow) to developing-annular flow occurs at lower qualities with higher liquid flow rates. The same conclusions can be drawn for the transitions from developing-annular flow to wavy-annular flow, and from wavy-annular flow to developed-annular flow, as well. Since the major purpose of the present study was to investigate the transition to annular flow, and the annular flow region after this transition, the remainder of the experimental conditions were all in the range of quality less than 30%, which is characterized in the present study as the "developing-annular" flow region.

In Figure 4.8, plots are made of total measured pressure drop vs. quality, with corresponding flow patterns, for R-113 liquid/vapor flow in circular and rectangular cross-section flow channels. A portion of the air-water data on Figure 4.7 for vertical up-flow in a circular cross-section flow channel with qualities less than 30% is also shown. As can be seen in Figure 4.8, in the range of quality from 0 -- 30%, the relation of flow pattern and pressure drop for R-113 is similar to that of air-water. The pressure drop gradient is seen to increase as the liquid flow rate or total flow rate increases. Also, the transition from slug flow to annular flow occurs at lower qualities with higher liquid flow rates (or total flow rates). It should be noted that all of the flow patterns for the R-113 data are in the intermittent or developing-annular flow regions. In addition, in the rectangular cross-section flow channel the transition is seen to occur at a higher quality and pressure drop compared to the circular cross-section flow channel (compare Figure 4.8(a) and (b)).

It should also be noticed that, unlike the transition from developing-annular flow to developed-annular flow for air-water flow, no special characteristics, such as a sharp increase, could be observed from the pressure drop vs. quality curves obtained from the three sets of data presented in Figure 4.8.

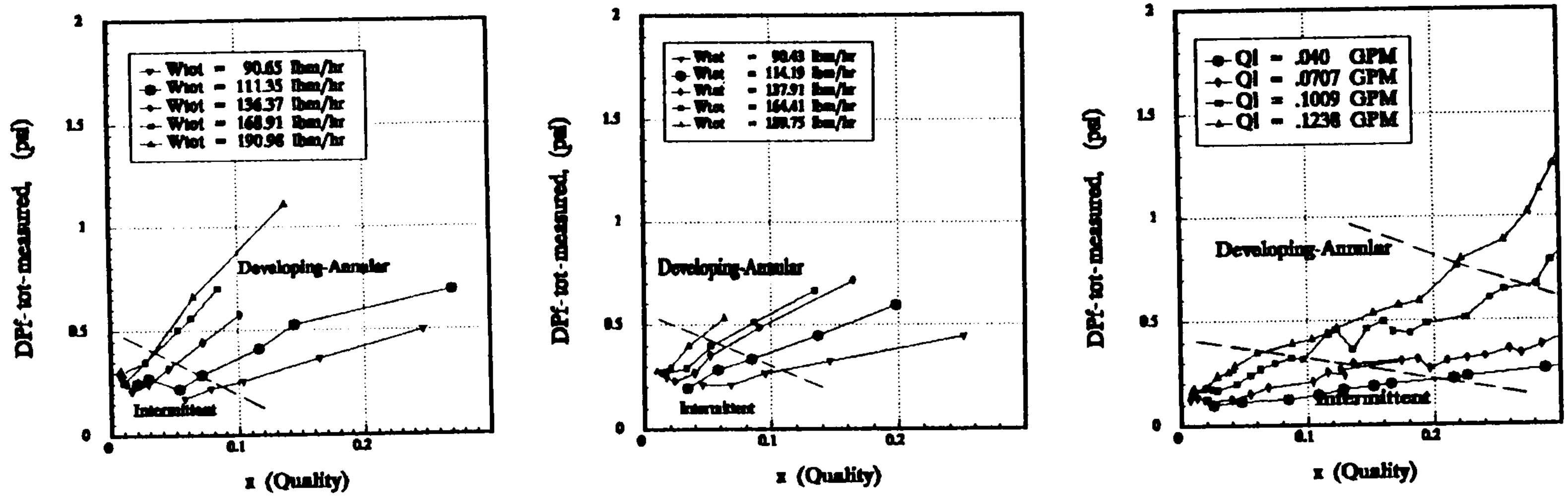

(a) R-113 liquid/vapor (circular tube)

(b) R-113 liquid/vapor (#1 rectangular tube, H/W=1.1)

(c) Air-water (circular tube)

Figure 4.8 Comparison of obtained pressure drops and their associated flow patterns of air-water and R-113 liquid/vapor in circular tube, and R-113 liquid/vapor in near rectangular tube

The preceding observations relative to the data of Figure 4.7 and 4.8 shows that different flow patterns yield different relations of pressure drop with respect to quality and flow rates. Therefore, the ability to predict flow pattern is again shown to be very important in predicting frictional two-phase pressure drop. Conversely, the pressure drop data may also provide useful information for flow pattern analysis, as revealed in Figure 4.7, for example, when the pressure drop experienced dramatic changes as the flow pattern changed from developing-annular flow to developed-annular flow.

Finally, in Figure 4.9 a comparison is made of two methods of calculating the density of a two-phase mixture by plotting the air-water pressure drop data obtained for the vertical up-flow case. In this figure, the solid symbols represent the values of measured total frictional pressure drop calculated from Equation (4.10), in which the two-phase mixture density is calculated by the void fraction method (equations (4.5) and (4.6)), while the open symbols indicate the values of measured total frictional pressure drop obtained by correcting the gravitational pressure drop using the "mass quality method" (homogeneous method, Equation (4.4)) to calculate the two-phase mixture density. Apparently, there is little difference shown by using the two methods here. The other two sets of data obtained in the present study for R-113 result in the same conclusion being drawn as well.

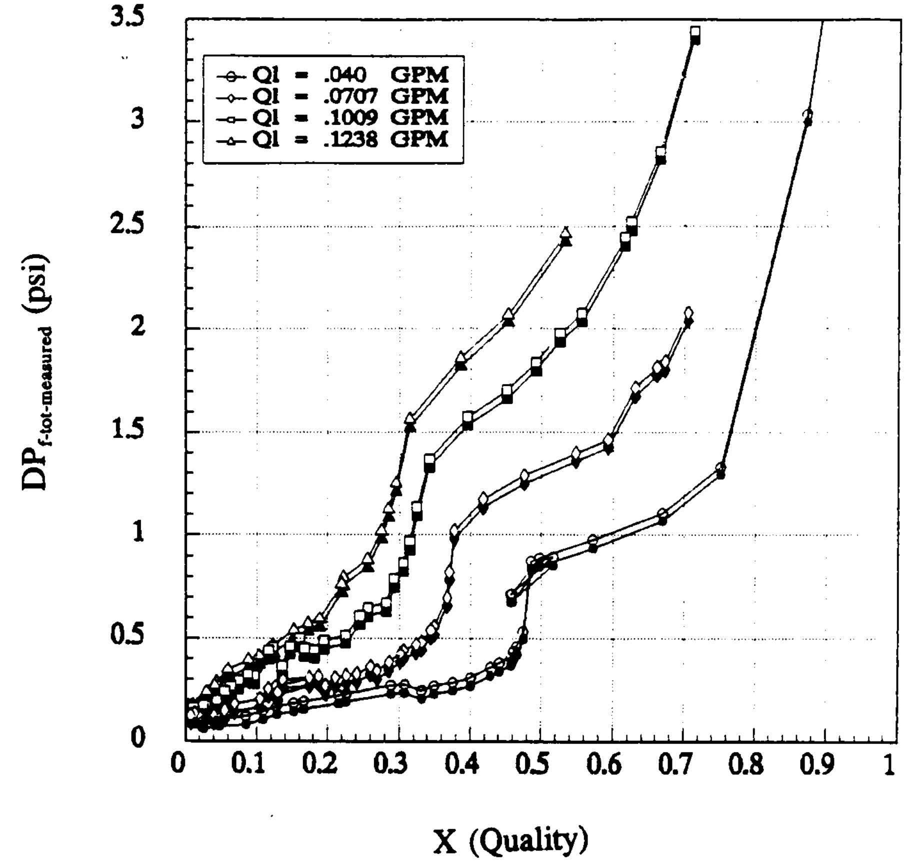

Figure 4.9 Comparison of Calculating the Density of Two-Phase Mixture by Mass Quality Method and Void Fraction Method [56]

4.4.2 Comparison of Measured Frictional Pressure Drop in Helical Coils with Existing Two-Phase Frictional Pressure Drop Correlations in Straight Tubes

There are two commonly used approaches for the experimental and analytical study of two-phase frictional pressure drop in coil geometries. One is to adopt and/or modify the existing single-phase frictional pressure drop models in coil geometries by using the homogeneous method to develop two-phase frictional pressure drop models in coil geometries. The second approach is to modify the existing two-phase frictional pressure drop models in straight tubes, such as the Lockhart-Martinelli model, by taking into account the curvature effect of coiled tubes to develop two-phase frictional pressure drop models in coiled tubes. In this and the following section, efforts were made through the two approaches to analyze two-phase frictional pressure drops for three sets of experimental data of helical vertical up-flow.

Since there is no existing two-phase frictional pressure drop correlations developed for helical coil vertical up-flows, the frictional pressure drop data obtained in the present study were compared with two commonly used two-phase frictional pressure drop correlations developed for flows in straight tubes -- the homogeneous model and the Lockhart-Martinelli model.

Figure 4.10 through 4.13 are plots of the total pressure drops across the test section for air-water flows in the circular tube flow channel. The data is compared with analytical predictions -- the homogeneous model and the Lockhart-Martinelli model. In Figure 4.10 and 4.11 no correction has

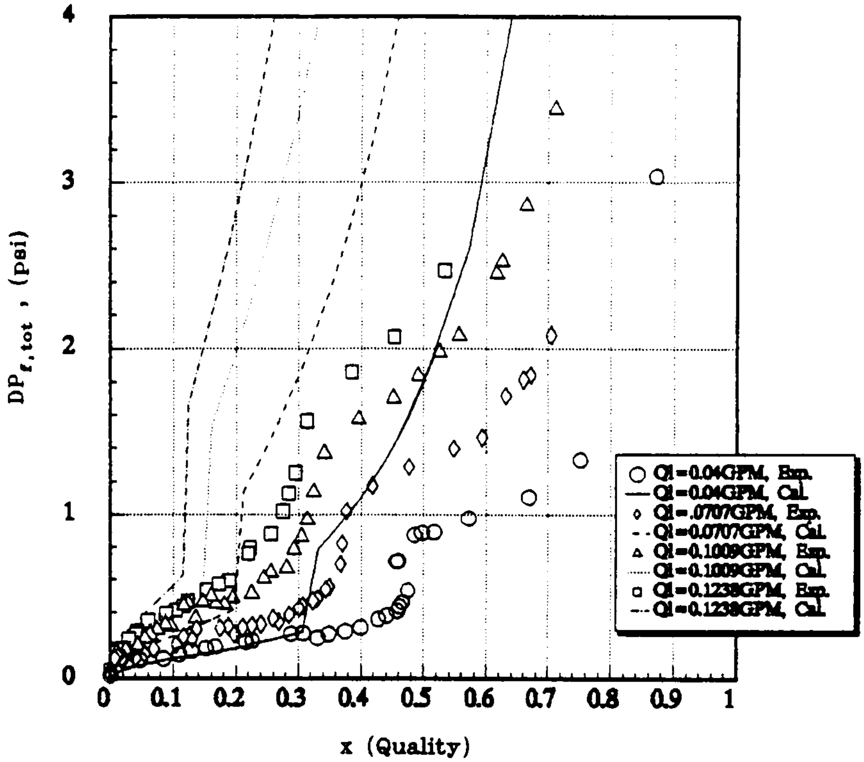

Figure 4.10 Comparison of Measured Total Pressure Drops of Air-Water Vertical Up-Flow With Predictions of Homogeneous Model Without Coil Correction. (Channel Type: Circular)

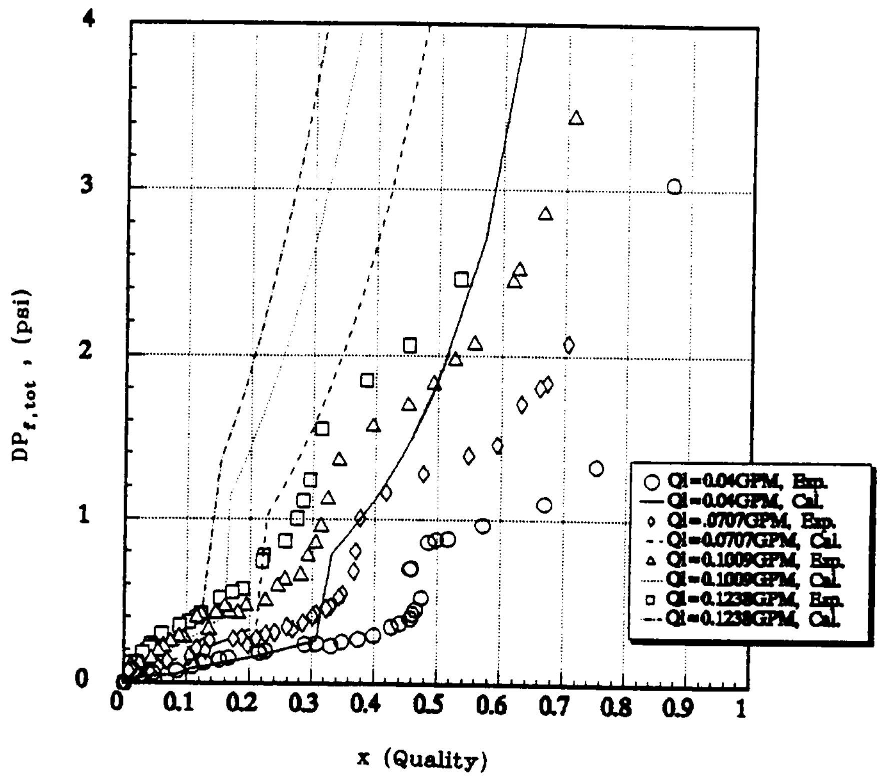

Figure 4.11 Comparison of Measured Total Pressure Drops of Air-Water Vertical Up-Flow With Predictions of Lockhart-Martinelli Model Without Coil Correction. (Channel Type: Circular)

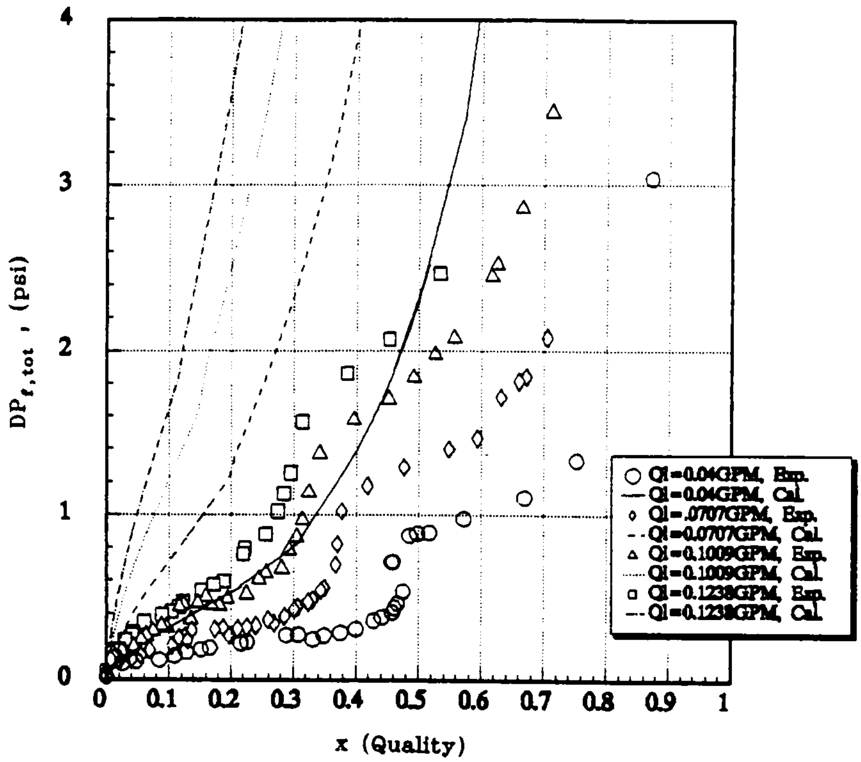

Figure 4.12 Comparison of Measured Total Pressure Drops of Air-Water Vertical Up-Flow With Predictions of Homogeneous Model With Coil Correction. (Channel Type: Circular)

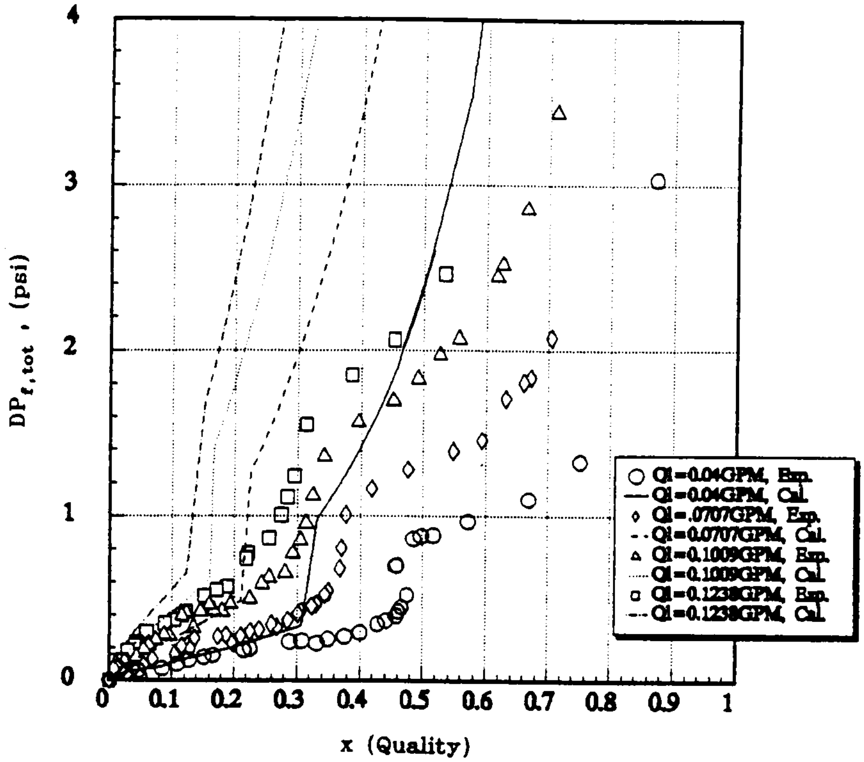

Figure 4.13 Comparison of Measured Total Pressure Drops of Air-Water Vertical Up-Flow With Predictions of Lockhart-Martinelli Model With Coil Correction. (Channel Type: Circular)

been made to the correlations for the curvature effect within the helical coil. In other words, both the homogeneous model and Lockhart-Martinelli model predictions apply to flow in straight channels. It is interesting to observe that the same knee in the curve of the pressure drop vs. quality curves occur in the predictions of the models. These abrupt changes in slope in the model calculations are due to a transition in flow from laminar to turbulent flow in the gas phase.

Figures 4.12 and 4.13 present the same data but in these cases the data is compared with analytical curves based on the homogeneous and Lockhart-Martinelli models which include corrections for coil curvature. The corrections are based upon equations (4.16) through (4.18). As expected from the behavior of single-phase flows, the pressure drops corrected for coil curvature effects are higher than those for the uncorrected, i.e. straight channel, predictions. These higher predicted values produce even larger discrepancies with the measured values beyond the knee in the curves. In general, for both the homogeneous and the Lockhart-Martinelli (L-M) methods, (1) the transition to turbulent flow (in the gas phase) occurs at a higher quality than predicted, and (2) the magnitude of the predicted pressure drop, particularly beyond the laminar-turbulent transition region are higher than those measured, using either the homogeneous or the L-M methods.

In Figures 4.14 through 4.17 similar comparisons are made for the two-phase flow of R-113. In Figures 4.14 and 4.15 the homogeneous and Lockhart-Martinelli methods are plotted for flow in a circular cross-section channel. In Figures 4.16 and 4.17 the same correlations are presented but with the coil corrections indicated by equations (4.16) through (4.18). For

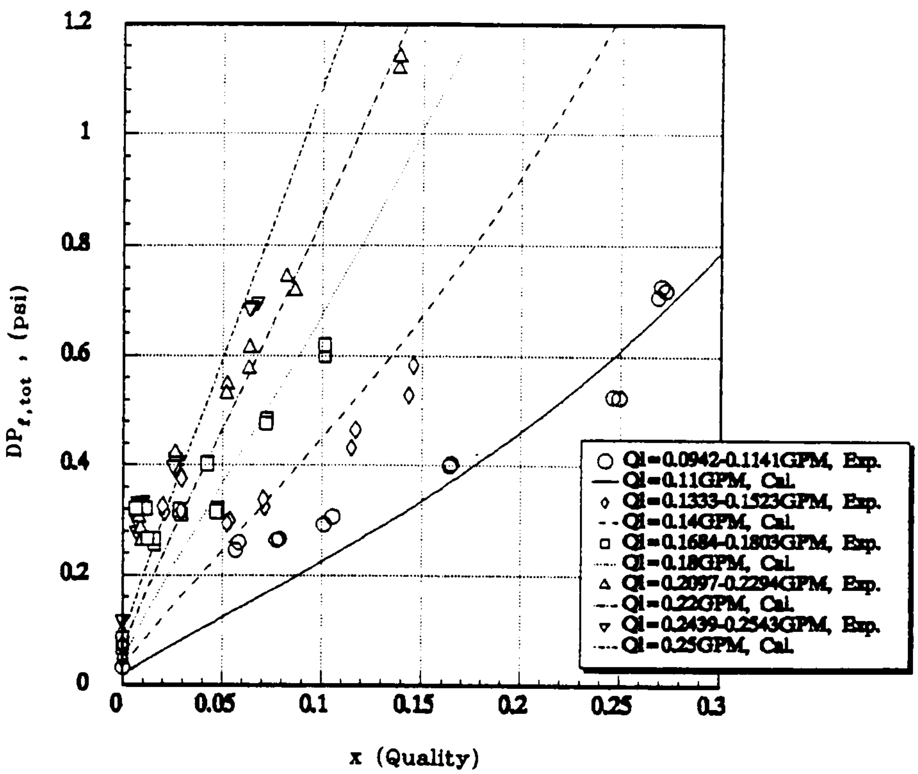

Figure 4.14 Comparison of Measured Total Pressure Drops of R-113 Liquid/Vapor Vertical Up-Flow With Predictions of Homogeneous Model Without Coil Correction. (Channel Type: Circular)

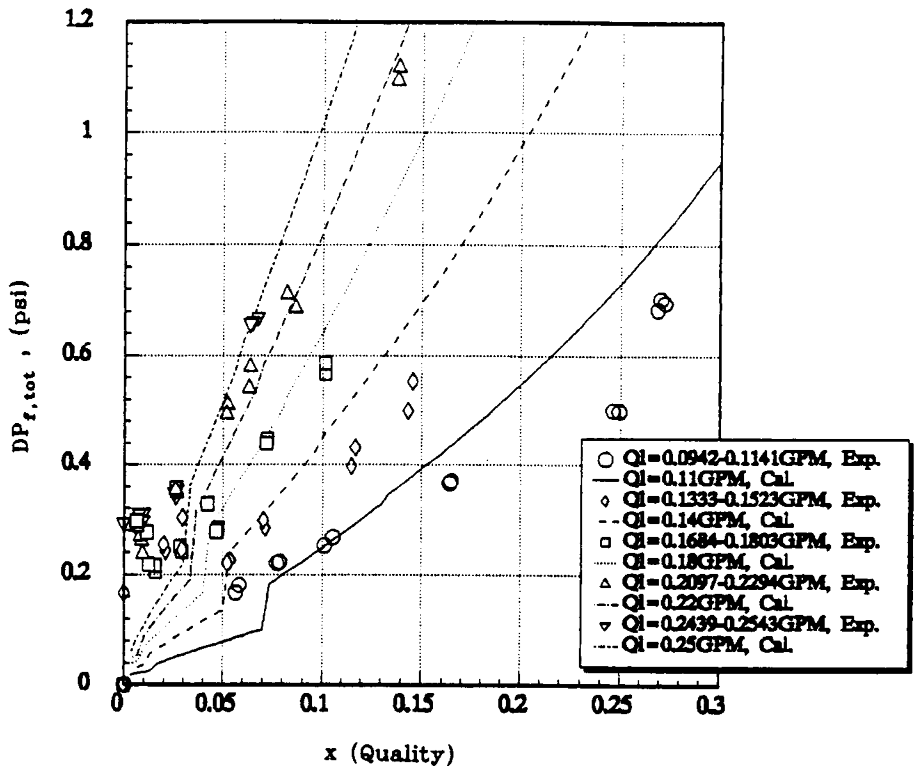

Figure 4.15 Comparison of Measured Total Pressure Drops of R-113 Liquid/Vapor Vertical Up-Flow With Predictions of Lockhart-Martinelli Model Without Coil Correction. (Channel Type: Circular)

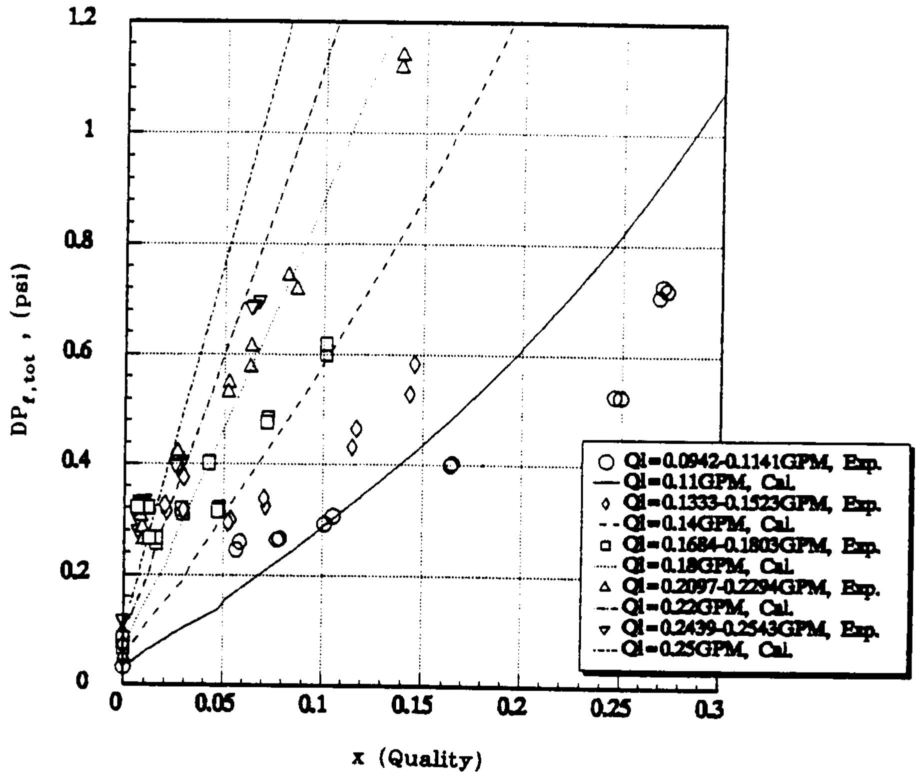

Figure 4.16 Comparison of Measured Total Pressure Drops of R-113 Liquid/Vapor Vertical Up-Flow With Predictions of Homogeneous Model With Coil Correction. (Channel Type: Circular)

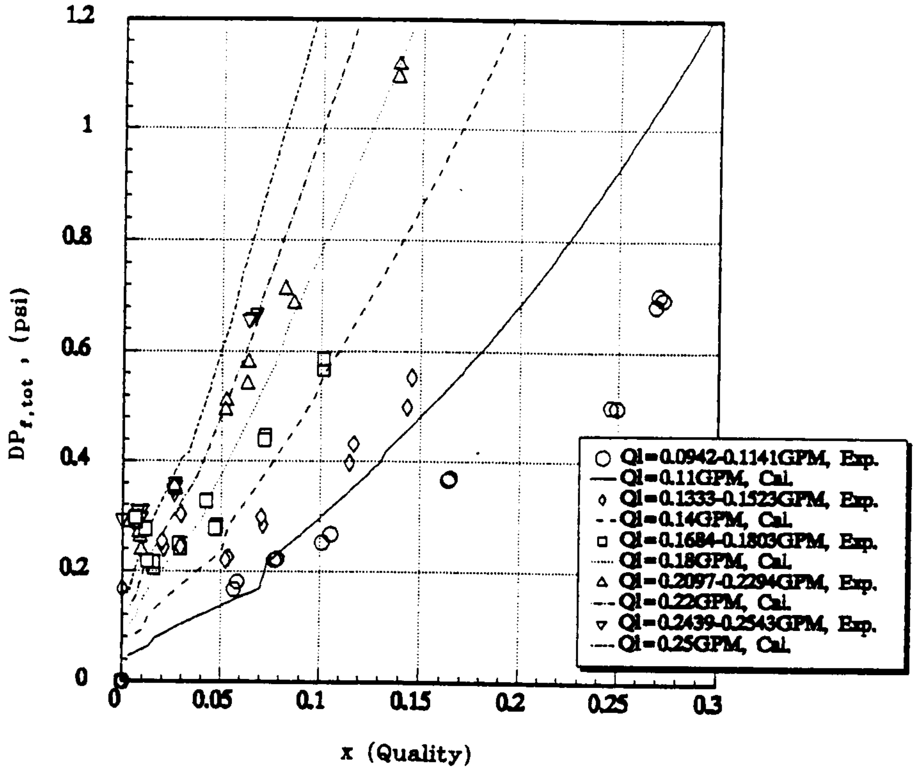

Figure 4.17 Comparison of Measured Total Pressure Drops of R-113 Liquid/Vapor Vertical Up-Flow With Predictions of Lockhart-Martinelli Model With Coil Correction. (Channel Type: Circular)

these R-113 flows, the magnitudes of the predicted and measured pressure drops are in better agreement.

Finally in figures 4.18 through 4.21 the same comparisons with correlations are made for the two-phase flow of R-113 and the coil test section of a rectangular cross-section flow channel. The predicted curves of pressure drop are also in reasonable agreements with the measured values in the sense that they are within comparable magnitude.

To broadly summarize the results presented in Figure 4.10 through Figure 4.21, for the air-water test, the trend of the pressure drop data is predicted by the analytical predictions. However, the quantitative agreement is only fair. For the R-113 flow in the circular cross-section channel both the qualitative and quantitative trends are predicted reasonably. However, for R-113 flow through the rectangular cross-section tube the quantitative agreement is poor, generally being lower than the actual measured pressure drop. In brief the agreement of data with predictive methods can be considered marginal.

4.4.3 Development of Empirical Correlations For Two-Phase Frictional Pressure Drop in Helical Coil Vertical Up-Flow

The general flow pattern and pressure drop analysis in Section 4.4.1 suggests that in the developing-annular and slug flow regions the difference between the gas velocity and liquid velocity is small, in which case the use of a homogeneous method based model to predict pressure drop could be considered reasonable.

As shown in Figure 4.8, the pressure drop data obtained for R-113

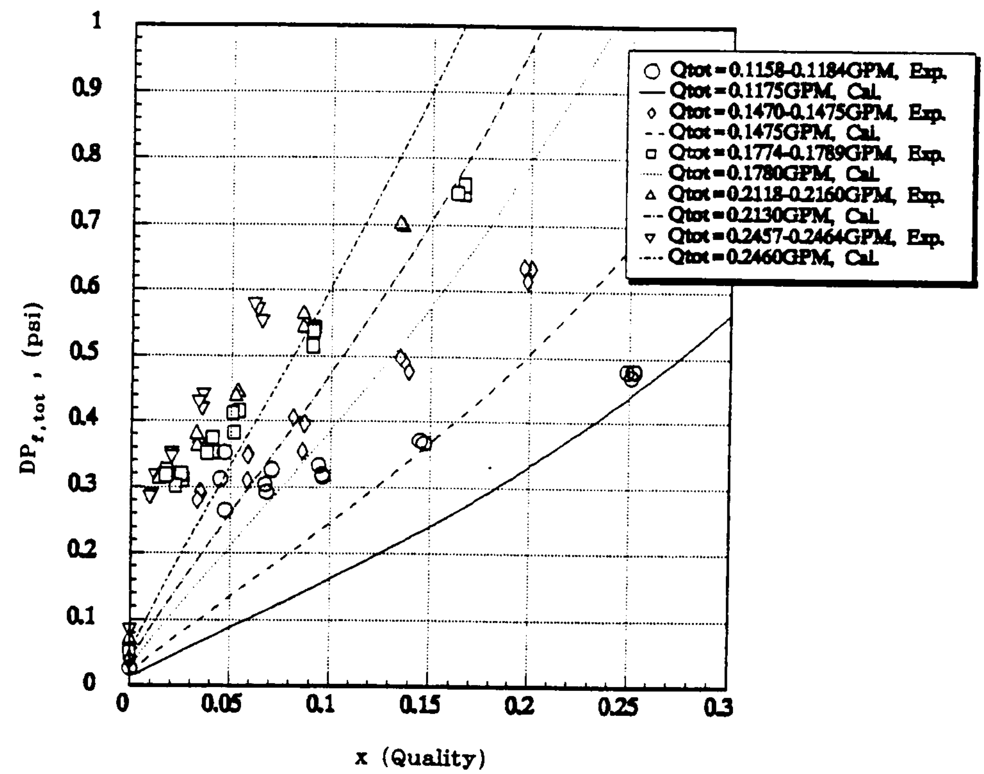

Figure 4.18 Comparison of Measured Total Pressure Drops of R-113 Liquid/Vapor Vertical Up-Flow With Predictions of Homogeneous Model Without Coil Correction. (Channel Type: Rectangular, H / W = 1.0)

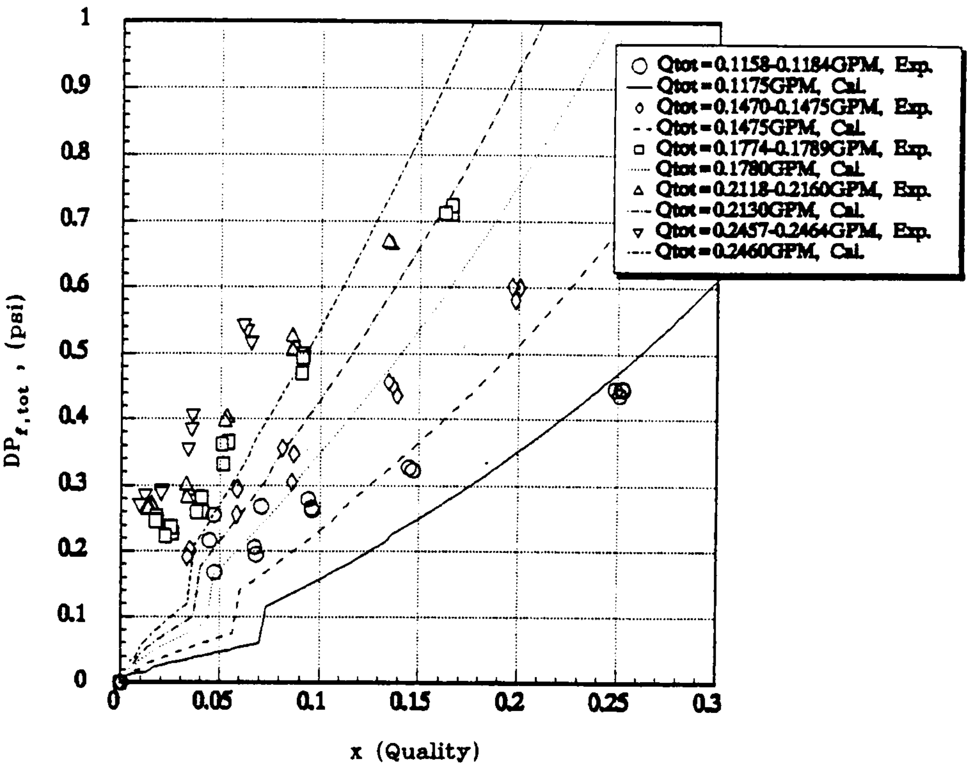

Figure 4.19 Comparison of Measured Total Pressure Drops of R-113 Liquid/Vapor Vertical Up-Flow With Predictions of Lockhart-Martinelli Model Without Coil Correction. (Channel Type: Rectangular, H / W = 1.0)

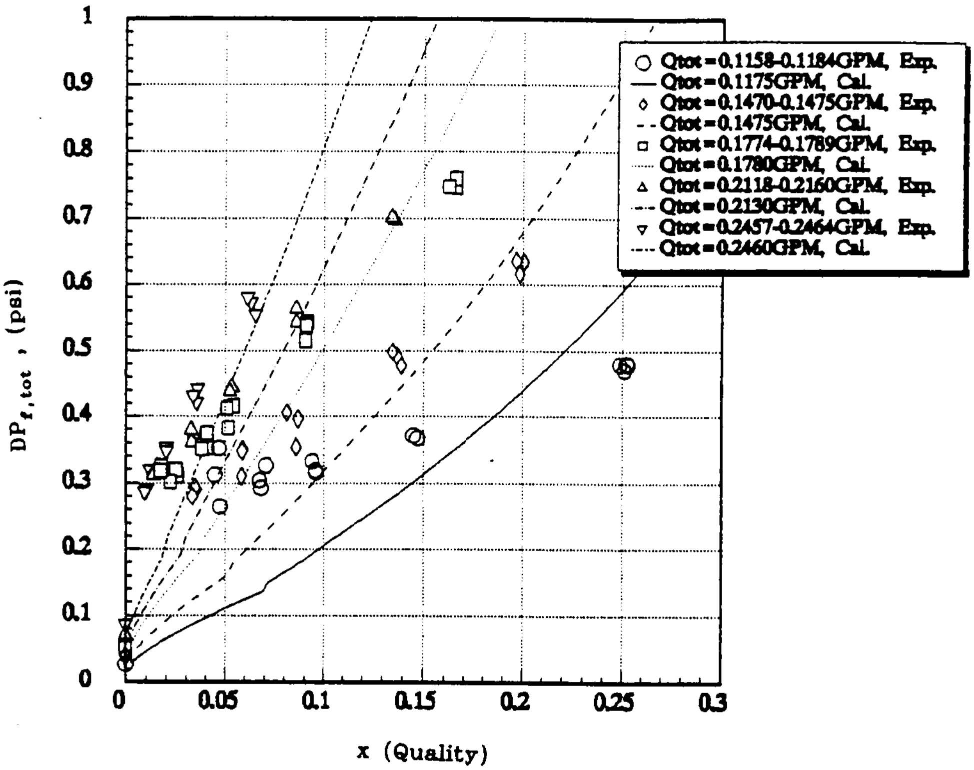

Figure 4.20 Comparison of Measured Total Pressure Drops of R-113 Liquid/Vapor Vertical Up-Flow With Predictions of Homogeneous Model With Coil Correction. (Channel Type: Rectangular, H / W = 1.0)

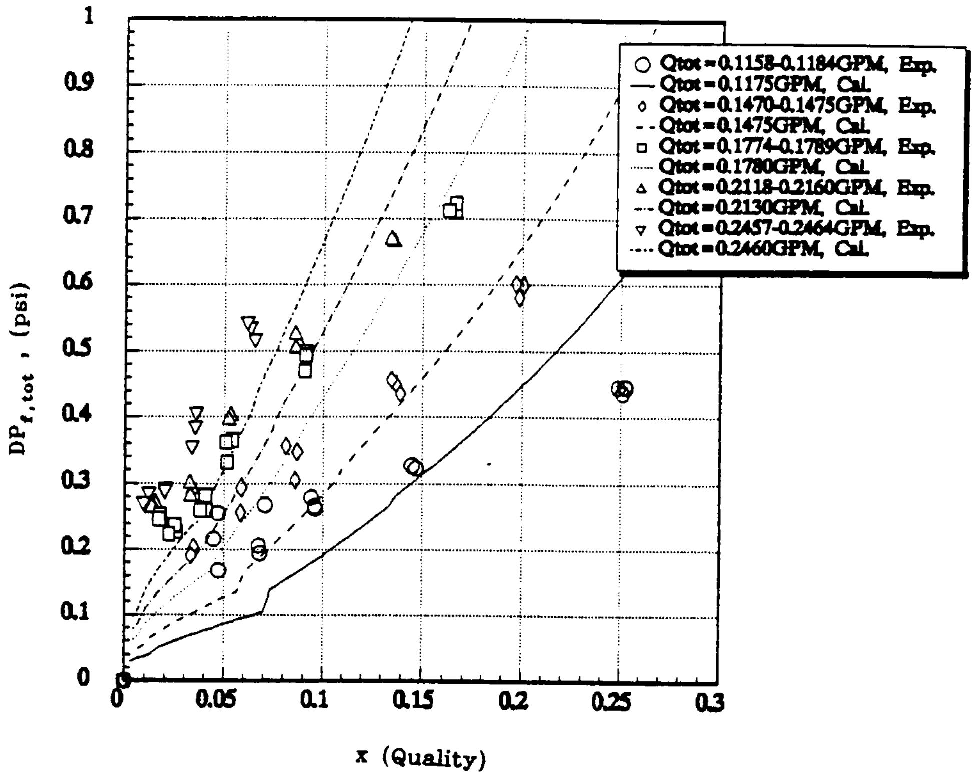

Figure 4.21 Comparison of Measured Total Pressure Drops of R-113 Liquid/Vapor Vertical Up-Flow With Predictions of Lockhart-Martinelli Model With Coil Correction. (Channel Type: Rectangular, H / W = 1.1)

are basically in the developing-annular and intermittent flow regions. Thus, efforts were made to develop an empirical correlation using the homogeneous method, to predict two-phase frictional pressure drop for helical coil vertical upflow in the developing-annular and intermittent flow regions. The pressure drop data obtained for R-113 in vertical up-flow in helical coils for both circular and near square rectangular cross-section flow channels were used to generate curves of friction factor as a function of Reynolds number.

Equations (4.13) through (4.18) are repeated here for convenience in the following discussion.

For single phase flow in straight tubes:

$$Re_{crit} = 2100, \qquad (4.13)$$

$$f_s = 16/Re, \quad \text{if } Re < Re_{crit}, \qquad (4.14)$$

$$f_s = 0.079\ Re^{-0.25}, \quad \text{if } Re > Re_{crit}. \qquad (4.15)$$

For single phase flow in coiled tubes:

$$Re_{crit} = 2100[1 + 12(d/D)^{0.5}], \text{ [Srinivasan]} \qquad (4.16)$$

$$f_c = (16/Re)*\{1+[0.090De^{1.5}/(70+De)]\}, \text{ if } Re < Re_{crit}, \text{ [Hart]} \qquad (4.17)$$

$$f_c = 0.079Re^{-0/25} + 0.0075(r/R_c)^{1/2}, \text{ if } Re > Re_{crit}, \text{ [Mishra]} \qquad (4.18)$$

For two-phase flow in a helical coil, the critical Reynolds number should be expected to yield higher values than in straight tubes as has been observed to occur in single phase flow due to secondary flow effects. This effect appears to be reflected in the data analyzed herein for two-phase flow.

In Figures 4.22 and 4.23, the measured homogeneous two-phase flow friction factors of R-113 in (1) the circular cross-section flow channel and (2) the near square rectangular cross-section flow channel, were plotted against the homogeneous Reynolds number of the two-phase mixture. The change of slope in the friction factor vs. Reynolds number curve of either plots implies a flow change from a laminar to turbulent condition. Furthermore, the corresponding Reynolds number at which this change occurs is in agreement with the value calculated from Equation (4.16), except for replacing the constant 2100 by 2300 for the present data, i.e.

$$Re_{crit,\ coil-tp} = 2300[1 + 12(d/D)^{0.5}] \tag{4.19}$$

When the homogeneous two-phase flow is identified to be in the turbulent flow regime, Equation (4.18), by Mishra for single phase turbulent flow in a coiled tube, gives good agreement with R-113 two-phase frictional pressure drop data for helical coil vertical upflow in a circular tube if the coefficient for curvature is changed slightly from 0.0075 to 0.01:

$$f_c = f_s + 0.01(r/R_c)^{1/2} \tag{4.20}$$

This correlation is applicable for $Re > Re_{crit,\ coil-tp}$, and $f_s = 0.079\ Re^{-0.25}$. It is shown as the dashed curve in Figure 4.22.

When the homogeneous two-phase flow is identified to be in the laminar flow regime, Equation (4.17), by Hart, for single phase laminar flow in a coiled tube, can not be similarly adopted to predict the R-113 pressure drop data for vertical upflow in a circular cross-section flow channel because it yields a much smaller slope in the friction factor vs. Reynolds number curve than for curve based on the measured values.

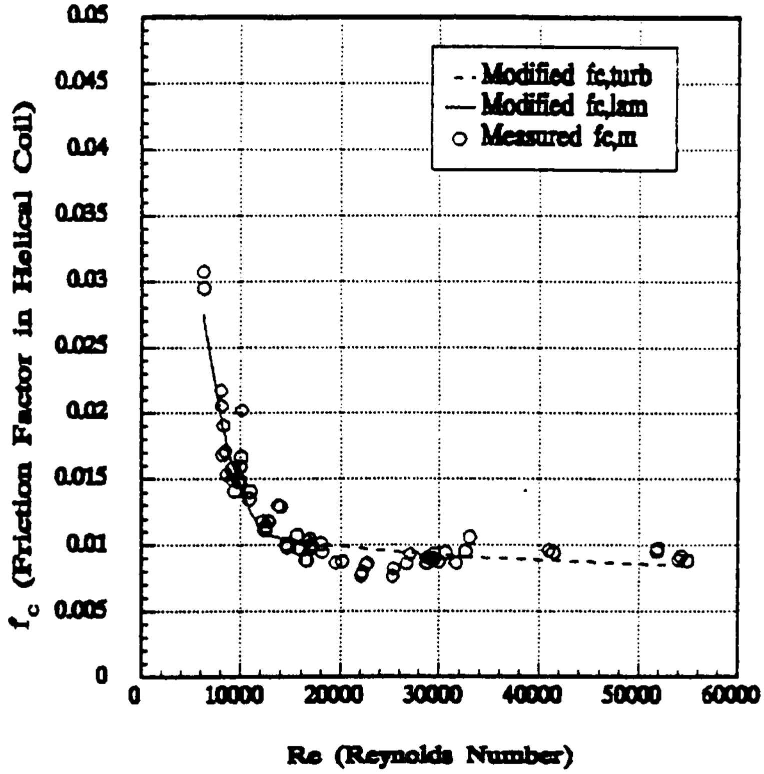

Figure 4.22 Comparison of Measured Friction Factors Based on Homogeneous Model With Predictions From Empirical Correlations, Equations (4.19) to (4.24b). (R-113 Liquid/Vapor, Circular Helical Coil Channel)

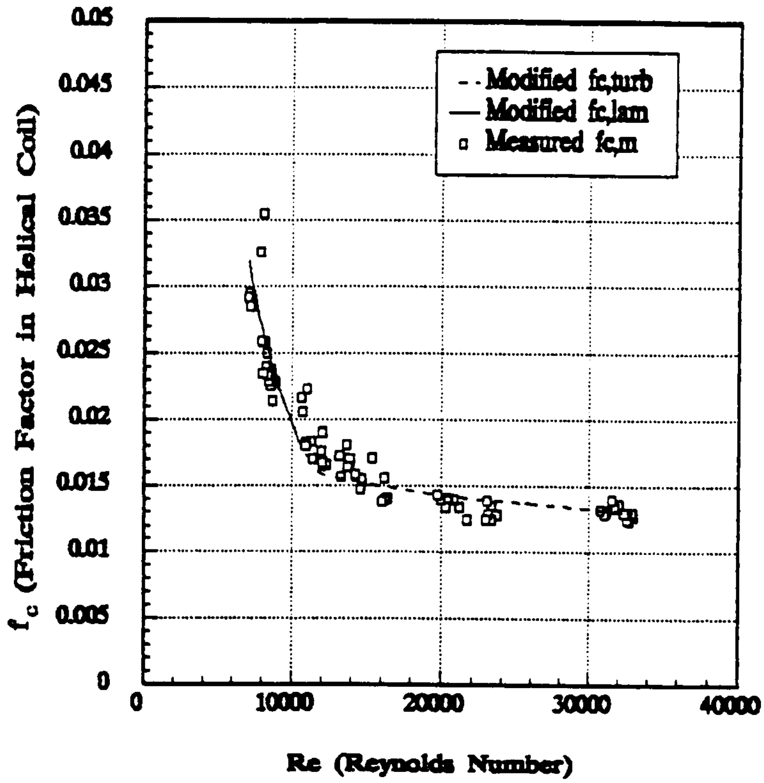

Figure 4.23 Comparison of Measured Friction Factors Based on Homogeneous Model With Predictions From Empirical Correlations, Equations (4.19) to (4.24b). (R-113 Liquid/Vapor, Square Helical Coil Channel)

Instead, for the laminar flow case it is proposed here that the friction factor for the coil geometry to be the friction factor for a straight channel flow times a constant C divided by the Dean number raised to the nth power(accounting for the coil curvature effect) as bellows:

$$f_c = f_s \ (C/De^n) \tag{4.21}$$

This equation is applicable for $Re < Re_{crit,\ coil\text{-}tp}$, and $f_s = 16/Re$. For the R-113 frictional pressure drop data for vertical upflow in a circular cross-section flow channel, the values of C and n were determined experimentally as 230 and 0.4, respectively. It is plotted as a solid curve in Figure 2.22.

For vertical upflow in a rectangular cross-section flow channel, the above correlations developed for circular cross-section flow channel (equations (4.20) and (4.21)) can also be found to give good predictions for the measured R-113 frictional pressure drop data in the near-square cross-section flow channel(near square), provided the friction factors f_s for straight flow channels given by equations (4.20) and (4.21) are modified to take into account the flow channel cross-sectional geometry factor in the form of:

$$f_s = C_A/Re^m \tag{4.22}$$

The coefficients in Equation (4.22) were obtained by analyzing experimental data and the model predictions; The best values of these coefficients were determined to be: $C_A = 22$ and $m = 1$ for laminar flow, and $C_A = 0.13$ and $m = .025$ for turbulent flow (analogous to Blasius equation with the geometry factor C_A). The predictions of Equation (4.22) are plotted in Figure 4.23, where the solid curve applies to laminar flow, while the dashed curve applies to turbulent flow.

The correlations developed herein, to predict the two-phase frictional pressure drop for vertical up-flow in helical coils for both circular and rectangular cross-section flow channels are summarized as follows:

$$Re_{crit} = 2300\ [1 + 12\ (d_i/D_c)^{0.5}\ ] \qquad (4.19)$$

For $Re < Re_{crit}$,

$$f_c = f_s\ (230/De^{0.4}) \qquad (4.23)$$

where $f_s = 16/Re$, in circular flow channel (4.23a)

$f_s = 22/Re$, in rectangular flow channel (4.23b)

For $Re > Re_{crit}$,

$$f_c = f_s + 0.01\ (r/R)^{1/2} \qquad (4.24)$$

where $f_s = 0.079\ Re^{-0.25}$, in circular flow channel (4.24a)

$f_s = 0.13\ Re^{-0.25}$, in rectangular flow channel (4.24b)

In the case of rectangular cross-section flow channels, the hydraulic diameter d_h should be used in place of d_i in the above equations.

In figures 4.24 and 4.25, plots are made of the same experimental data, together with curves from different predictions, for comparison purpose. The dotted curves in the figures are predictions made by equations (4.13) through (4.15) for single-phase flow in straight flow channels, which have been modified by assuming a homogeneous two-phase flow in the straight channel. It is apparent that they considerably under-predict the measured values of two-phase flow in coiled tubes. The dashed curves in figures 4.24 and 4.25 are predictions of equations (4.16) through (4.18) by Hart et [26] and Mishra [37], which have been modified by assuming a homogeneous two-phase flow to occur in the system. It should be noted that these predictions of pressure drop in coil geometries are based upon equations valid only for single phase flow. In general,

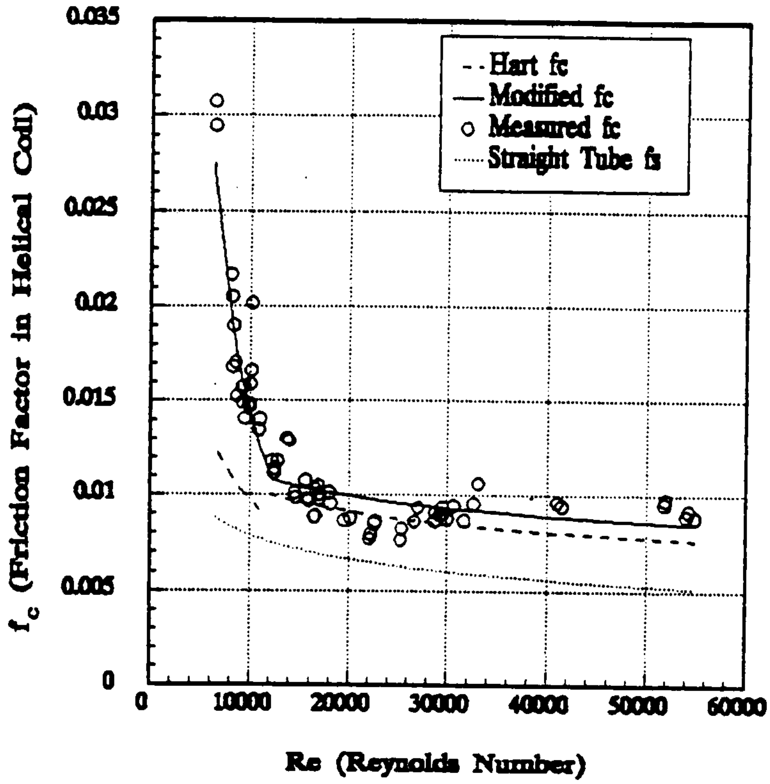

Figure 4.24 Comparison of Measured Friction Factors Based on Homogeneous Model With Predictions From Various Empirical Correlations. (R-113 Liquid/Vapor, Circular Helical Coil Channel)

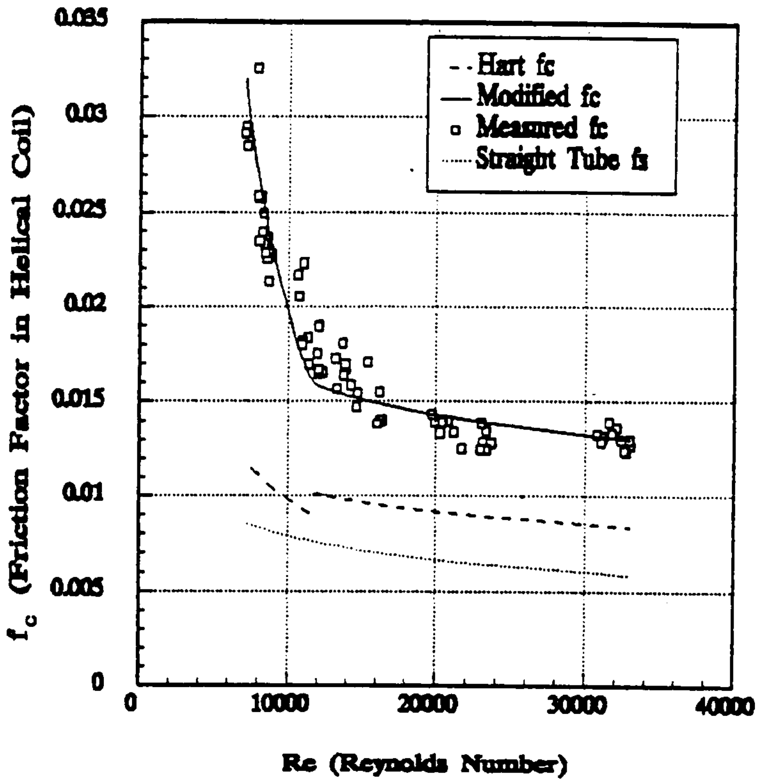

Figure 4.25 Comparison of Measured Friction Factors Based on Homogeneous Model With Predictions From Various Empirical Correlations. (R-113 Liquid/Vapor, Near Square Helical Coil Channel)

they all under-predict the measured pressure drop values of two-phase flow in coil geometries. However, for the circular tube geometry the modified Mishra predictions for friction factor agree reasonably well with the data in the turbulent range. For laminar flow, however, there is a considerable difference between the modified Hart et al predictions and the data obtained. For flow in a near square cross-section channel the Hart-Mishra modified predictions result in even larger differences with the experimental data in either the turbulent or laminar flow regimes.

In summary, two-phase vertical upflow appears to be characterized by a higher critical Reynolds number, which may be attributable to secondary flow effects in the coil geometry. This critical Reynolds number can be calculated by using the equation proposed herein, Equation (4.19), for flow conditions similar to those of the present study. The two-phase friction factor is higher than that of single phase vertical upflow in helical coils in both laminar and turbulent flow regimes; These friction factors can be calculated from Equations (4.23) and (4.24) if the flow conditions are similar to those of the present study. Finally, for the same vertical upflow conditions in helical coils, the friction factor in the near square cross-section channel geometry is higher than that in the circular cross-section channel geometry, especially in the turbulent regime. This comparison is depicted in Figure 4.26.

It should be mentioned that because of the large discrepancies between the measured values of air-water pressure drop data and the predicted values of pressure drop by the homogeneous and Lockhart-Martinelli models (as shown in preceding Section 4.4.2), the air-water pressure drop data was not used in the development of the above modified

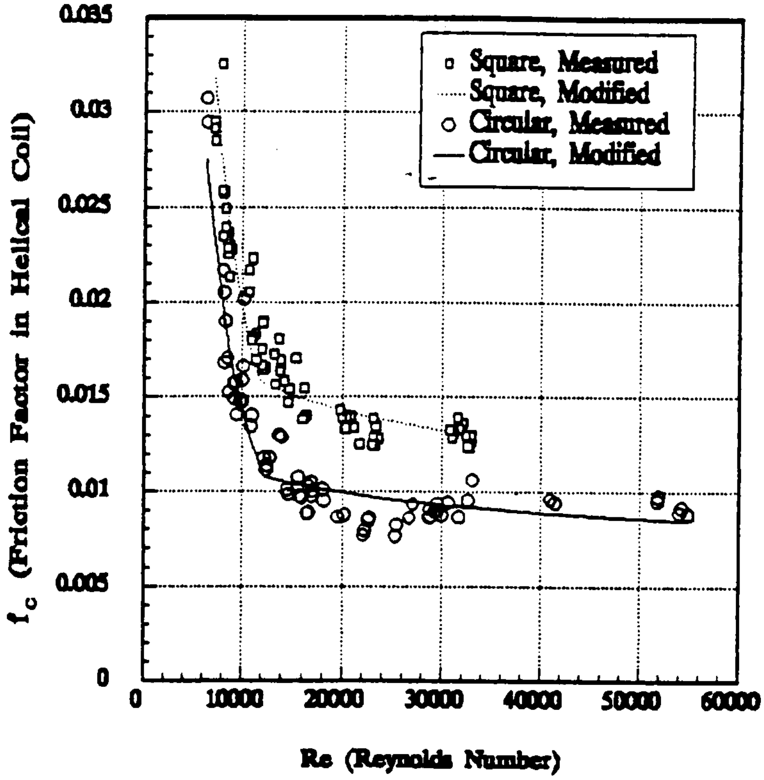

Figure 4.26 Comparison of Measured Friction Factors Based on Homogeneous Model With Predictions From Empirical Correlations, Equations (4.19) to (4.24b). (R-113 Liquid/Vapor, Circular and Near Square Helical Coil Channels)

correlations for predicting frictional pressure drop in helical coil vertical up-flow. Further confirmation of the applicability of these modified correlations to air-water two-phase flow in helical coil vertical up-flow is left for future investigation.

4.5 Summary

The measured single phase (liquid) frictional pressure drop data for vertical upflow of water and R-113 in helical coils in a circular flow channel agreed well with the existing correlations by Hart et al [26,28,37,49]. Good agreement for R-113 liquid data in a near square flow channel was also shown by these correlations provided the hydraulic diameter is used in place of channel diameter. Through the use of these three test data sets the critical Reynolds number was shown to be higher in coiled tubes than in straight tubes. Higher frictional pressure drops were measured for water, as compared to R-113 liquid in the same circular tube. For the R-113 liquid, the frictional pressure drop in a near square tube is about the same as that in a circular tube if the tube diameter is the same as the hydraulic diameter of the near-square tube.

For two-phase vertical upflow of air-water and R-113 in helical coils, the frictional pressure drop characteristics were found to be related to different flow patterns and their characteristics (see figures 4.7 and 4.8). It was observed that the transition from slug flow to developing-annular flow does not affect the slope of pressure drop vs. quality curve, whereas the slope does change during the transition from developing-annular to developed-annular flow. If the liquid flow rate is kept constant and the gas flow rate is increased gradually, the transition from slug to annular flow occurs at lower quality values for higher liquid flow rates. The slug-annular transition occurs at higher quality values in the near-square cross-section flow channel than in the circular flow channel for the same flow rates.

Three sets of experimental pressure drop data -- air-water and R-113 in a circular cross-section flow channel and R-113 in a near square rectangular channel -- in a helical coil vertical up-flow configuration were compared. The comparison was made using the two-phase homogeneous and Lockhart-Martinelli models, using friction factors based upon single phase flow in straight and coiled channels proposed by Mishra [37] and Hart [26]. In general, these models were found to be unable to predict the pressure drop for flows in wavy-annular and developed-annular flow pattern regions, perhaps due to the high interfacial frictional losses and high slip velocity in the two-phase flow. For flow in slug and developing-annular flow pattern regions, quantitative predictions of two sets of R-113 experimental data by the analytical methods are predicted reasonably well. However, for air-water pressure drop data, the agreement is poor. In brief, these analytical methods appear to be able to give only approximate predictions of frictional pressure drop in the slug and developing-annular flow regions in helical coil vertical up-flow conditions.

Empirical correlations of critical Reynolds number and two-phase frictional pressure drop were developed in the present study for R-113 liquid/vapor two-phase in helical coil vertical up-flow for both circular cross-section and near square cross-section flow channels. The friction factor values in the near square cross-section flow channel are higher than those in the circular cross-section channel for helical coil vertical up-flow. Confirmation of the applicability of these developed empirical correlations to air-water two-phase flow in such geometry is left for future investigation.

CHAPTER 5 SUMMARY AND CONCLUSIONS

Experimental Results

A total of 609 experimental data points of two-phase pressure drop and flow pattern identifications were obtained for the following 15 flow and geometry conditions:

(1) helical coil vertical-up flow

  (a) in circular tube for air-water and R-113 mixtures, respectively

  (b) in rectangular tubes (three aspect ratios) for air-water and R-113 mixtures, respectively

(2) helical coil horizontal flow

  (a) in circular tube for air-water

  (b) in rectangular tubes (three aspect ratios) for air-water

(3) helical coil vertical-downward flow in a circular tube for air-water

(4) spiral coil of circular cross-section for air-water and R-113 mixtures, respectively

The experimental data obtained for both air-water and R-113 liquid/vapor mixtures in rectangular cross-section channels for the vertical upflow orientation is believed to be first available in the published literature. Also, for flow in the circular cross-section coils, the experimental data of obtained for R-113 liquid/vapor mixtures for the horizontal orientation and vertical downward flow direction were the first available in the literature to the writer's knowledge.

Five sets of data were obtained herein as a basis the study of flow patterns. Three sets of data were obtained as a basis for the study of pressure drops. The analysis of the remainder of the data obtained is left for future investigations because of the limited time for the present thesis study.

The following sets of test data were studied for the flow pattern analysis:

(1) air-water helical coil vertical up-flow in a circular cross-section flow channel

(2) R-113 liquid/vapor helical vertical up-flow in a circular cross-section flow channel

(3) R-113 liquid/vapor helical vertical up-flow in a near square cross-section flow channel

(4) air-water spiral coil horizontal outward flow in a circular cross-section flow channel

(5) R-113 liquid/vapor spiral coil horizontal outward flow in a circular cross-section flow channel

The pressure drop of three sets of test data were studied, which are:

(1) air-water helical coil vertical up-flow in a circular cross-section flow channel

(2) R-113 liquid/vapor helical vertical up-flow in a circular cross-section flow channel

(3) R-113 liquid/vapor helical vertical up-flow in a near square cross-section flow channel

The flow patterns observed in helical coil vertical up-flow and spiral coil horizontal outward flow were found to be similar to those in horizontal straight flow channel, except for the absence of the stratified flow pattern, believed due to the small pitch (inclination angle of helical coil), the coiled tube curvature, and the relatively small flow channel diameter. The observed flow patterns are BUBBLE, PLUG, SLUG, and ANNULAR (which is further delineated into DEVELOPING-ANNULAR, WAVY-ANNULAR and DEVELOPED-ANNULAR flow patterns). A special phenomenon, a backward motion of the liquid film at the channel bottom, between slug surges, was observed for helical coil vertical up-flow at some low gas and liquid flow rates. This is due to the flow channel inclination and has also been observed by other investigators [46].

The transition of greatest interest here was the slug-annular transition. This transition occurs when periodic liquid slugs break away from touching the upper part of the flow channel, allowing a continuous gas passage throughout the flow channel, while a liquid film is maintained along the entire flow channel periphery.

The flow patterns observed for the five test conditions are compared with four existing flow maps, i.e., the modified Baker flow map, the Taitel & Dukler map, the Choe et al map, and the Uddin map. None of these maps were able to adequately predict both the helical coil and spiral coil test data. However, the Choe map gives the closest prediction for the transition to annular flow if the separated flow pattern in the map is replaced by the intermittent flow pattern.

An empirical correlation of the slug-annular flow pattern transition for circular cross-section helical coil vertical up-flow was developed based upon both the air-water and R-113 liquid/vapor test data which takes into account the effects of coil curvature and fluid properties.

For the spiral coil, in which the coil diameter varies along the flow channel, the slug-annular transition was designated by a band, accounting for the largest and smallest curvature ratios existing within the spiral coil. The correlations for predicting the upper and lower slug-annular transition lines for outward flow are generated by substituting the largest coil diameter and smallest coil diameter into the empirical correlation of the slug-annular transition for helical coil vertical up-flow. Good agreement is obtained for both the air-water and R-113 test data.

Using a shape factor correction, an empirical correlation of the slug-annular transition in rectangular cross-section flow channels for helical vertical up-flow was developed. Further study is recommended to confirm this empirical correlation using data from rectangular flow channels over a range of aspect ratios.

The experimental results observed herein for both helical coil and spiral coil, indicate that the coil curvature, fluid properties, and flow channel cross-section geometry have an influence upon the slug-annular transition. Helical coils or spiral coils with a large coil curvature experience an earlier slug-annular transition(i.e. at lower quality). For flow in a near square cross-section flow channel the slug-annular transition occurs at lower quality(lower gas flow rate) than that in a circular cross-section flow channel for the same liquid flow rate. Also, this transition occurs at lower gas flow rates for R-113 liquid/vapor that for air-water, at a certain liquid flow rate. Among these effects, the properties effect is the most dominant one. Somewhat surprisingly, the curvature effect on the slug-annular transition was not as significant as that of the effect of fluid properties for the range of coil curvatures in this study.

Frictional pressure drop data were obtained for vertical up-flow of water in the circular tube coil and R-113 (liquid) in circular and square tubes. The data agreed well with the existing critical Reynolds number and friction factor correlations developed by Srinivasan [49], Hart et al [26], and Mishra et al [37], for single phase flow inside coils. Also, by using the hydraulic diameter the frictional pressure drop test data agreed well with the above correlations which were developed for circular tubes.

For two-phase air-water and R-113 liquid/vapor vertical up-flow in helical coils, curves for pressure drop vs. quality were obtained for both the circular and near-square channels. The experimental results indicate that the pressure drop along a helical coil is directly affected by the flow patterns within, indicating the importance of being able to predict the flow pattern in calculating two-phase pressure drop. It was evident from the present study that when the pressure gradient exhibits dramatic changes, it should imply that a flow pattern change is probably occurring in the system.

Following are the observations made from the experimental results:

- Pressure drop increases in helical coil vertical up-flow with the increasing of total flow rate or liquid flow rate.
- At the slug-annular transition the pressure drop does not show any special characteristic changes in the pressure drop vs. quality curve. However, when the flow pattern changes from a developing-annular flow to a developed-annular (or wavy-annular) flow, the pressure gradient increases sharply.
- The slug-annular transition occurs at a lower quality for a higher total flow rate or liquid flow rate.

- For the same flow rate condition, the slug-annular transition occurs at higher quality in the near-square cross-section flow channel than that in a circular cross-section flow channel, based upon the flow pattern observations.

The measured pressure drop results of the three sets of test conditions were compared with the homogeneous method and Lockhart-Martinelli method using the friction factors developed for straight channels and for single phase flow in coiled tubes, respectively. All of them only approximately predict pressure drops in the slug and developing-annular flow pattern regions, which is similar to results obtained by earlier investigators [1,8,42,32]. For flows in wavy-annular and developed-annular flow pattern regions, these methods gives much higher predicted pressure drop values than the values measured for air-water test data. This discrepancy implies a high slip ratio existing in such flow patterns so that the homogeneous and Lockhart-Martinelli methods are no longer applicable in these flow regions.

The experimental results indicate that the measured two-phase friction factor in helical coil vertical up-flow is higher than that calculated from expressions for single phase friction factor for coiled tubes, modified to account for a homogeneous two-phase flow. Also, the two-phase friction factor in a near-square cross-section flow channel is higher than in a circular cross-section flow channel. This is not the case in single phase flow, where the pressure drops in both circular and near square flow channels were observed to be about the same. This suggests that in a rectangular flow channel secondary flow effects in a two-phase flow cause a more appreciable frictional pressure drop loss than in single phase flow.

Empirical correlations were developed to calculate the critical Reynolds number and friction factors for R-113 liquid/vapor helical coil vertical up-flow for both a circular flow channel and a near-square flow channel, using a homogeneous two-phase fluid model. Efforts to similarly correlate the air-water test data were not successful, however.

BIBLIOGRAPHY

BIBLIOGRAPHY

1. Akagawa, K., Sakaguchi, T., and Ueda M., "Study on a Gas-Liquid Two-Phase Flow in Helically Coiled Tubes," *Bulletin of the JSME*, Vol. 14, No. 72, pp. 564-571, 1971.

2. Baker, O., "Simultaneous Flow of Oil and Gas," *Oil and Gas Journal*, Vol. 53, No. 12, pp. 185, 1954.

3. Banerjee, S., Edward. Rhodes and D. S. Scott, "Film Inversion of Cocurrent Two-Phase Flow in Helical Coils," *AIChE Journal*, Vol. 13., No. 1, pp. 189-191, January 1967.

4. Banerjee, S., "The Nature of Two-Phase Flow: II. Two-Phase Flow Regimes," Short Course Notes in Chemical Engineering Department, Stanford University, 1980.

5. Barnea, D., O. Shoham, Y. Taitel, and A. E. Dukler, "Gas-Liquid Flow In Inclined Tubes: Flow Pattern Transitions For Upward Flow," A Short Course.

6. Barnea, D., "A Unified Model For Predicting Flow-Pattern Transitions For The Whole Range of Pipe Inclinations," *Int. J. Multiphase Flow*, Vol. 13, No. 1, pp. 1-12, 1987.

7. Barua, S. N., "On Secondary Flow in Stationary Curved Pipes," *Quart. J. Mech. Appl. Math.* **16**, 61-77 (1962).

8. Boyce, B. E., J. G. Collier, and J. Levy, "Hold-Up and Pressure Drop Measurements in the Two-Phase Flow of Air-Water Mixtures in Helical Coils," *Proceedings of the International Symposium on Research in Concurrent Gas-Liquid Flow*, pp. 203-231, September 18-19, 1963.

9. Butterworth, D., "Brief Communications: A Comparison of Some Void-Fraction Relations for Co-Current Gas-Liquid Flow," *Int. J. Multiphase Flow*, Vol. 1, pp. 845-850, 1975.

10. Butterworth, D. and G. F. Hewitt, Two-Phase Flow And Heat Transfer, Oxford University Press, 1977.

11. Chen, I., Downing, R. Scott, Parish, R. and Keshock, E., "A Reduced Gravity Flight Experiment: Observed Flow Regimes and Pressure Drops of Vapor and Liquid Flow in Adiabatic Piping," *AIChE Symposium Series;* No. 263, Vol. 84, pp. 203-216, Heat Transfer, Houston, TX, 1988.

12. Chen, I., Downing, R. Scott, Keshock, E. and Al-Sharif, M., "An Experimental Study and Prediction of a Two Phase Pressure Drop in Microgravity," *AIAA Aerospace Science Meeting*, Reno, Nevada,

January, 1989 (submitted for Publication to AIAA Journal of Thermophysics).

13. Chen, X., Zhou, F., and Guo, L., (Xian Jiaotong University) "Investigations on flow pattern transition of gas-liquid two-phase downflow in vertical helical coils," J. Engng. Thermophysics., vol.8, no.1, Feb. 1987,p55-59.

14. Chen, Xue-Jun, and Zhang, Ming-Yuan, "An Investigation on Flow Pattern Transition for Gas-Liquid Two-Phase Flow in Helical Coils," *Multi-Phase Flow and Heat Transfer III. Part A: Fundamentals*, edited by T. N. Veziroglu and A. E. Bergles, Elsevier Science Publishers B. V., Amsterdam, 1984 - Printed in The Netherlands, pp. 185-200.

15. Chisholm, D., Two-Phase Flow In Pipelines And Heat Exchangers, George Godwin, London and New York, **in association with** The Institution of Chemical Engineers, 1983.

16. Choe, W. G., L. Weinberg, and J. Weisman, "Observation and Correlation of Flow Pattern Transitions in Horizontal Cocurrent Gas-Liquid Flow," Two-Phase Transport and Reactor Safety, Hemisphere Publishing Co., 1978.

17. Choudhury, K., "Two-Phase Flow Visualization in a Helical Coil in High Gravity Fields," Sundstrand Advanced Technology Group Memo, 1988.

18. Churchill, Stuard W., "Friction-factor equation spans all fluid-flow regimes," Chemical Engineering, November 7, 1977.

19. Collier, J. G., Convective Boiling and Condensation, McGraw-Hill Inc., 1981.

20. Crain, B. Jr., and Bell, K. J., "Forced Convection Heat Transfer to a Two-Phase Mixture of Water and Steam in a Helical Coil," *A.I.Ch.E. Symposium Series*, Vol. 69, No. 131, pp. 30-36, 1973.

21. Crowley, C. J., "Unified Flow Regime Predictions at Earth Gravity and Microgravity," report TN-483 of Creare Inc., Hanover, New Hampshire 03755.

22. Dean, W. R., "Note on the Motion of Fluid in a Curved Pipe," *Phil. Mag.* 4, 208-223 (1927); *Phil. Mag.* 5, 637-695 (1928).

23. Fei, Te-Tai, Error Theory and Data Processing, Machinary Industry Press, Beijing, China, 1987.

24. Ginwala, Kymus, Thomas A. Blatt, Robert W. Bilger, et al, "Engineering Study of Vapor Cycle Cooling Components for Space Vehicles," Technical Report No. ASD-TDR-63-582, Wright-Patterson Air Force Base, Ohio, September 1963.

25. Guo, Liejin, Fangde Zhou, and Chen Xuejun, "Investigation on Flow Pattern Transitions of Gas-Liquid Two-Phase Flow in the Horizontal Helical Coiled Tubes," Particulate Phenomena and Multiphase Transport, Vol. 1, Hemisphere Publishing Corp., 1988.

26. Hart, J., J. Ellenberger, and P. J. Hamersma, "Single- and Two-Phase Flow Through Helically Coiled Tubes," *Chem. Eng. Sci.*, v43, n4, pp. 775-783, 1988.

27. Hasan, A. Rashid, "Inclined Two-Phase Flow: Pattern Transition, Void Fraction, and Pressure Drop," Particulate Phenomena and Multiphase Transport, Vol. 1, Hemisphere Publishing Corp., 1988.

28. Ito, H., "Friction Factors for Turbulent Flow in Curved Pipes," *J. Basic Engineering, Trans. ASME*, D81, pp. 123-134, 1959.

29. Jensen, M. K., and Bergles, A. E., "Boiling Heat Transfer and Critical Heat Flux in Helical Coils," *Trans. ASME, Series C, J. Heat Transfer*, **103**,pp. 660-666, 1981.

30. Jensen, M. K., and Bergles, A. E., "Critical Heat Flux in Helical Coils with a Circumferential Heat Flux Tilt toward the Outside Surface," *Int. J. Heat Mass Transfer*, Vol. 25, No. 9, pp. 1383-1395, 1982.

31. Kaji, M., K. Mori, S. Nakanishi, and S. Ishigai, "Flow Regime Transitions for Air-Water Flow in Helically Coiled Tubes," *Multi-Phase Flow and Heat Transfer III. Part A: Fundamentals*, edited by T. N. Veziroglu and A. E. Bergles, Elsevier Science Publishers B. V., Amsterdam, 1984 -Printed in The Netherlands, pp. 201-214.

32. Kasturi, G. and J. B. Stepanek, "Two Phase Flow — I. Pressure Drop and Void Fraction Measurements in Cocurrent Gas-Liquid Flow in a Coil," *Chemical Engineering Science*, Vol. 27, pp. 1871-1880, 1972.

33. Lockhart, R. W. & Martinelli, R. C., "Proposed correlation of data for isothermal two-phase, two-component flow in pipes," *Chem. Engng. Prog.*, **45**, 39-48, 1949.

34. Lopina, Robert F., and Arthur E. Bergles, "Heat Transfer and Pressure Drop in Tape Generated Swirl Flow," Wright-Patterson Air Force Base technical report, No. 70281-47, June, 1967.

35. Lyczkowski, Robert W., Gidaspow, Dimitri, and Solbrig, Charles W., Advances in Transport Processes, Volume II --- Multiphase Flow Models for Nuclear, Fossil and Biomass Energy Production, edited by Arun S. Mujumdar and R. A. Mashelkar, Wiley Eastern Ltd., 1982.

36. Mandhane, J. M., G. A. Gregory and K. Aziz, "A Flow Pattern Map For Gas-Liquid Flow In Horizontal Pipes," *Int. J. Multiphase Flow*, Vol. 1, pp. 537-553, 1974.

37. Mishra, P and S. N. Gupta, "Momentum Transfer in Curved Pipes. 1. Newtonian Fluids," *Ind. Eng. Chem. Process Des. Dev.*, Vol. 18, No. 1, 1979.

38. Mori, Yasuo and Nakayama, Wataru, "Study on Forced Convective Heat Transfer in Curved Pipes (1st Report, Laminar Region)", *Int. J Heat Mass Transfer*, Vol. 8, pp. 67-82, 1965.

39. Mori, Yasuo and Nakayama, Wataru, "Study on Forced Convective Heat Transfer in Curved Pipes (2nd Report, Turbulent Region)," *Int. J Heat Mass Transfer*, Vol. 10, pp. 37-59, 1967.

40. Mori, Yasuo and Nakayama, Wataru, "Study on Forced Convective Heat Transfer in Curved Pipes (3rd Report, Theoretical Analysis Under the Condition of Uniform Wall Temperature and Practical Formulae)," *Int. J Heat Mass Transfer*, Vol. 10, pp. 681-695, 1967.

41. Niggemann, R. E., W. J. Greenlee, D. G. Hill, W. Ellis, and P. Mardhall, "A Swirl Flow Evaporative Cold Plate," *AIAA 20th Thermophysics Conference*, Williamsburg, Virginia, U.S.A., June 19-21, 1985.

42. Owhadi, A., K. J. Bell and B. Crain, Jr., "Forced Convective Boiling Inside Helically-Coiled Tubes," *Int. J. Heat Mass Transfer*, Vol. 11, pp.1779-1793, 1968.

43. Rippel, G. R., Eidt, C. M. Jr., and Jordan, H. B. Jr., "Two-Phase Flow in a Coiled Tube -- Pressure Drop, Holdup, and Liquid Phase Axial Mixing," *Industry and Engineering Chemistry Process Design and Development*, Vol. 5, pp. 32-39, 1966.

44. Rouhani, S. Z. and Sohal, M. S., "Two-Phase Flow Patterns: A Review of Research Results," *Progress in Nuclear Energy*, Vol. 11, No. 3, pp. 219-259, 1983.

45. Sadatomi, M. and Y. Sato, "Two-Phase Flow In Vertical Noncircular Channels," *Int. J. Multiphase Flow*, Vol. 8, No. 6, pp. 641-655, 1982.

46. Saxena, A. K., Schumpe, A., Nigam, K. D. P., and Deckwer, W. D.(Univ. Oldenburg, Oldenburg, West Germany), "Flow regimes, hold-up and pressure drop for two phase flow in helical coils," Canadian Journal of Chemical Engineering, v. 68, n. 4, Aug. 1990, p.553-550.

47. Sekoguchi, K., Y. Sato, and A. Kariyasaki, "The Influence of Mixers, Bends, and Exit Sections on Horizontal Two-Phase Flow," *Proceedings of the International Symposium on Research in Concurrent Gas-Liquid Flow*, pp. 109-144, September 18-19, 1963.

48. Shu, Ming-tsai, J. A. Hamshar, and C. B. Weinberger, "Cocurrent Flow of Gas-Particulate Mixtures Through Helical Tubular Coils: Particle Velocity Measurement and Prediction," *AIChE Journal*, Vol. 32, No. 4, pp. 529-536, April, 1988.

49. Srinivasan P. S. et al, "Friction Factors For Coils," *Trans. Inst. Chem. Engrs*, **48**, T156-T161, 1970.

50. Taitel, Y., and A. E. Dukler, "A Model for Predicting Flow Regime Transitions in Horizontal and Near Horizontal Gas-Liquid Flow," *AIChE Journal*, Vol.22, No.1, pp. 47-55, January 1976.

51. Taitel, Y., Dvora Bornea and A. E. Dukler, "Modelling Flow Pattern Transitions for Steady Upward Gas-Liquid Flow in Vertical Tubes," *AIChE Journal*, Vol. 26, pp. 345-354,1980.

52. Thomas, G. B., Jr., Calculus, Addison-Wesley Publishing Co., Inc. (London), 2nd ed., p. 464, 1964.

53. Uddin, A. K. M., "A Model to Predict Two-Phase Flow Patterns in Helically Coiled Tubes," Particulate Phenomena and Multiphase Transport, Vol. 1, Hemisphere Publishing Corp., 1988.

54. Vafaie, F. N., and J. R. Dunn, "Forced-Convection Heat Transfer for Single and Two-Phase Helical Flow in a Solar Receiver," *Transactions of ASME*, Vol 108, pp. 76-83, February, 1986.

55. Venkateswarlu, K., R. C. Sastry, and A. Satyanarayan, "Heat Transfer to Single and Two Phase Flow in a Helical Coil," *IE(I) Journal-CH*, Vol. 63, June 1983, pp. 68-72.

56. Wallis, G. B., One-Dimensional Two-Phase Flow, McGraw-Hill Inc., 1969.

57. Weisman, J., D. Duncan, J. Gibson, and T. Crawford, "Effects of Fluid Properties and Pipe Diameter on Two-Phase Flow Patterns in Horizontal Lines," *Int. J. Multiphase Flow*, Vol.5, pp. 437-462, 1979.

58. Weisman, J., "Flow Pattern Identification in Concurrent Vapor-Liquid Flow," Two-Phase Flow Dynamic, edited by Arthur E. Bergles and Seikan Ishigai, Japan-US Seminar, 1979, Hemisphere Publication Corp.

59. Whalley, P. B., "Air-Water Two-Phase Flow in a Helically Coiled Tube," *Int. J. Multiphase Flow*, Vol. 6, pp. 345-356, 1980.

60. White, C. M., "Streamlines flow through curved pipes," *Proc. R. Soc.* **A123**, 645-663, 1929.

61. White, C. M., "Fluid friction and its relation to heat transfer," *Trans. Inst. Chem. Engrs*, **18**, pp.66-86, 1932.

62. Williams, G. S., C. W. Hubbell, and G. H. Fenkell, "Experiments at Detroit, Mich., on the Effect of Curvature Upon the Flow of Water in Pipes," *Trans. ASCE*, vol.47, pp.1-369, 1902.

63. Zhou, F., and Chen, X., "Friction pressure drop variation along tube length of air-water two-phase flow in helical coils," Two-phase flow

and heat transfer Conference, Xian, China, May 9-14,1984; Proceeding published by Hemisphere Publ. Corp., Washington D.C., USA, 1985, p. 89-95.

APPENDIX

APPENDIX A

UNCERTAINTY ANALYSIS

The uncertainties in calculated quantities based upon experimentally measured variables may be estimated by the following method of Fei [23], given by:

$$e_R = \left[\left(e_1 \frac{\partial R}{\partial x_1}\right)^2 + \left(e_2 \frac{\partial R}{\partial x_2}\right)^2 + \cdots\cdots + \left(e_n \frac{\partial R}{\partial x_n}\right)^2 \right]^{\frac{1}{2}} \tag{A-1}$$

where e_R is the uncertainty in the result and e_1, e_2, ..., e_n are uncertainties in the independent variables.

1. AIR-WATER TESTS

Uncertainty in Liquid Volumetric Flow Rate

The volumetric flow rate was calculated from the expression:

$$Q_1 = C_0 + C_1 * f \tag{A-2}$$

Q_1 = Liquid volumetric flow rate (GPM)

f = Output frequency of the flowmeter pickup (HZ)

C_0 = Flowmeter calibration curve fitting constant, $C_0 = 9.23484 \times 10^{-3}$ (GPM)

C_1 = Flowmeter calibration curve fitting constant, $C_1 = 1.52920\times10^{-4}$ (GPM/HZ)

The major contributions to the uncertainty of the liquid volumetric flow rate measurement are: (1) the calibration curve fitting uncertainty, for which the standard deviation, $\sigma_{Q,0}$, is 2.467×10^{-3} GPM; (2) the flowmeter frequency pickup reading uncertainty, with a standard deviation, σ_f, equal to 3.333 HZ, which results in a transferred uncertainty in the volumetric flow rate, denoted by the standard deviation, $\sigma_{Q,f}$, through equation (A-2) , which may be calculated by:

$$\sigma_{Q,f} = C_1 * \sigma_f = 5.097\times10^{-4} \text{ (GPM)} \qquad \text{(A-3)}$$

The combined uncertainty for the liquid volumetric flow rate measurement can be represented by a standard deviation, σ_Q, which may be calculated by:

$$\sigma_Q = (\sigma_{Q,0}^{\;2} + \sigma_{Q,f}^{\;2})^{1/2} = 2.519\times10^{-3} \text{ (GPM)} \qquad \text{(A-4)}$$

For the present study, the liquid volumetric flow rate test range is from 0.040 to 0.254 GPM. Therefore, for this range of flow rates, the relative uncertainty on a percentage basis, σ_Q/Q_1, has minimum, average, and maximum values equal to 0.984%, 2.18%, and 6.24%, respectively.

Uncertainty in Test Section Inlet Quality

The inlet quality is calculated from the expression:

$$x = W_g \,/\, (W_g + \rho_l Q_l) \qquad \text{(A-5)}$$

where x = Test section inlet quality

W_g = Air mass flow rate (lb_m/sec)

Q_l = Water volumetric flow rate (ft^3/sec).

Applying equation (A-1) to (A-5),

$$\frac{e_x}{x} = \frac{\rho_l Q_l}{W_g + \rho_l Q_l}\sqrt{\left(\frac{e_{W_g}}{W_g}\right)^2 + \left(\frac{e_{\rho_l}}{\rho_l}\right)^2 + \left(\frac{e_{Q_l}}{Q_l}\right)^2} \qquad \text{(A-6)}$$

Sample calculation values and the resulting uncertainty in the inlet quality are as follows:

$\rho_l = 62.31 \dfrac{lb_m}{ft^3}$ $\qquad e_{\rho_l} = 0.5\%$

$Q_l = 1.575\times10^{-4} \dfrac{ft^3}{sec}$ $\qquad e_{Q_l} = 10.69\%$

$W_g = 2.869\times10^{-3} \dfrac{lb_m}{sec}$ $\qquad e_{W_g} = 2.0\%$

$x = 0.226$ $\qquad e_x = 8.42\%$

Uncertainty in Measured Total Frictional Pressure Drop Between Differential Pressure Drop Transducer Taps

The total frictional pressure drop is given by:

$$\Delta P_{f-m} = \Delta P_{tr} + (\rho_{l-rm} - \rho_{TP})(g/g_c)\Delta z \qquad \text{(A-7)}$$

where ΔP_{f-m} = Measured total frictional pressure drop between differential pressure drop transducer taps, including the coiled tubing length of the test section and the inlet and exit straight tubing lengths connected to the test section (lb_f/ft^2)

ΔP_{tr} = Direct output reading of the differential pressure drop transducer (lb_f/ft^2)

ρ_{l-rm} = Density of liquid inside the measuring lines of the differential pressure drop transducer at room temperature (lb_m/ft^3)

ρ_{TP} = Density of two-phase mixture inside coiled test section (lb_m/ft^3)

g = Gravitational acceleration (=32.2 ft/sec^2)

g_c = Gravitational conversion factor (=32.2 (lb_m-ft)/(lb_f-sec^2))

Δz = Elevation between ΔP transducer taps (ft)

Applying equation (A-1) to (A-7),

$$e_{\Delta P_{f-m}} = \left[\left(\frac{g}{g_c}\Delta z\right)^2 (e_{\rho_{l-rm}})^2 + \left(\frac{g}{g_c}\Delta z\right)^2 (e_{\rho_{TP}})^2 + (e_{\Delta P_{tr}})^2 + \left[(\rho_{l-rm} - \rho_{TP})\frac{g}{g_c}\right]^2 (e_{\Delta z})^2\right]^{\frac{1}{2}} \qquad \text{(A-8)}$$

The density of two-phase mixture, ρ_{TP}, can be obtained by the following equation, assuming the two-phase flow is homogeneous:

$$\frac{1}{\rho_{TP}} = \frac{x}{\rho_g} + \frac{(1-x)}{\rho_l} \qquad \text{(A-9)}$$

where x = Quality inside test section

ρ_l = Liquid density (lb_m/ft^3)

ρ_g = Gas density (lb_m/ft^3)

The uncertainty in ρ_{TP}, denoted by $e_{\rho,TP}$, consists of two sources as indicated in the following equation:

$$e_{\rho,TP} = [(e_{\rho,TP,v})^2 + (e_{\rho,TP,model})^2]^{1/2} \qquad \text{(A-10)}$$

The first term in the brackets, $e_{\rho,TP,v}$, is the uncertainty transferred through equation (A-9) from the uncertainties of each independent variable, and can be determined by applying equation (A-1) to equation (A-9):

$$\frac{e_{\rho_{TP,v}}}{\rho_{TP}} = \frac{1}{x\upsilon_g + (1-x)\upsilon_l} \left[(x\upsilon_g)^2\left(\frac{e_{\upsilon_g}}{\upsilon_g}\right)^2 + [(1-x)\upsilon_l]^2\left(\frac{e_{\upsilon_l}}{\upsilon_l}\right)^2 + [(\upsilon_g-\upsilon_l)x]^2\left(\frac{e_x}{x}\right)^2 \right]^{\frac{1}{2}}$$

where υ_g = *gas specific volume,* $\left(\frac{ft^3}{lb_m}\right)$ (A-11)

υ_l = *liquid specific volume,* $\left(\frac{ft^3}{lb_m}\right)$

The second term in the bracket, $e_{\rho,TP,model}$ is the uncertainty in calculating the two-phase mixture density, ρ_{TP}, by using equation (A-9). Two values, $e_{\rho,TP,model}$ = 1% and 90%, are selected in the following sample calculation.

Sample calculation values and the resulting uncertainty in the total measured frictional pressure drop are as follows:

$$\upsilon_g = 13.42 \frac{ft^3}{lb_m} \qquad e_{\upsilon_g} = 1.0\%$$

$$\upsilon_l = 0.01605 \frac{ft^3}{lb_m} \qquad e_{\upsilon_l} = 0.5\%$$

$$x = 0.226 \qquad e_x = 8.42\%$$

$$\rho_{l-rm} = 62.26 \frac{lb_m}{ft^3} \qquad e_{\rho_{l-rm}} = 0.5\%$$

$$\Delta z = 0.551\ ft \qquad e_{\Delta z} = 3.0\%$$

$$\Delta P_{tr} = 11.66 \frac{lb_f}{ft^2} \qquad e_{\Delta P_{tr}} = 4.8\%$$

$$\rho_{TP} = 0.328 \frac{lb_m}{ft^3} \qquad e_{\rho_{TP,V}} = 8.44\%$$

(a) $e_{\rho,TP,model} = 1.0\%$ $\qquad e_{\rho,TP} = 8.50\%$

$$\Delta P_{f-m} = 45.79 \frac{lb_f}{ft^2} \qquad e_{\Delta P_{f-m}} = 2.58\%$$

(b) $e_{\rho,TP,model} = 90.0\%$ $\qquad e_{\rho,TP} = 90.4\%$

$$\Delta P_{f-m} = 45.79 \frac{lb_f}{ft^2} \qquad e_{\Delta P_{f-m}} = 2.60\%$$

2. R-113 LIQUID/VAPOR TESTS

Uncertainty in Total Mass Flow Rate of R-113 Two-Phase Mixture Through the Test Section

The total mass flow rate of R-113 two-phase mixture through the test section is obtained from:

$$W_{tot} = \rho_{l-m} * Q_{l-m} \qquad \text{(A-12)}$$

where W_{tot} = Total mass flow rate through the test section (lb_m/sec)

Q_{l-m} = Volumetric flow rate measured by the flow meter in the liquid line before stainless steel heater (ft^3/sec)

ρ_{l-m} = Density of R-113 liquid passing through the flow meter (lb_m/ft^3)

Applying (A-1) to (A-12),

$$\frac{e_{W_{tot}}}{W_{tot}} = \sqrt{\left(\frac{e_{\rho_{l-m}}}{\rho_{l_{l-m}}}\right)^2 + \left(\frac{e_{Q_{l-m}}}{Q_{l-m}}\right)^2} \qquad \text{(A-13)}$$

Sample calculation values and the resulting uncertainty in the total mass flow rate of R-113 two-phase mixture through the test section are as follows:

$$\rho_{l-m} = 97.12 \ \frac{lb_m}{ft^3} \qquad e_{\rho_{l-m}} = 1.0\%$$

$$Q_{l-m} = 3.90\times10^{-4} \ \frac{ft^3}{sec} \qquad e_{Q_{l-m}} = 4.28\%$$

$$W_{tot} = 3.817\times10^{-2} \ \frac{lb_m}{sec} \qquad e_{W_{tot}} = 4.40\%$$

Uncertainty in the Power Input To the Stainless Steel Heater

The power input is obtained from the equation:

$$Power = V \times I \qquad \text{(A-14)}$$

where Power = Power input to stainless steel heater (Watts)

I = Current (amps)

V = Voltage drop across the heater (volts)

The uncertainty in power is given by:

$$\frac{e_{power}}{Power} = \sqrt{(\frac{e_I}{I})^2 + (\frac{e_V}{V})^2} \qquad \text{(A-15)}$$

Sample calculation values and the resulting uncertainty in the power input are as follows:

I = 525.0 (amps) e_I = 1.59%

V = 1.578 (volts) e_V = 1.0%

Power = 828.4 (Watts) e_{Power} = 1.88%

Uncertainty in the Heat Losses to Room From the Stainless Steel Heater Through Fiberglass Insulation

This loss is calculated from the expression:

$$Q_{Loss} = \frac{2\,\pi\,K\,l}{\ln(r_o\,/\,r_i)} \times \Delta T \qquad \text{(A-16)}$$

where Q_{Loss} = Rate of heat loss to room (Watts)

K = Thermal conductivity of fiberglass insulation (Watts/m°C)

l = Length of insulation (m)

r_o = Outside radius of fiberglass insulation (m)

r_i = Inside radius of fiberglass insulation (m)

ΔT = Temperature difference between the inside and outside of insulation (°C)

The uncertainty in the calculated heat loss is given by:

$$\frac{e_{Q_{Loss}}}{Q_{Loss}} = [(\frac{e_K}{K})^2 + (\frac{e_l}{l})^2 + (\frac{e_{\Delta T}}{\Delta T})^2 + (\frac{e_{r_o}}{r_o \ln(r_o/r_i)})^2 + (\frac{e_{r_i}}{r_i \ln(r_o/r_i)})^2]^{\frac{1}{2}} \qquad \text{(A-17)}$$

Sample calculation values and the resulting uncertainty in the heat loss are as follows:

K = 0.034 (Watts/(m°C)) e_K = 3%

l = 3 (m) e_l = 1%

r_i = 0.012 (m) e_{ri} = 1%

r_o = 0.040 (m) e_{ro} = 1%

ΔT = 60 (^oC) $e_{\Delta T}$ = 6%

Q_{Loss} = 31.9 (Watts) e_{QLoss} = 6.88%

Uncertainty in the Inlet Quality to the Coil Test Section

The inlet quality is calculated as follows:

$$x = [\frac{Power - Q_{Loss}}{\rho_{l-m} Q_{l-m}} - (h_{fo} - h_{fi})] \frac{1}{h_{fgo}} \tag{A-18}$$

where x = Test section inlet quality

Power = Power to stainless steel heater (Watts)

Q_{Loss} = Heat losses to room (Watts)

ρ_{l-m} = Liquid density of R-113 passing through flow meter (kg/m^3)

Q_{l-m} = Volumetric flow rate of liquid R-113 before heater (m^3/sec)

h_{fo} = Liquid enthalpy of R-113 at outlet of heater (J/kg)

h_{fi} = Liquid enthalpy of R-113 at inlet of heater (J/kg)

h_{fgo} = Latent heat of vaporization at outlet of heater (J/kg)

The uncertainty in quality is given by:

$$e_x = [(\frac{1}{\rho_{l-m}Q_{l-m}h_{fgo}}e_{Power})^2 + (\frac{1}{\rho_{l-m}Q_{l-m}h_{fgo}}e_{Q_{Loss}})^2 +$$

$$(\frac{Power - Q_{Loss}}{\rho_{l-m}{}^2Q_{l-m}h_{fgo}}e_{\rho_{l-m}})^2 + (\frac{Power}{\rho_{l-m}Q_{l-m}{}^2h_{fgo}}e_{Q_{l-m}})^2 +$$

$$(\frac{1}{h_{fgo}}e_{h_{fo}})^2 + (\frac{1}{h_{fgo}}e_{h_{fi}})^2 + ((\frac{Power - Q_{Loss}}{\rho_{l-m}Q_{l-m}} - h_{fo} + h_{fi})\frac{e_{h_{fgo}}}{h_{fgo}^2})^2]^{\frac{1}{2}}$$

Sample calculation values and the resulting uncertainty in the quality are as follows:

Power = 828.4 (Watts)	e_{Power} = 1.88%
Q_{Loss} = 31.9 (Watts)	e_{QLoss} = 6.88%
$Q_{l-m} = 1.113\times10^{-5}$ (m^3/sec)	e_{Ql-m} = 4.28%
ρ_{l-m} = 1556 (kg/m^3)	$e_{\rho,l-m}$ = 1.0%
$h_{fi} = 5.944\times10^4$ (J/kg)	$e_{h,fi}$ = 1.0%
$h_{fo} = 9.205\times10^4$ (J/kg)	$e_{h,fo}$ = 1.0%
$h_{fgo} = 14.12\times10^4$ (J/kg)	$e_{h,fgo}$ = 1.0%
x = 0.09476	e_x = 17.1%

Uncertainty in Measured Total Frictional Pressure Drop Between Pressure Transducer Taps

The same method used previously to calculate the uncertainty of ΔP_{f-m} of the air-water test data can be used here to calculate the uncertainty of ΔP_{f-m} of the R-113 liquid/vapor test data. The following results are presented for a sample data calculation. Similarly, the unknown method-determined portion of the uncertainty of the two-phase mixture density($e_{\rho,TP}$), denoted by $e_{\rho,TP,model}$, is set to be 1% and 90% for the sample calculation, respectively.

Sample calculation values and the resulting uncertainty in the frictional pressure drop are as follows:

$$\upsilon_g = 1.355 \frac{ft^3}{lb_m} \qquad e_{\upsilon_g} = 1.0\%$$

$$\upsilon_l = 0.01089 \frac{ft^3}{lb_m} \qquad e_{\upsilon_l} = 1.0\%$$

$$x = 0.0948 \qquad e_x = 17.1\%$$

$$\rho_{l\text{-}rm} = 97.77 \frac{lb_m}{ft^3} \qquad e_{\rho_{l\text{-}rm}} = 1.0\%$$

$$\Delta z = 0.525\ ft \qquad e_{\Delta z} = 3.0\%$$

$$\Delta P_{tr} = 38.63 \frac{lb_f}{ft^2} \qquad e_{\Delta P_{tr}} = 4.8\%$$

$$\rho_{TP} = 7.23 \frac{lb_m}{ft^3} \qquad e_{\rho_{TP,V}} = 15.8\%$$

(*a*) $e_{\rho,TP,model} = 1.0\%$ $\qquad e_{\rho,TP} = 15.8\%$

$$\Delta P_{f\text{-}m} = 86.16 \frac{lb_f}{ft^2} \qquad e_{\Delta P_{f\text{-}m}} = 5.16\%$$

(*b*) $e_{\rho,TP,model} = 90.0\%$ $\qquad e_{\rho,TP} = 91.4\%$

$$\Delta P_{f\text{-}m} = 86.16 \frac{lb_f}{ft^2} \qquad e_{\Delta P_{f\text{-}m}} = 6.51\%$$

VITA

An Yan was born in Chong-Qing city, Si-Chuan province, P. R. China, on November 24, 1962. She attended elementary and high schools in Shanghai, P. R. China, and graduated from high school in June 1979. Upon graduation, she entered Shanghai Jiao Tong University in Shanghai, P. R. China and received her Bachelor of Science degree in Nuclear Engineering in June 1983. In the fall of 1983, she continued her graduate study in the same institution and received her first Master of Science degree in Nuclear Engineering in July 1986. In the same month, July 1986, she married Zhichao Guo who has been a wonderful husband and friend since then. After graduation, she accepted a position of Research Associate in the CAD Division of Computing Center in Shanghai Jiao Tong University from July 1986 to July 1988.

She entered the Graduate School of the University of Tennessee, Knoxville, in January, 1989. She received the research and/or teaching assistantship at the University of Tennessee from September 1988 to August 1990. From April 1, 1991 to February 14, 1992, she worked full-time at Aluminum Company of America as a Mechanical Engineer. After her thesis defense on April 24, 1992, she continued her career as a research engineer at Carrier Corporation, Syracuse, NY, on May 1, 1992. In August 1992, she will receive her second Master of Science degree in Mechanical Engineering at the University of Tennessee, Knoxville, upon the completion of the degree requirements.